MILLING OF FLEXIBLE STRUCTURES

By

Darcy Thomas Montgomery

B.A.Sc (Mechanical Engineering)

University of British Columbia

A THESIS SUBMITTED IN PARTIAL FULFILLMENT OF

THE REQUIREMENTS FOR THE DEGREE OF

MASTER OF APPLIED SCIENCE

in

THE FACULTY OF GRADUATE STUDIES

MECHANICAL ENGINEERING

We accept this thesis as conforming

to the required standard

THE UNIVERSITY OF BRITISH COLUMBIA

February 1990

In presenting this thesis in partial fulfilment of the requirements for an advanced degree at the University of British Columbia, I agree that the Library shall make it freely available for reference and study. I further agree that permission for extensive copying of this thesis for scholarly purposes may be granted by the head of my department or by his or her representatives. It is understood that copying or publication of this thesis for financial gain shall not be allowed without my written permission.

Department of MECHANICAL ENGINEERING

The University of British Columbia
Vancouver, Canada

Date MARCH 30TH 1990

DE-6 (2/88)

Abstract

Current manufacturing research aims at increasing productivity by optimal selection of process parameters. This is accomplished by understanding the fundamental physics of individual manufacturing processes.

In this thesis, peripheral milling of very flexible cantilevered plates is studied. The static and dynamic deflections of the plate under periodic milling forces are modelled. A new dynamic cutting force model is developed which considers five discrete zones of relative motion between the tool and the workpiece. The kinematics of both milling and vibratory motions are modelled, which is an original research contribution in this area. It is shown that the penetration of the tool into the workpiece during vibratory cutting has a strong influence on the damping and stiffness characteristics of the milling process.

A structural model of a discontinuous cantilevered plate is determined using the finite element method. A reduced order structural model at the tool-workpiece contact zone is implemented for discrete time response analysis of the plate under cutting force excitations during milling. The closed loop dynamic behaviour of the system is modelled and taken into account in the analysis. Simulations of plate machining are compared with experimental results. A model of the surface finish generation mechanism is deduced from the analysis and experimental results.

Applications of this research include peripheral milling of integral jet engine impellers, computer disk drives and other flexible mechanical components.

Table of Contents

List of Tables

List of Figures

Nomenclature

a :axial depth of cut (milling) or width of cut (general)

A_1 : ploughing model shearing contact area

A_2: ploughing model normal contact area

c : feed per tooth

c_i: damping of a SDOF dynamic system at node i

C: damping matrix of a MDOF dynamic system

f: feedrate

f_n: natural frequency

f_{nc}: vibration frequency during cutting

f_s : shearing force from ploughing model

f_n : normal force from ploughing model

f_t : tangential dynamic cutting force

f_r : radial dynamic cutting force

$F_i(t)$: excitation force at node i as a function of time

$F(t)$: excitation force vector as a function of time

F_x : resultant cutting force in x direction on a tooth

F_y: resultant cutting force in y direction on a tooth

F_X : resultant cutting force in x direction on the tool

F_Y: resultant cutting force in y direction on the tool

F_t: tangential cutting force

F_r: radial cutting force

G: transfer function

$|G|$: magnitude of transfer function

h: uncut chip thickness

h_c: cut chip thickness

h_f: height of feed marks on workpiece surface

h_m: mean uncut chip thickness

h^* : equivalent flank component of uncut chip thickness

k_i: stiffness of a SDOF dynamic system at node i

K: stiffness matrix of a MDOF dynamic system

K_s: specific cutting pressure

l_1: ploughing model shearing contact length

l_2: ploughing model normal contact length

m_i: mass of a SDOF dynamic system at node i

M: mass matrix of a MDOF dynamic system

N : washboarding multiplication factor

p_o: workpiece yield pressure

P: modal displacement matrix

$q_i(t)$:generalized displacement at node i as a function of time

$q(t)$: generalized displacement vector as a function of time

r: washboarding period ratio

r_1: cutting force ratio

r_2: edge force ratio

r_c: cutting force ratio

R: resultant cutting force

R: tool's nominal radius

R_p : distance of surface point from spindle center

R_t: tooth radius from spindle center

t: time

T: time step used in simulations

T_a: aliasing or washboarding period

T_c: cutting period

T_v: vibration period

x_c, y_c: x, y coordinates of tool center

x_p, y_p: x, y coordinates of point on workpiece

x_t, y_t: x, y coordinates of tooth

x : feeding direction coordinate axis

y : normal direction coordinate axis

z : axial direction coordinate axis

x_o, y_o, z_o: previous x, y, z values

Z : number of flutes on the cutter

Δx: change in x position of workpiece

Δy: change in y position of workpiece

$SURF(i, j, k)$: surface array of the workpiece

$\vec{v}$: oriented velocity of tool relative to the workpiece during ploughing

$\vec{v}_c$: velocity of tool center

$\vec{v}_p$: velocity of vibrating workpiece

$\vec{v}_t$: velocity of tooth on the cutter

$\vec{v}_{t/p}$:velocity of tooth relative to the workpiece

α: tool's rake angle

β: oriented direction of tool travel relative to the workpiece

γ: tool's clearance angle

ζ: structural damping ratio

η: effective angle of the clearance face to the horizontal axis

θ: process immersion angle

η: direction of tool travel relative to the workpiece

λ: surface finish wavelength

μ: coefficient of friction

ν: Poisson's ratio

τ: shear stress on the cutting shear plane

ϕ: shear angle of cutting

ϕ: phase angle of a transfer function

ϕ_i: mode shape for mode number i

ψ: instantaneous immersion angle of the tool in the workpiece

ω: circular frequency

ω_n: natural circular frequency

ω_d: damped circular frequency

Φ: modal matrix

Ω: angular speed of the tool

æ

Acknowledgement

I would like to thank my supervisor Dr. Yusuf Altintas for his support and instruction during this work for which I am grateful. I would like to thank Philip Chan, Jimmy Yang and Fariborz Ordubadi for their valuable technical assistance. I am indebted to Lourdes and my family, whose support and patience have made this work possible.

This work was supported by NSERC of Canada under Grant Number OGP-0006164 and by The Centre for Integrated Computer Systems Research (CICSR) UBC.

Chapter 1

Introduction

Current manufacturing research is mostly aimed at increasing productivity and developing unmanned operations. This is accomplished by taking one of two basic approaches. The first approach is development and improvement of manufacturing systems such as sensors and control schemes. The second approach is more fundamental and attempts to investigate the physics of individual processes. The second approach is taken here to investigate milling of flexible workpieces.

Milling is a common machining operation used to profile prismatic and sculptured parts. The versatility of the end milling process has resulted in widespread use of this operation by industry. Current milling machines and machining centres utilize sophisticated computer numerical control (CNC) technologies and require limited operator presence.

One application of end milling is the manufacture of flexible workpieces such as jet engine impellers, microwave guideway systems and aircraft structural components. The periodic forces of milling result in both static and dynamic deflections of the workpiece and corresponding surface errors. Current industrial practice uses conservative speeds and feeds to reduce the surface errors of the finished workpiece. This is an unacceptable solution because of the corresponding loss in productivity. It is the purpose of this research to investigate and model the physics of machining flexible workpieces and to determine methods of improving on current practice.

Chapter 2 is the Literature Review, and provides a theoretical base for the remainder

of this thesis. Topics from metal cutting, milling geometry, friction theory, vibrations, machine-tool chatter and machining flexible workpieces are discussed.

Chapter 3 presents the geometric modelling of dynamic milling and the metal cutting theory used in this thesis. Simulation and experimental results, along with analytical explanations, are given for both static and dynamic milling.

In Chapter 4 the dynamic characteristics of a stepped cantilevered plate are discussed and modelled using the finite element method. Experimental verification of this model is given.

Chapter 5 discusses the machining of flexible workpieces. This work integrates the results of Chapters 2, 3 and 4. Simulation and experimental results are presented for four cases of plate maching. Some recommendations for future work are presented.

The thesis is concluded with a short summary of the main results.æ

Chapter 2

Literature Review

2.1 Introduction

The nature of manufacturing research is highly interdisciplinary. When considering a complex manufacturing process from an engineering perspective, there are several considerations to be made. In the body of this report the subjects introduced in this chapter are integrated to analyze the problem of peripheral milling of flexible structures. In this chapter topics from the following subjects are reviewed: metal cutting, geometry of milling, friction theory, vibrations, machine-tool chatter and machining of flexible workpieces. The purpose of reviewing these topics is to provide a theoretical base for the remainder of this work and also to present approaches taken by other authors of similar projects.

2.2 Metal Cutting Process

In this section the metal cutting process is defined and its physics are discussed. A general definition of metal cutting includes, "operations in which a thin layer of metal, the chip or swarf, is removed by a wedge-shaped tool from a larger body" [46]. The resultant machined surface should have a desired shape and surface finish, and measure within required tolerances.

Although metal cutting operations are performed by a wide configuration of machine-tools, the basic mechanics of most of these cutting processes may be idealized by considering the orthogonal cutting process, see Fig.2.1. Orthogonal cutting is defined as, "cutting with the cutting edge perpendicular to the relative velocity between tool and work"[32].

A tool, with rake angle (α) and clearance angle (γ), moves along the workpiece surface at an uncut chip thickness (h). The workpiece material shears along plane (AB) and forms a chip. The deformed chip is of thickness (h_c) and the cutting ratio is defined as[32]:

$$r_c = h/h_c \tag{2.1}$$

The shear angle (ϕ) is given as a function of the cutting ratio and the rake angle by[32]:

$$\phi = \arctan \frac{r_c \cos \alpha}{1 - r_c \sin \alpha} \tag{2.2}$$

This cutting geometry is not valid for oblique cutting where the tool cutting edge is not orthogonal to the cutting velocity. Oblique cutting is thoroughly explained in [2].

Forces encountered in metal cutting depend on several factors: geometric orientation of the tool, cutting speed, workpiece material and the lubricant used [2]. The various forces are shown in Fig.2.2. The resultant force acting on the tool is (R). It is useful to consider two fundamental sets of forces equivalent to the resultant force. (F_{fr}) and (N) are the friction and normal forces respectively acting on the tool rake face. (F_s) and (F_n) are the shearing and normal forces respectively acting on the shear plane (AB). (F_t) and (F_r) are the tangential and radial and components of (R). The relationship between these forces is apparent from the geometry of Fig.2.2, [2]:

$$F_{fr} = F_t \sin\alpha + F_r \cos\alpha \tag{2.3}$$

$$N = F_t \cos\alpha - F_r \sin\alpha$$

$$F_s = F_t \cos\phi - F_r \sin\phi \tag{2.4}$$

$$F_n = F_t \sin\phi + F_r \cos\phi$$

Merchant [25] developed a thin zone model for analytically predicting the cutting forces on the tool. A minimum energy condition was used to show that the forces could be given by:

$$F_t = 2ha\tau \cot\phi \tag{2.5}$$

$$F_r = ha\tau(\cot^2\phi - 1)$$

where,

$$\phi = \frac{\pi}{4} - \frac{1}{2}(\beta - \alpha) \tag{2.6}$$

and (τ), (ϕ) and (β) are the shear stress on the shear plane, the shear angle and the angle between the resultant force and the normal to the rake face respectively. This model is rather simple and based on assumptions which are "open to considerable doubt"[2]. Results of experiments [2] show that the above equations don't accurately represent the physics of actual cutting. Different models have been presented by other authors [2] but none have proved to be very accurate, and for this reason empirical models of the cutting force are used most frequently.

Assumptions inherent to the orthogonal cutting model include[2],[16]:

- a truly planar shear plane

- process independence of thermal effects
- a rigid tool-workpiece system
- a perfectly sharp tool
- uniformly distributed stresses on the shear plane
- homogeneous workpiece material
- continuous chip formation
- constant cutting speed
- two dimensional deformation.

Although the orthogonal cutting model is not exact the analysis "qualitatively describes the cutting process satisfactorily" [2].

(F_t) and (F_r) can usually be measured with a dynamometer for given cutting conditions. For a specific cutter-workpiece pair an empirical formulation for (F_t) and (F_r) can be derived if sufficient cutting tests are carried out. One commonly used linear model for the cutting forces is [37]:

$$F_t = K_s a h \tag{2.7}$$

$$F_r = r_1 K_s a h$$

where the specific cutting pressure (K_s), and the cutting force ratio (r_1) are both experimentally determined parameters which may or may not vary with the cutting conditions. Here the cutting force is assumed to be proportional to the width of cut (a) and to the instantaneous uncut chip thickness (h). This model neglects the effect of cutting speed which is often a good approximation [37].

Another linear model for the cutting forces is[1]:

$$F_t = K_s a(h + h^*) \tag{2.8}$$

$$F_r = K_s a(r_1 h + r_2 h^*)$$

where (K_s), (r_1), (r_2) and (h^*) are all experimentally determined parameters. In this case the cutting force is proportional to the uncut chip thickness plus some constant (h^*) which represents the effect of the so called edge-cutting forces due to rubbing at the edge and flank of the tool. It should be noted that other, perhaps nonlinear, models could be developed to fit experimental data if required.

This section has thus far considered only static cutting (when there is no relative vibration between the tool and the workpiece). The effects of cutting under dynamic conditions will be considered next.

During metal cutting operations the structural properties of the machine-tool or the workpiece (discussed later) may give rise to vibrations which cause changes in the instantaneous uncut chip thickness (h). The cutting force will also be variable since it has been shown to be roughly proportional to (h). The nature of how the cutting force varies with instantaneous changes of the cutting conditions is reviewed.

The most obvious method of analysing dynamic cutting is to use the simple orthogonal cutting model. In this case the cutting forces would vary as the uncut chip thickness. This solution would be sufficient if the amplitude and frequency of vibration were small enough such that other effects could be neglected.

When the amplitude and frequency of vibration become significant more detailed models must be used to obtain a high level of confidence in theoretical predictions. The reasons for vibrations becoming large during cutting are not obvious and are discussed in Section 2.6. Assuming that a dynamic cutting model is required there are several

methods of force prediction available. This area has been the topic of several research projects and three theories are briefly reviewed here.

The first theory considers Dynamic Cutting Force Coefficients (DCFC). The process of dynamic cutting is shown in Fig.2.3. As noted by Tlusty [37] "The tool is removing a chip from an undulated surface which was generated during the previous pass when the tool vibrated with an amplitude (z_o). Simultaneously the tool is vibrating with an amplitude (z)." By decomposing the dynamic cutting process into wave removing and wave generating the dynamic components (f_t and f_r) of the cutting forces are given by [37]:

$$f_t = a(K_{ci}z + K_{co}z_o) \tag{2.9}$$

$$f_r = a(K_{di}z + K_{do}z_o)$$

The DCFC's (K_{di},K_{do},K_{ci} and K_{co}) are considered to be complex numbers. Subscript (d) represents direct coefficients because (f_r) is the cutting force in the direction of vibration (z). Subscript (c) represents cross coefficients because (f_t) is the cutting force perpendicular to (z). Subscripts (i) and (o) represent inner and outer modulations respectively.

Under extreme conditions of vibration Tlusty [40] has noted that the cutting tool may "jump out" of the workpiece. Under this condition there is no contact between the tool and the workpiece and the cutting force is therefore zero.

The DCFC's are measured by harmonically exciting the tool during orthogonal cutting and comparing the tool vibration and the cutting forces during the process. "The whole equipment is very sophisticated, it needs considerable maintenance and calibration effort and, of course, contains many potential error sources" [40]. A major result of DCFC measurements indicate that, "modes of vibration with direction close to the normal to

the cut are affected by the damping in the cutting process much more than the modes in other directions" [37]. This model requires specialized test equipment but gives insight into the dynamics of cutting from the results obtained for various changes in the cutting conditions.

The second approach to the dynamic cutting process discussed here considers an elastic plastic deformation zone located at the tool tip and on the clearance face. As shown in Fig.2.4 [50], the workpiece material passes both above and below the tool. Point A is known as the separation point. The material passing above point A forms a chip and is removed from the workpiece in the usual manner. The material passing below point A is compressed in an elastic plastic deformation process and remains as part of the workpiece.

The cutting force on the rake face is calculated using orthogonal cutting theory. The forces on the clearance face are determined using a ploughing theory which assumes the force is proportional to the volume of material displaced by the tool motion. This theory assumes small vibrations of the tool. The ploughing forces (f_t and f_r are components of the overall cutting force due to ploughing, see Fig.2.4) are given as [50]:

$$f_t = f_{sp} V \tag{2.10}$$

$$f_r = \mu_c V$$

where (f_{sp}) is the specific ploughing force, (μ_c) is the mean friction coefficient on the contact surface and (V) is the volume of material displaced. The model neglects side spread of workpiece material and permanent plastic deformation of the ploughed surface. The nose AB is neglected from the ploughing calculation because the force is said to be constant on this part of the tool. The results are verified experimentally for a sinusoidally varying case [50].

The third theory for the dynamic cutting process considers the effects of varying both the feedrate and the cutting speed. Tobias notes that [45]: "it is quite sufficient to determine how the cutting force changes when small variations in these factors take place."

The variation of the cutting force is defined in terms of the variation of three parameters: the instantaneous uncut chip thickness (h), the cutting speed (v) and the rate of penetration (r). The variation of the cutting force is given as [45]:

$$dF = k_1 dh + k_2 dr + k_3 dv \tag{2.11}$$

These dynamic coefficients require a significant amount of work to obtain but are simple in terms of physical understanding, as explained by Tobias [45].

The descriptions of the metal cutting process given in this section have all made physical assumptions of reality. A brief introduction to some of the phenomena which have not yet been discussed, but are important in the field of metal cutting, will be reviewed here.

Tool wear occurs in all metal cutting operations. As noted by Armarego and Brown [2]:

"Cutting tools are subjected to an extremely severe rubbing process. They are in metal-to-metal contact with the chip and workpiece under conditions of very high stress at high temperature. The situation is further aggrivated by the existence of extreme stress and temperature gradients near the surface of the tool."

Rubbing and diffusion cause the tool to form craters on the rake face and wear lands on the clearance face. Chipping off of small particles may also occur on the cutting edge. The results of a worn tool are changes in both the static and dynamic cutting forces and variations in the tool geometry (which may affect the dimensions and surface quality of

the finished workpiece).

The previous analyses have all assumed the formation of a continuous chip under static cutting conditions. It should be noted that for certain workpiece materials and cutting conditions the formation of a built up edge or cutting with a discontinuous chip due to vibrations may occur. Brittle materials tend to form discontinuous chips while ductile materials are more likely to form a built up edge [2]. Built up edge and discontinuous chips produced by vibrations result in a deteriorated surface quality and "if surface finish is an important requirement, the cutting conditions will have to be adjusted to avoid these features" [2].

In industrial machining operations cutting fluids are often used to lubricate the chip tool contact area in order to reduce the friction. The decreased cutting friction results in lower cutting forces and increased tool life. Other benifits of using a cutting fluid include an improved surface finish and reduced distortion due to temperature rise in the workpiece. The use of a cutting fluid strongly affects the metal cutting process and this must be accounted for in any analysis where a cutting fluid is used.

2.3 Geometry of Milling

A physical description of the milling process is given by Martellotti [22]: "a process of removing the excess material from the workpiece in the form of small individual chips. These chips are formed by the intermittent engagement with the workpiece of a plurality of cutting edges or teeth integral with or inserted in a cylindrical body known as the milling cutter. This intermittent engagement is produced by feeding the workpiece into the field dominated by the rotating cutter." A wide variety of machining operations are possible on a milling machine. These operations can mostly be defined as either peripheral or face milling. In peripheral milling the surface being generated is parallel

to the axis of the tool. In face milling operations the working surface is perpendicular to the axis of the tool. A typical end mill is shown and geometrically defined in Fig.2.5 [2].

Martellotti [22] gives a precise mathematical formulation for the geometry of the milling process. He derives relationships for the looped trochoidal path generated by a milling cutter tooth, the uncut chip thickness, amplitude of the tooth marks, the angle of approach of teeth and the relative velocity along the tooth path.

The equation for amplitude of the tooth marks is used in a later section and is therefore repeated here [22]:

$$h_f = \frac{R}{8}(\frac{c}{R \pm r})^2 \tag{2.12}$$

where (h_f) is the height of the tooth mark above its lowest level, (R) is the radius of the cutter, (r) is the feed per revolution divided by (2π) and (c) is the feed per tooth. The $(+)$ sign represents up milling and the $(-)$ sign represents down milling.

The equations given by Martellotti are correct only for a completely rigid system. If vibrations occur they must be added to the path of the tool to accurately model its motion. The dynamic motion of milling is shown in Fig.2.6.

When the feed per tooth (c) is small the trochoidal path of the tool may simply be approximated as a circle [22]. In this case the uncut chip thickness is given by:

$$h = c \sin \psi \tag{2.13}$$

where (ψ) is the immersion angle of the tooth in cut.

2.4 Friction Theory

Due to the nature of the metal cutting process a great deal of frictional resistance is generated in various regions of the cutting zone. This is especially true during dynamic

cutting when the clearance face rubs and ploughs into the workpiece. A general definition of friction is [12]: "the resistance to motion which is experienced whenever one solid body slides over another." Frictional resistance of contacting metals is primarily due to the processes of adhesion and material displacement [12]. Theories of adhesion and ploughing (a particular case of material displacement) will be briefly discussed here.

The dynamic coefficient of friction (μ) is defined as the ratio of the frictional to the normal force acting on contacting bodies in relative motion. Bowden and Tabor [12] define the coefficient of friction due to adhesion in their simple theory as:

$$\mu_a = s_o/p_o \tag{2.14}$$

where (s_o) and (p_o) are the critical shear stress and the yield pressure respectively. The frictional force is calculated by multiplying the coefficient of friction by the normal force on the surface. The theory ignores work hardening and the effect of any contaminant layer which might be present.

Ploughing is the result of "asperities on a hard metal penetrating into a softer metal and 'ploughing' out a groove by plastic flow in the softer metal"[12]. The coefficient of friction due to ploughing is given by [12]:

$$\mu_p = A_v/2A_h \tag{2.15}$$

where (A_v) and (A_h) are the vertically and horizontally projected areas of contact for a given asperity. The normal (N) and shearing (F_s) forces are given by:

$$N = A_h p_o \tag{2.16}$$

$$F_s = A_v p_o$$

The total frictional forces are calculated by combining those due to adhesion and ploughing.

2.5 Vibration Theory

A large variety of methods for the analysis of dynamic systems is available. Topics reviewed in this section include: free vibration, forced vibration, self excited vibration, modal testing and identification, the finite element method and system reduction.

Free vibration of linear discrete systems is defined by one or more ordinary differential equations representing one or more degrees of freedom (dof) of motion. During free vibration there are no external forces applied to the structure and its motion is determined by its inertial, damping and restoring forces. The equation of motion of a linear, damped, non-gyroscopic, coupled dynamic system is given in general by [24]:

$$M\ddot{q}(t) + C\dot{q}(t) + Kq(t) = 0 \tag{2.17}$$

where $(q(t))$ is the generalized displacement n-vector and is of the form:

$$q(t) = [q_1(t)\, q_2(t) \ldots q_n(t)]^T \tag{2.18}$$

(M), (C) and (K) are the $n \times n$ matrices of the systems mass, damping and stiffness respectively. Eq. 2.17 is usually determined using either Newton's formulation (equating forces) or Lagrange's formulation (energy method). Experimental methods may also be used to obtain the equation of motion in an indirect manner. The eigenvalue problem for Eq. 2.17 can be solved for the mode shapes and modal frequencies of the system [24] if proportional damping is assumed. The characteristics of the system are determined by performing modal analysis on the equations of motion. This leads to n uncoupled linear ordinary differential equations each corresponding to a mode shape and frequency

of the system. This process is explained in most mechanical vibration textbooks [47]. The modal solution gives insight into how the system will respond to various external excitations.

When external forces are applied to a dynamical system the problem becomes one of forced vibration. The applied forces must balance with the inertial, damping and restoring forces which leads to a forced equation of motion [24]:

$$M\ddot{q}(t) + C\dot{q}(t) + Kq(t) = F(t) \tag{2.19}$$

where (F) is the generalized excitation force and is of the form:

$$F(t) = [F_1(t)\ F_2(t) \ldots F_n(t)]^T \tag{2.20}$$

(F_i) is the force or moment applied to dof-i.

The response of a system to a given excitation may be considered as a function of either time or frequency. The time domain solution is considered first. Since all linear multiple degree of freedom (MDOF) systems of the form of Eq. 2.19 can be reduced to sets of linear single degree of freedom (SDOF) systems by modal analysis, the response of a SDOF system will be considered here.

Consider the system shown in Fig.2.7. The general equation of motion of such a SDOF system can be given by:

$$m\ddot{x}(t) + c\dot{x}(t) + kx(t) = f(t) \tag{2.21}$$

The exact solution for such a system, provided that $(f(t))$ is known, is found in many textbooks [47]. The solution gives a continuous time equation for $(q(t))$. Eq. 2.21 can also be solved in the discrete time domain and this is the approach taken here. Taking the Laplace transform of Eq. 2.21 gives:

$$ms^2x(s) + csx(s) + kx(s) = f(s) \tag{2.22}$$

or,

$$x(s) = \frac{f(s)}{ms^2 + cs + k} \tag{2.23}$$

where (s) is the Laplacian operator. The discrete time equivalent of the Laplacian operator may be approximated using the bilinear transformation method as [29]:

$$s = \frac{2}{T}\left(\frac{1 - z^{-1}}{1 + z^{-1}}\right) \tag{2.24}$$

where (z) is the Z-transform operator and (T) is the time step. By substituting Eq.2.24 into Eq.2.23 and carrying out the z-operator reductions it can be shown that:

$$x_i = \frac{f_i + 2f_{i-1} + f_{i-2} - Ax_{i-1} - Bx_{i-2}}{C} \tag{2.25}$$

where,

$$A = -\frac{8}{T^2}m + 2k$$

$$B = \frac{4}{T^2}m - \frac{2}{T}c + k$$

$$C = \frac{4}{T^2}m + \frac{2}{T}c + k$$

and the subscript denotes the time step of the parameter when (i) is the current value.

For the solution of Eq.2.25 $(f(t))$ is not required as a closed form function. Such a discrete time equation is ideal for computation on a digital computer. The accuracy of the result can be increased by reducing the size of the time step (T). Eq. 2.25 is the

solution for only one mode of a MDOF problem. It is usually only required to solve a few of the modal responses in a desired range of frequencies, choosing (T) accordingly. The principle of superposition [24] allows the modal solutions to be added to obtain the complete system response.

The frequency domain transfer function of Eq.2.21 is found by substituting ($s = i\omega$) into Eq. 2.23 to obtain:

$$G(\omega) = \frac{X(\omega)}{F(\omega)} = \frac{1}{-\omega^2 m + i\omega c + k} \tag{2.26}$$

The response may be considered in terms of the magnitude and phase of the transfer function. These are given as:

$$|G| = \frac{1}{\sqrt{(k - \omega^2 m)^2 + (\omega c)^2}} \tag{2.27}$$

$$\phi = arctan \frac{-\omega c}{k - \omega^2 m}$$

Physical interpretations of the magnitude ($|G|$) and the phase (ϕ) of the transfer function are simple. For a sinusoidally varying input force of constant amplitude and frequency, ($|G|$) represents the ratio of the amplitude of the response to the amplitude of the input and (ϕ) is the phase angle between the response and the input.

Both time domain and frequency domain solutions give important insight into the behaviour of dynamical systems.

The next topic of discussion is self excited vibration. Self excited vibrations occur when [6]: "The external forces applied to the system are now determined by the motion of the system. But the internal forces governing free vibration are also of this sort, so it is now as if the external forces augment the inertia-, the damping- and the stiffness-forces." This differs from forced vibration where the motion and excitation forces are independent. The other criterion for self excited vibration to occur is that there must

be some source of energy for the vibration to "tap" and the motion must be such that the energy can be extracted [6]. Some examples of self excited systems are: machine tool chatter (discussed later in detail), stick-slip friction and flutter of aircraft wings. If the vibration extracts energy from the source, the response may grow until it is limited by some nonlinearity. In each case of self excited vibration the physical process of self excitation is slightly different.

There are two fundamentally different ways to obtain the dynamic characteristics (M,C and K) of mechanical systems. Either theoretical calculations or experimental testing may be used as the first step in identifying these parameters. Theoretical results generally determine (M), and (K) directly. Experimental methods usually measure the system response to a known input and manipulate this data to further obtain (M), (C) and (K). Experimental modal testing will be reviewed next with the finite element method being briefly discussed later on.

Modal testing is defined as [10]:"the processes involved in testing components or structures with the objective of obtaining a mathematical description of their dynamic or vibration behaviour." The testing procedure and the mathematical description of the data may vary considerably from test to test. The process generally consists of physical excitation of the system and measurement of both the input and the response. The excitation is usually accomplished with one or more shakers or an impact hammer. The response is measured with one or more accelerometers, velocity transducers or proximity sensors located at various points on the structure. Modern frequency analysis equipment can transform the measured data into useful transfer functions (by use of Fourier analysis) in the frequency domain. From these transfer functions one can "work backwards" (with respect to to the analytical methods of vibration analysis) to obtain the dynamic characteristics of the system.

A brief review of modal testing for SDOF systems is given here. This is useful because

linear MDOF systems are just a linear combination of a number of SDOF systems. Most of the discussion follows directly from [10] which covers the entire scope of the subject. The generalized equation of motion for a SDOF system was given by Eq. 2.21 which is repeated here:

$$m\ddot{x}(t) + c\dot{x}(t) + kx(t) = f(t) \tag{2.28}$$

Some well known equations relating the parameters of Eq.2.28 are:

$$\omega_n = \sqrt{k/m} \tag{2.29}$$

$$\zeta = \frac{c}{2\sqrt{km}} \tag{2.30}$$

$$\omega_d = \omega_n\sqrt{1-\zeta^2} \tag{2.31}$$

where (ω_n), (ζ), (c), (ω_d), (m) and (k) are the natural frequency, damping ratio, damping factor, damped natural frequency, mass and stiffness respectively of the system. The receptance frequency response function (FRF) was given by Eq. 2.26:

$$G(\omega) = \frac{X(\omega)}{F(\omega)} = \frac{1}{(k - m\omega^2) + ic\omega} \tag{2.32}$$

Other forms of the FRF are the mobility ($\dot{X}(\omega)/F(\omega)$=$i\omega G(\omega)$) and the accelerance ($\ddot{X}(\omega)/F(\omega)$=$-\omega^2 G(\omega)$). Graphical display of FRF data may be presented in three common forms [10]:

- modulus (of FRF) *vs* frequency, and phase *vs* frequency
- real part (of FRF) *vs* frequency, and imaginary part *vs* frequency

- real part *vs* imaginary part

Typical FRF response curves for a SDOF system are shown in Fig.2.8. The various parameters which can be obtained from the curves are noted on the figures. For SDOF systems the above curves give a complete physical description of the dynamic characteristics.

Analytical tools may also be used to compute the dynamic characteristics of vibratory systems. "The finite element method is a numerical procedure for solving a continuum mechanics problem with an accuracy acceptable to engineers" [9]. It is beyond the scope of this work to give any quantitative details of the method and interested readers are referred to standard textbooks on the subject [9], [51]. A finite element model defines a continuum by first dividing it into small parts or finite elements. Each element has several nodal points which are either restricted by continuity requirements of neighbouring elements or constrained by the boundary conditions of the system. Trial functions are found to describe the behaviour of the system for each element by minimizing some energy condition of the continuum.

The equations of motion obtained from a finite element analysis of a dynamic system are often of a very large dimension. Several reduction methods are available to reduce the size of the model at various stages of the analysis. The purpose of these methods is usually to "minimize computer time/cost or to deal with a reduced model for forced response studies" [28]. The method considered here is known as the system equivalent reduction expansion process (SEREP) and is presented by O'Callahan et al [28]. Some of the unique qualities of SEREP are[28]:

- the arbitrary selection of modes that are to be preserved in the reduced system model

- the quality of the reduced model is not dependent upon the location of the selected active dof
- the frequencies and mode shapes of the reduced system are exactly equal to the frequencies and mode shapes (for the selected modes) of the full system model.

Assume the equation of motion of an n_{FE}-dof undamped dynamic system, determined by finite elements (FE) or some other method, is given by Eq.2.33:

$$M_{FE}\ddot{x}_{FE} + K_{FE}x_{FE} = F_{FE} \tag{2.33}$$

The finite element solution is assumed to give a (n_M) mode solution. The generalized coordinates are defined as:

$$x_{FE} = \Phi_{FE}P \tag{2.34}$$

where (P) is the $n_M \times 1$ modal coordinate vector, and (Φ_{FE}) is the $n_{FE} \times n_M$ eigenvector matrix of the finite element equations of motion. One or more dof's is kept from Eq.2.33 which are usually points where forces are applied or deflections are required. The equation relating the reduced (R) dof's and the modal coordinates is:

$$x_R = \Phi_R P \tag{2.35}$$

where (Φ_R) is the $n_R \times n_M$ eigenvector matrix of the reduced system. The modal coordinates are found explicitly by:

$$P = \Phi_R^g x_R \tag{2.36}$$

where (Φ_R^g) is the generalized inverse of (Φ_R) and, if $n_R \leq n_{FE}$, is given by [28]:

$$\Phi_R^g = (\Phi_R^T \Phi_R)^{-1} \Phi_R^T \tag{2.37}$$

It can be easily determined from Eq's. 2.34 and 2.36 that:

$$x_{FE} = \Phi_{FE} \Phi_R^g x_R = T x_R \tag{2.38}$$

where (T) is the global mapping transformation matrix. The n_R-dof reduced system equation of motion is given by:

$$M_R \ddot{x}_R + K_R x_R = F_R \tag{2.39}$$

where,

$$M_R = T^T M_{FE} T \tag{2.40}$$

$$K_R = T^T K_{FE} T \tag{2.41}$$

$$F_R = T^T F_{FE} \tag{2.42}$$

A computer program has been written to compute the SEREP reduction of large dynamic models [27].

2.6 Machine Tool Vibrations

During a machining operation various disturbances may act independantly or combine to result in some form of vibration of the machine tool or workpiece. Some of these causes are [2]: impact or shock, unbalance of rotating parts, discontinuous chip formation and self induced vibration of the dynamic cutting process.

Vibration of a machine tool during a cutting operation can have a wide range of effects. If the vibration amplitude is small and of a transient nature, the consequences may be negligable. On the other hand if the vibration grows to a large amplitude the result may be damage to the workpiece, damage to the machine tool or premature failure of the tool.

In this section only vibrations due to the cutting process itself are considered. These fall broadly into two categories: forced vibrations and self excited vibrations (chatter).

By definition forced vibrations can only occur in open loop systems, that is when the excitation and response are independent. For this reason the analysis of forced vibrations of machine tools is a relatively easy matter. If the input force from the cutting process is known, the response can always be determined assuming correct knowledge of the dynamic characteristics of the machine tool.

Even the simple orthogonal cutting model of the metal removal process shows that the cutting force is dependent on the deflection of the tool. It is obvious that the deflection of the tool is also dependent on the cutting force. Thus all machining processes should most properly be considered as closed loop dynamic systems. The importance of the feedback loop is a function of the process parameters. Analysis of machine tool vibrations as a closed loop system considers the process to be a self excited vibration problem. The type of self excited vibration encountered during machining operations is known as chatter. As noted by Tobias [45], "The most important characteristic property of chatter vibration is that it is not induced by external periodic forces, but rather that the forces which bring it into being and maintain it are generated in the vibratory process itself."

The general theory of chatter outlined here makes several assumptions [39] following the analysis given by Tlusty [16]:

- the vibratory system is linear

- the direction of the variable component of the cutting force is constant
- the variable component of the cutting force depends only on vibration in the direction of the normal to the cut surface
- the value of the variable component of the cutting force varies proportionately and instantaneously with the vibrational displacement
- the frequency of the vibration and the mutual phase shift of undulations in subsequent overlapping cuts are not influenced by the relationship of wavelength to the length of cut.

It is generally accepted that two mechanisms of chatter exist; mode coupling and regeneration.

"Mode coupling is a mechanism of self-excitation that can only be associated with situations where the relative vibration between the tool and the workpiece can exist simultaneously in at least two directions in the plane of the orthogonal cut"[16]. Consider the cutting process shown in Fig.2.9 with two perpendicular modes of vibration. Assume that the two modes vibrate simultaneously in the elliptical pattern shown. Since the cutting force is assumed to be proportional to the uncut chip thickness (h), it will be greater from $B \rightarrow A$ than from $A \rightarrow B$. "Periodically there is a surplus of energy sustaining the vibrations against damping losses"[16]. Under certain conditions the process may become unstable which is discussed later on.

Regeneration is a mechanism of self excitation that occurs only when "the tool removes the chip from a surface which was produced by the tool in the preceding pass" [16]. If during the preceding pass the tool was vibrating, the surface removed during the current pass will be wavy, see Fig.2.10. This results in a periodically varying cutting force. As for

the case of mode coupling chatter, regenerative chatter may be either stable or unstable depending on the process parameters.

Consider again the system shown in Fig.2.9. The cutting forces may be defined as:

$$F_x = -F_t \sin\theta + F_r \cos\theta \tag{2.43}$$

$$F_y = F_t \cos\theta + F_r \sin\theta$$

where,

$$F_t = K_s a h = K_s a(h_m - z) \tag{2.44}$$

$$F_r = r_1 K_s a(h_m - z)$$

$$z = y \sin\theta + x \cos\theta \tag{2.45}$$

where (h_m) is the mean uncut chip thickness and (z) is the time dependent normal deflection of the tool. The equation of motion for the system of Fig.2.9 can be reduced to:

$$m_x\ddot{x} + c_x\dot{x} + k_x x = K_s a(h_m - y\sin\theta - x\cos\theta)(-\sin\theta + r_1\cos\theta) \tag{2.46}$$

$$m_y\ddot{y} + c_y\dot{y} + k_y y = K_s a(h_m - y\sin\theta + x\cos\theta)(\cos\theta + r_1\sin\theta)$$

or alternatively,

$$\begin{bmatrix} m_x & 0 \\ 0 & m_y \end{bmatrix} \begin{Bmatrix} \ddot{x} \\ \ddot{y} \end{Bmatrix} + \begin{bmatrix} c_x & 0 \\ 0 & c_y \end{bmatrix} \begin{Bmatrix} \dot{x} \\ \dot{y} \end{Bmatrix} + \tag{2.47}$$

$$\begin{bmatrix} k_x + K_1\cos\theta & K_1\sin\theta \\ K_2\cos\theta & k_y + K_2\sin\theta \end{bmatrix} \begin{Bmatrix} x \\ y \end{Bmatrix} = h_m \begin{bmatrix} K_1 \\ K_2 \end{bmatrix}$$

where,

$$K_1 = K_s a(-\sin\theta + r_1 \cos\theta)$$

$$K_2 = K_s a(\cos\theta + r_1 \sin\theta)$$

From Eq.2.47 it is apparent that the motion of the two modes will be coupled, thus the name "mode coupling" type chatter. Tlusty[16] notes that "for the limit of stability the open-loop transfer function is equal to -1". The limiting factor for mode coupling chatter is the axial depth of cut ($b_{lim,mc}$) and is given as [16]:

$$b_{lim,mc} = -1/K_s Re[(G)_{min}] \tag{2.48}$$

If regeneration is considered, the uncut chip thickness contains a phase lag term and is given by [16]:

$$h = h_m - z + z_o \tag{2.49}$$

where (z_o) is the (z) position of the previous tooth which accounts for regeneration in the cutting process. The equation of motion is given by:

$$\begin{bmatrix} m_x & 0 \\ 0 & m_y \end{bmatrix} \begin{Bmatrix} \ddot{x} \\ \ddot{y} \end{Bmatrix} + \begin{bmatrix} c_x & 0 \\ 0 & c_y \end{bmatrix} \begin{Bmatrix} \dot{x} \\ \dot{y} \end{Bmatrix} + \tag{2.50}$$

$$\begin{bmatrix} k_x + K_1 \cos\theta & K_1 \sin\theta \\ K_2 \cos\theta & k_y + K_2 \sin\theta \end{bmatrix} \begin{Bmatrix} x \\ y \end{Bmatrix} -$$

$$\begin{bmatrix} K_1 \cos\theta & K_1 \sin\theta \\ K_2 \cos\theta & K_2 \sin\theta \end{bmatrix} \begin{Bmatrix} x_o \\ y_o \end{Bmatrix} = h_m \begin{bmatrix} K_1 \\ K_2 \end{bmatrix}$$

where (K_1) and (K_2) are the same as before.

The limit of stability for regenerative chatter has been given by Tlusty [16] as:

$$b_{lim,regen} = -1/2K_s Re[(G)_{min}] \tag{2.51}$$

Comparing Eq's. 2.48 and 2.51, it can be seen that the limit of stability for regenerative type chatter is half of that for mode coupling chatter. For this reason regenerative chatter is usually dominant in most practical machining operations. Still there are some special cases, milling with alternating helix tools or thread cutting in turning, where regenerative chatter is suppressed and mode coupling becomes dominant.

The previous analyses assumed that the cutting force can be modelled using the simple orthogonal cutting model presented earlier. A more realistic approach would use a dynamic cutting model accounting for flank face interference and the possibility of the tool "jumping out" of the workpiece material.

2.7 Machining of Flexible Structures

The theories presented in earlier sections of this chapter can be applied in various degrees to the application of machining flexible structures. In machining operations, a flexible structure may be defined as a workpiece whose static or dynamic flexibilities are significant when compared to similar parameters of the machine tool itself. Such structures find application in the aerospace and communication industries as ribbed structural components, turbine blades and microwave guideways. Few works have been carried out on the topic of machining flexible structures. Two research projects are discussed here.

Tlusty has experimentally investigated the use of steadies to reduce chatter when machining thin blades on a milling machine. The steadies used were constructed of either rubber or stainless steel and were said to decrease the severity of chatter vibrations.

This result was explained by an argument that the steadies increased the static stiffness and increased damping of the higher vibrational modes. The use of steadies to reduce chatter vibrations has two drawbacks: first, the dynamics of the coupled workpiece-steady system are difficult to model and second, this method cannot be used on components with very complex geometry such as jet engine impellers. In this study the workpiece vibration was assumed to be closely represented by the cutting forces measured on a dynamometer. The validity of this assumption depends strongly on which vibrational modes are active and where the displacement of the workpiece is of interest relative to the nodal lines of each mode. It was observed that the machined surface did not exhibit the chatter wavelengths which are regenerated on the arc of the cut. This was explained graphically as the machined surface is only being generated during a small fraction of the cutting period. Reasons for reducing the severity of chatter during such an operation are decreased tool wear and to lessen the deep tight grooves left on the surface by chatter vibrations.

Kline [18] developed and experimentally verified an analytical approach to modelling the machining of flexible structural components used in the aircraft industry. The process considered was machining of a CCCF plate with a flexible end mill. Deflections of both the workpiece and the tool were considered. The tool was modelled using beam theory and the plate was modelled using both finite differences and the finite element method. The problem was considered to be static with the author arguing that the excitation frequency was an order of magnitude less than the lowest natural frequency of either the plate or the end mill. This is valid only if chatter is not present in the particular machining operation and thus limits the range of validity of the work. Runout was modelled and experimentally verified for the rigid machining process. Kline notes that [18]: "The effects of runout are most severe for cuts with long lengths of engagement between flutes and workpiece and light feeds." This is the case investigated in Kline's

research and is justification for implementation of a runout model when considering such low feed systems. The cutting forces were defined as deflection independent functions of the cutting conditions. This approach will introduce errors into the predicted cutting forces and the resultant deflections of the tool and workpiece. Surface profiles were predicted by adding deflections of both the tool and the workpiece. The approach taken by Kline is valid only if dynamic effects are not significant to the machining operation.

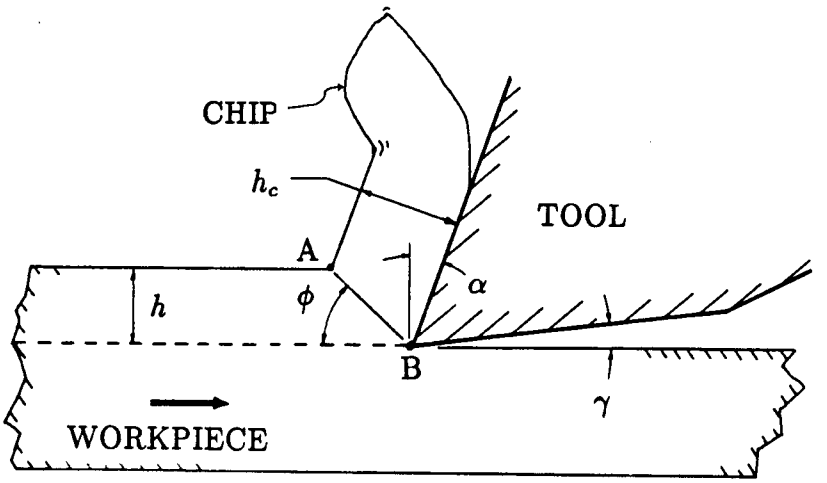

Figure 2.1: Orthogonal cutting process geometry.

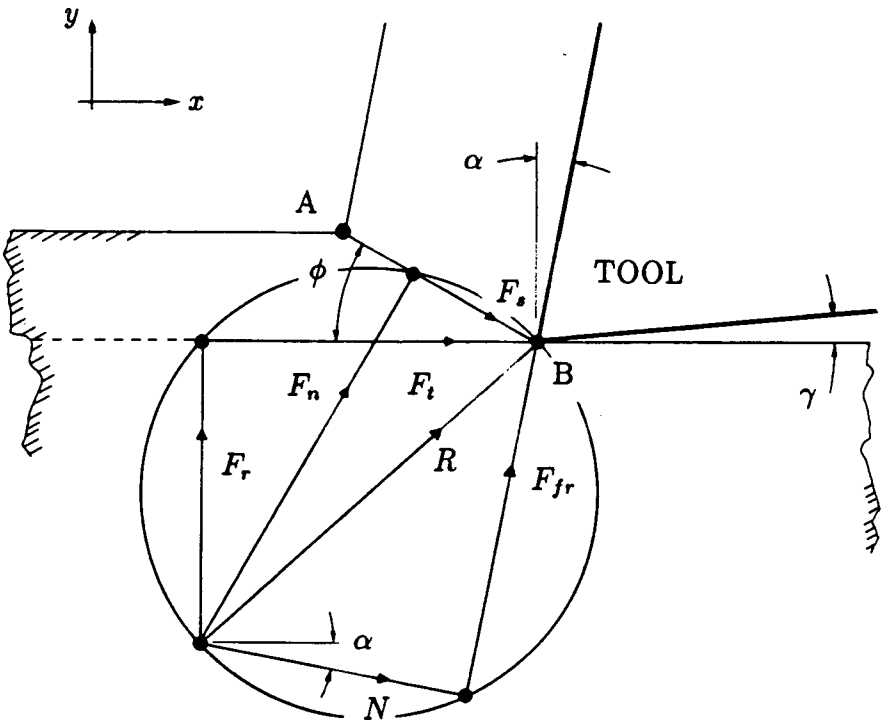

Figure 2.2: Forces in the orthogonal cutting process.

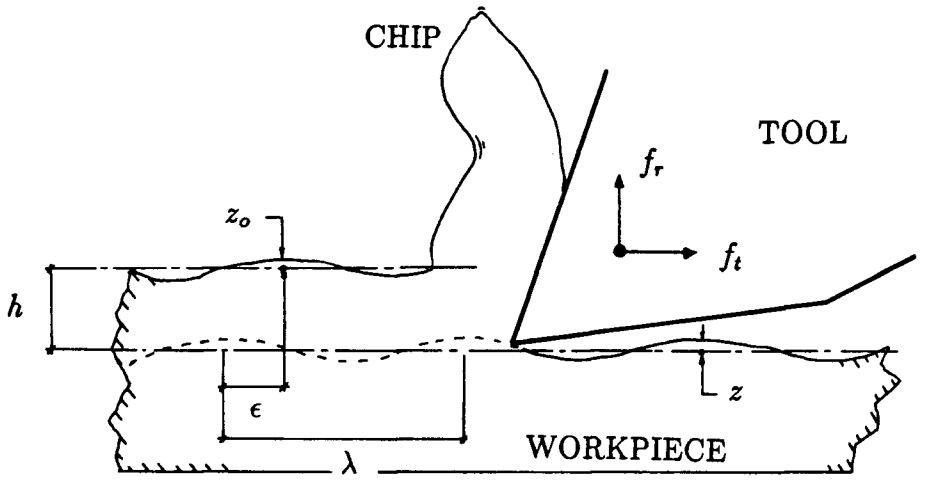

Figure 2.3: Dynamic cutting process geometry.

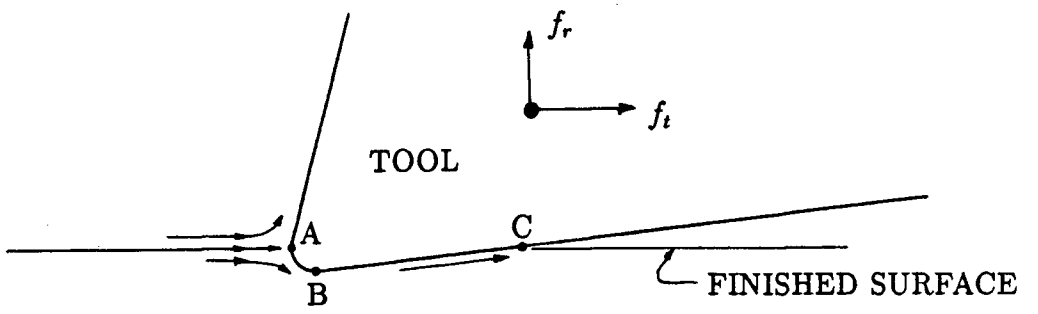

Figure 2.4: Cutting process detail.

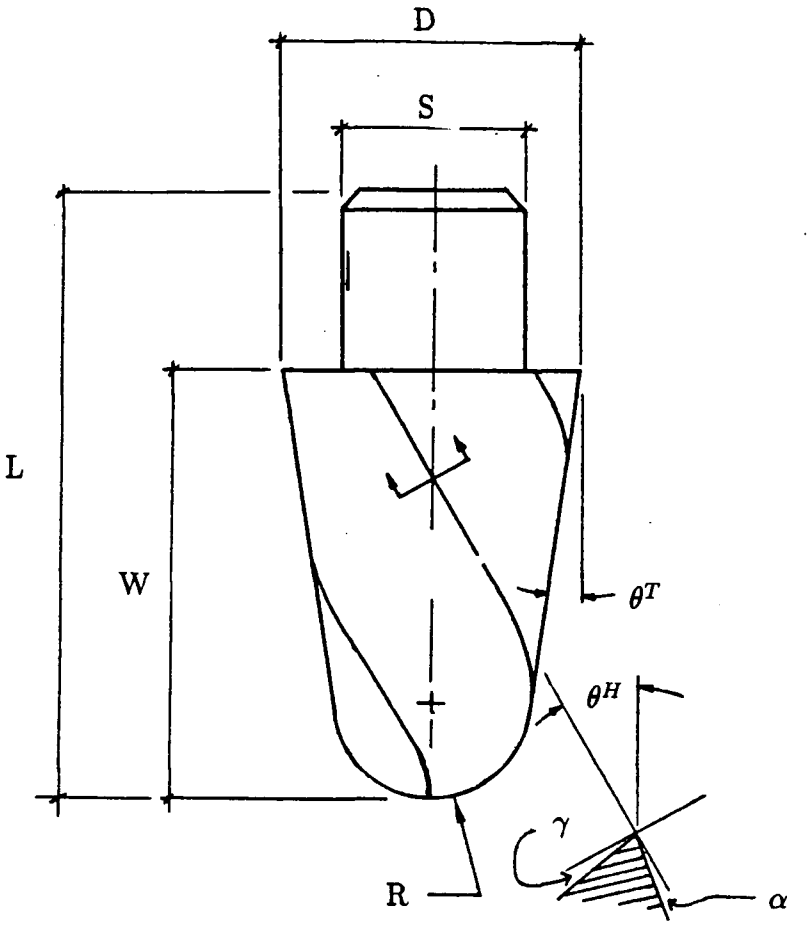

Figure 2.5: End mill geometry.

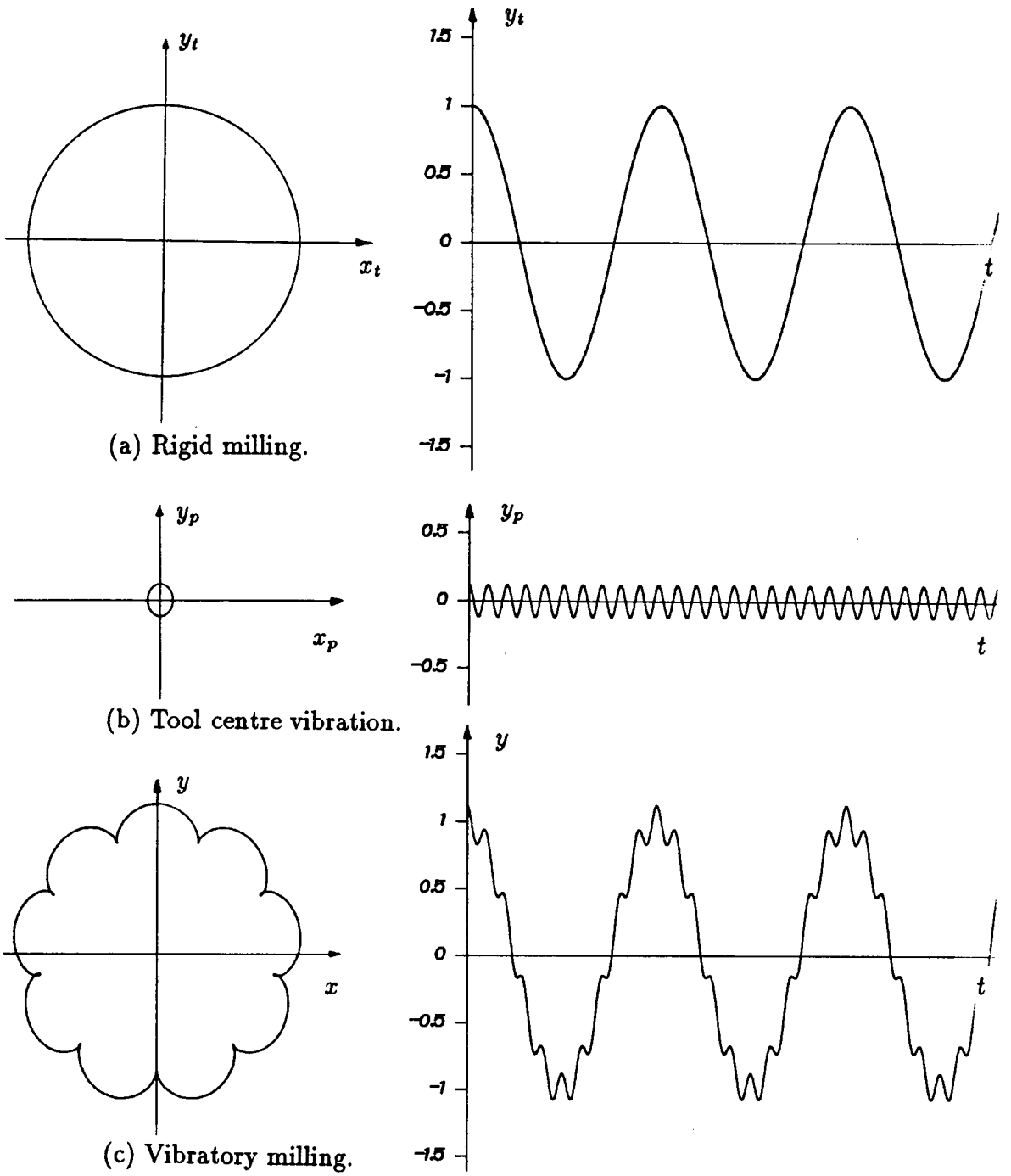

(a) Rigid milling.

(b) Tool centre vibration.

(c) Vibratory milling.

Figure 2.6: Vibratory motion of the milling process.

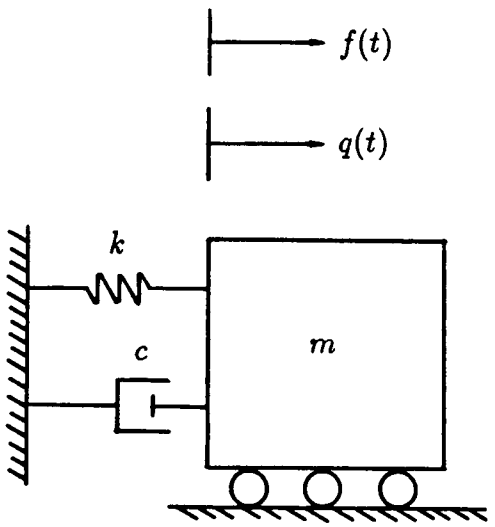

Figure 2.7: Single degree of freedom forced dynamical system.

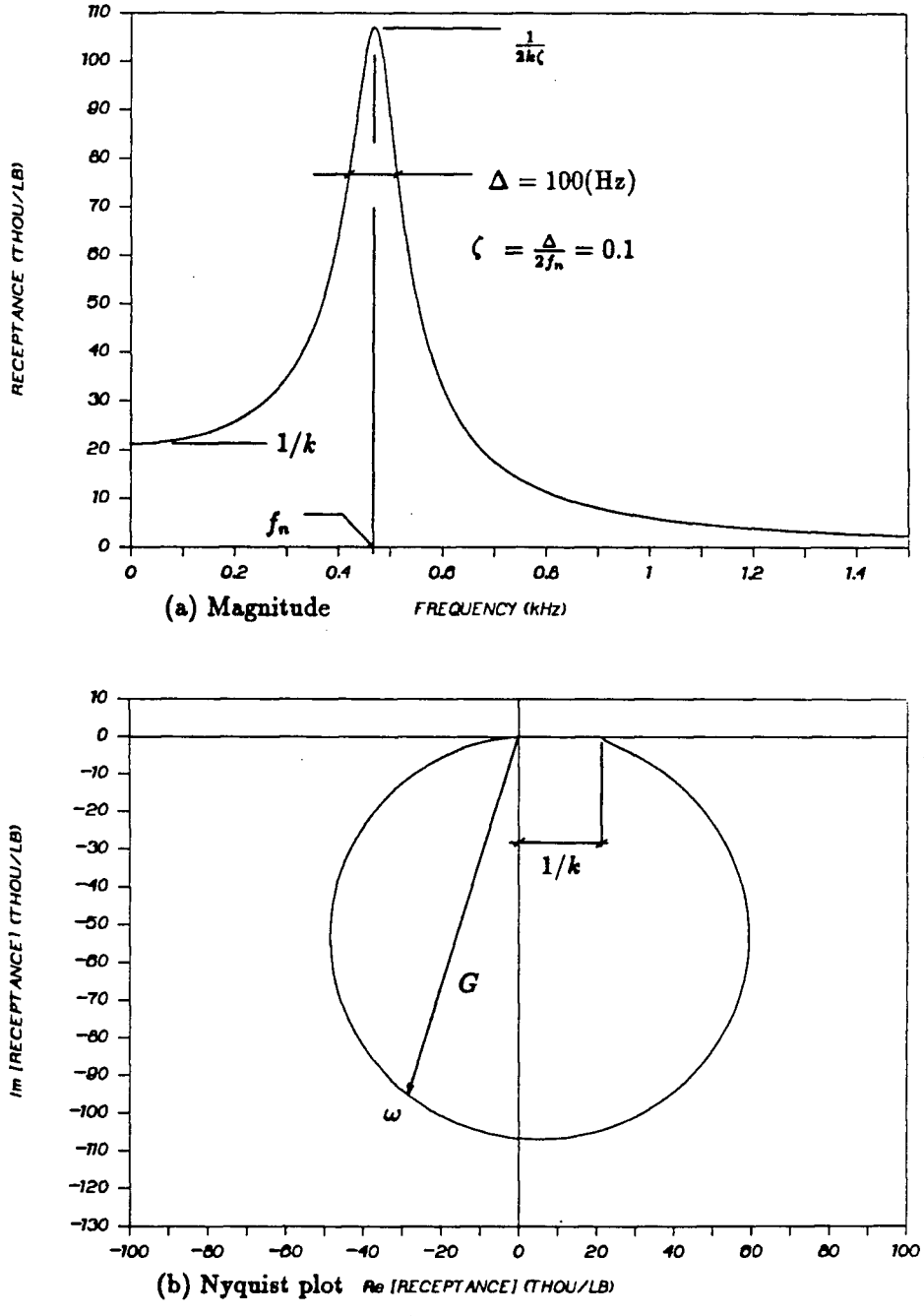

Figure 2.8: Frequency domain characteristic curves for a SDOF dynamic system.

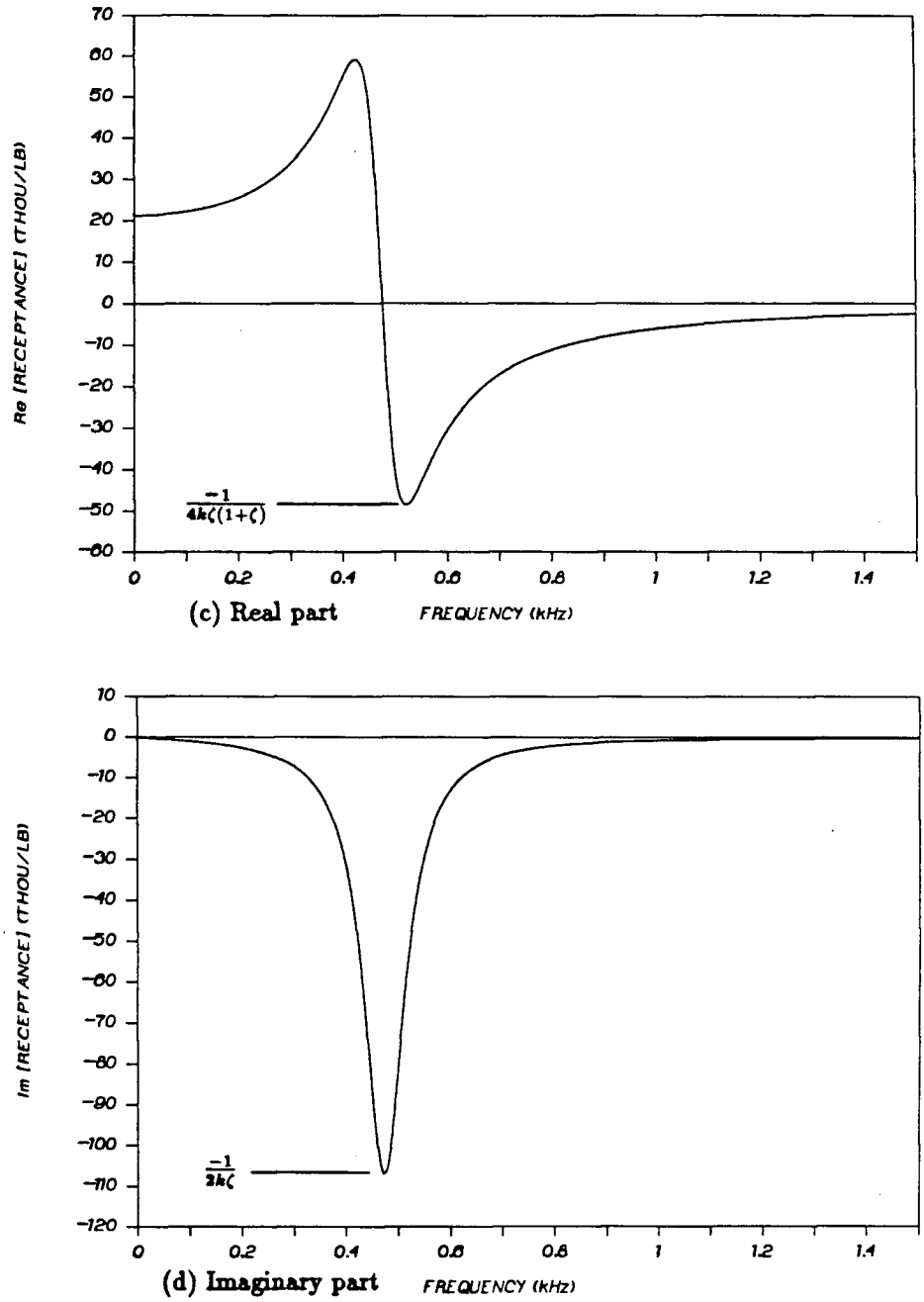

Figure 2.8: Frequency domain characteristic curves for a SDOF dynamic system.

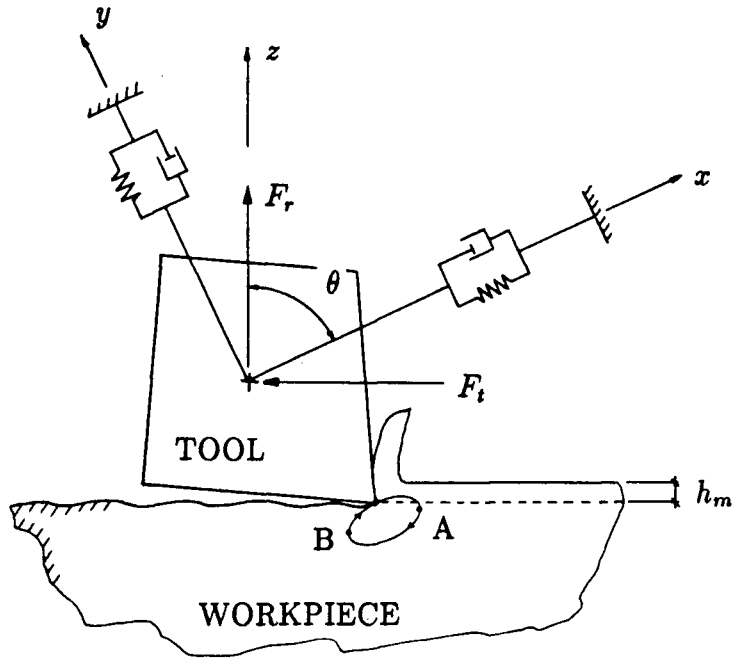

Figure 2.9: Mechanism of mode coupling.

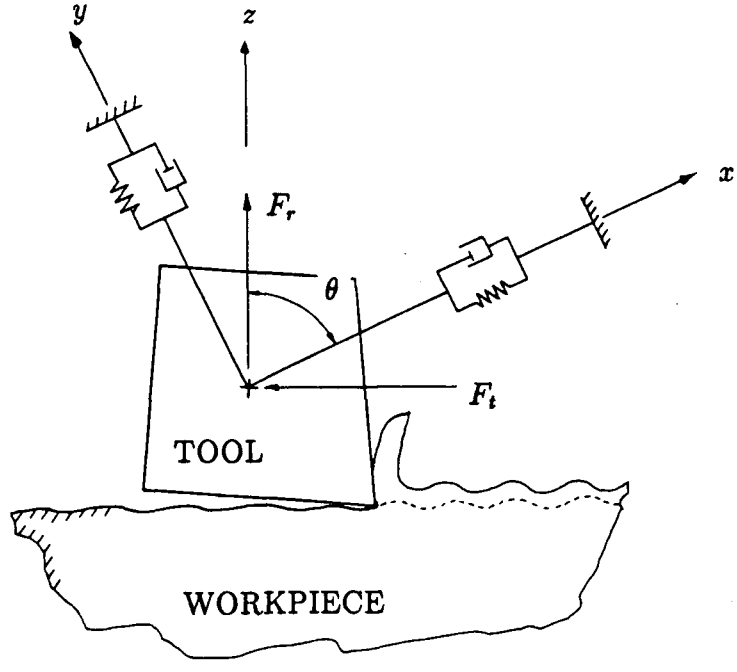

Figure 2.10: Mechanism of regeneration

Chapter 3

Mechanism of the Dynamic Milling Process

3.1 Introduction

The milling process is widely used in industry for the manufacturing of mechanical components. The process can be as simple as face milling the top of a flat surface with a rigid cutter, or very complex such as peripheral milling of flexible aircraft engine impellers on five axis CNC machining centers. Although the dynamics of milling has been addressed by several authors, the process is rather complex and more research is required for a thorough understanding of its physics.

Past research has been concentrated mostly in the mechanistic modelling of cutting forces. Martellotti [22], Tlusty et al. [43] and DeVor et al. [17,11] have contributed to the understanding of the geometry and mechanistic modelling of cutting forces. In these studies, the workpiece and tool system were assumed rigid, hence the influence of structural vibrations on cutting forces (called vibratory cutting here) were not considered. Early work in vibratory cutting was confined to orthogonal cutting where the directions of the cutting forces and the structural dynamics of the tool workpiece system were assumed constant. Tobias [45] and Tlusty [39] proposed stability theories which analytically predict chatter free cutting conditions when the cutting stiffness, cutting force direction and the transfer function of the tool-workpiece structure in the same direction are known. However, milling has a complex geometry with varying cutting force direction and cutting stiffness. Tlusty has contributed a significant amount of knowledge in

modelling the physics of dynamic cutting. Time domain simulations of a vibrating end mill were developed to illustrate chatter growth and the loss of contact between the tooth and the workpiece by Tlusty et al. [40] and by Sutherland [35,34]. Recently, Lin, Devor and Kapoor [20] presented results of experiments where chatter growth was avoided by varying the spindle speed.

This chapter presents a comprehensive simulation model of dynamic milling where the tool geometry and the vibrations of both workpiece and tool in any direction are included. The model has been developed primarily to analyze the stability of peripheral milling of very flexible workpieces, see Fig.3.1. However, the analysis is valid for milling with rigid tool-rigid workpiece, rigid workpiece-flexible tool, flexible workpiece-rigid tool or flexible workpiece-flexible tool systems. The model predicts the topology of finished workpiece surfaces, cutting forces in the feeding and normal directions and vibrations of both the tool and workpiece simultaneously. The cutting model developed differs from the previous approaches in several aspects as shown in the following sections.

In what follows, geometric modelling of the vibratory tool and workpiece system is given. Calculation of the dynamic uncut chip thickness for force calculation and finished surface prediction is presented. A material removal model, which separates the cutting zones into five distinct regions, is introduced in section 3.3. The model verification with simulation and experimental studies is given in section 3.4. The chapter is concluded by summarizing the contributions.

3.2 Models of the Vibrating Tool and Workpiece Geometries

Geometric models are developed to represent the tool and workpiece for a general milling process. These models are used to calculate cutting forces, represent the kinematics of motion and construct the finished workpiece geometry.

3.2.1 The Geometry of Tool Motion

A detailed drawing of one milling cutter tooth is shown in Fig. 3.2. The tool geometry is defined by the radius of each tooth (R), the rake angle (α; negative as shown), the clearance angle (γ; positive as shown) and the number of teeth on the cutter (Z). Tool center vibrations are defined as the position (x_c, y_c) and velocity ($\vec{v_c}$) of the tool centre relative to the stationary spindle axis. These vibrations are calculated from the structural dynamic model of the end mill. The spindle speed (Ω) is assumed to be constant and unaffected by the process. The instantaneous velocity of the cutting edge ($\vec{v_t}$) can be calculated as the vectorial sum of the velocity of the tool center ($\vec{v_c}$) and the cutting speed ($\vec{R\Omega}$). The following analysis refers to a single tooth of an end mill.

$$\vec{v_t} = \vec{v_c} + \vec{R\Omega} \tag{3.52}$$

The instantaneous position of the cutting edge can be calculated if the position of the tool center (x_c, y_c) and the angle of edge rotation (ψ) are known.

$$\left.\begin{aligned} x_t &= R\sin\psi + x_c \\ y_t &= R\cos\psi + y_c \end{aligned}\right\} \tag{3.53}$$

The effective angle of the clearance face with respect to the horizontal axis (ζ) may be calculated as:

$$\zeta = \gamma - \psi \tag{3.54}$$

All of the parameters of Eqs. 3.52, 3.53 and 3.54 are time varying, with the exception of (R) and (γ) which are constant. The calculated parameters accurately define the geometry and state of the tool cutting edge with respect to the spindle or coordinate center.

The inclusion of more complex cutting geometries, such as runout or taper and helix angles, is considered here. These complexities require consideration of the tool's axial variations. For this purpose the tool is divided into several equally spaced axial slices. The geometry of each flute is assumed to vary continuously in the axial direction.

Runout is assumed to be constant along the tool axis. This geometry is accounted for by simply adding a different constant value to the radius of each tooth on the cutting tool. This simplistic approach is only considered here for tools with zero helix angle. More complex models can be divised, if appropriate, for particular applications.

A helix angle can be included in the tool geometry by varying the starting angle of a flute as a function of its axial position. For a mill with helix angle (θ^H) the immersion angle is given by:

$$\psi^H = \psi + (z \tan \theta^H)/R \tag{3.55}$$

where (z) is the axial distance along the tool. This modified value of the initial rotation angle is used to calculate the instantaneous rotation angle for tools with nonzero helix angles.

A taper angle (θ^T) is included with the tool geometry by varying the tool radius as a function of its axial position. The modified tool radius (R^T) is given by:

$$R^T = R - z \tan \theta^T \tag{3.56}$$

This value is substituted into the previous equations for the tool radius (R) when a nonzero taper angle is used.

3.2.2 The Geometry of Workpiece Motion

The workpiece geometry is digitized by a number of points on the surface, and is stored as an array in Cartesian coordinates. The kinematics of the workpiece are independent of the tool motion. The centre of the coordinate system is selected as the stationary spindle center, see Fig.3.3. Each tooth generates a surface which is used in the force calculation for the next tooth to come along. The process is discretized in time, and the time increment (T) is selected at least 14 times smaller than the period of the highest vibration mode of the tool-workpiece system. A tooth generates a new point on the surface every time step when it is cutting. The surface array is stored as "$SURF(i,j,k)_{mT}$", where (mT) is the time at the m'th integration step. Dimension (i) indicates the tooth which has generated the surface and is of size (Z), where (Z) is the number of teeth. Dimension (j) indicates whether the value is for the (x) or (y) coordinate $(1 = x,\ 2 = y)$, and is of size 2. Dimension (k) indicates the discrete position of the point within the surface vector. The size of dimension $k = (\theta)/(\Omega T)$, where (θ) is the immersion angle of the cutter in the workpiece.

As an example; "$SURF(3,1,256)$" is the x-coordinate of the 256'th point on the surface generated by tooth number 3 (see Fig.3.3).

Initial conditions of $SURF(i,j,k)$ are set to represent the workpiece geometry. The points on the surface are equally spaced at angular positions with radii corresponding to the tool's nominal radius.

For each integration time step (T), three modifications are made to update the surface vector. First, the feeding motion of the workpiece is added to every point of the surface vector. In this work it is assumed that feeding occurs in the x-direction only. This is not a necessary assumption but is made here to reduce the complexity of the surface modelling procedure. Second, the dynamic motion of the workpiece is added to both the (x) and

(y) surface vectors at every point. The dynamic motion can be determined by calculating the structural response of the workpiece. The dynamic response of a cantilevered plate workpiece is discussed in Chapter 4. In this chapter it is assumed that the dynamic motion of the workpiece is known. Third, the cutting action of the tool is accounted for on the surface vector. If the tooth is cutting then the instantaneous location of the tool is used to update the surface. If the tool isn't cutting, due to excessive vibrations, the surface generated by the previous tooth is used to update the surface.

The coordinate of the surface in the feeding direction is updated by translating the surface a distance $(-f \cdot T + \Delta x)$, where (f) is the feeding velocity:

$$SURF(i,1,k)_{(m+1)T} = SURF(i,1,k)_{mT} - fT + \Delta x \tag{3.57}$$

The coordinate in the normal direction is updated as:

$$SURF(i,2,k)_{(m+1)T} = SURF(i,2,k)_{mT} + \Delta y \tag{3.58}$$

where (Δx) and (Δy) are changes in the surface which are calculated from the dynamic response of the workpiece.

The metal removal process is accounted for in two ways when a tooth is in the cutting zone. If the tooth is cutting then the surface is updated as:

$$\left.\begin{aligned} SURF(i,1,k) &= x_{t,i} \\ SURF(i,2,k) &= y_{t,i} \end{aligned}\right\} \tag{3.59}$$

If the tooth is out of cut, due to excessive vibration, the surface is updated as:

$$\left.\begin{aligned} SURF(i,1,k) &= SURF(i-1,1,k^*) \\ SURF(i,2,k) &= SURF(i-1,2,k^*) \end{aligned}\right\} \tag{3.60}$$

where (k^*) represents a point on the surface generated by the tooth $(i-1)$ at the angular position of the tooth (i). These three modifications to the surface vector completely define any possible motion of the workpiece.

3.3 Cutting Mechanics Model

In vibratory cutting, the tool having an elliptical motion, the cutting edge may travel in five distinct regions as shown in Fig.3.4. The cutting region is determined depending on the edge geometry (i.e. rake and clearance angles) and the relative motion between the tool and the workpiece. The tool rake (α) and clearance (γ) angles are shown in Fig.3.5. The velocity of a tooth relative to the workpiece $(\vec{v}_{t/p})$ is calculated as:

$$\vec{v}_{t/p} = \vec{v}_t - \vec{v}_p \tag{3.61}$$

where $(\vec{v}_t)$ is shown in Fig.3.5 and $(\vec{v}_p)$ is the absolute vibration velocity of the workpiece. The angular orientation of this relative velocity is given by (η):

$$\eta = \pi/2 - \arctan\left[(\vec{v}_{t/p})_y/(\vec{v}_{t/p})_x\right] \tag{3.62}$$

In order to orient this direction with the geometry of Fig.3.5, angle (β) $(0 \leq \beta < 2\pi)$ is defined as:

$$\beta = \eta - \psi \tag{3.63}$$

(β), (α) and (γ) are used to determine the current cutting region. Conditions which determine the cutting region are:

Region 1: $\pi/2 - \gamma < \beta \leq \pi + \alpha$

Region 2: $\pi + \alpha < \beta \leq 3\pi/2 - \gamma$

Region 3: $3\pi/2 < \beta$ *or* $\beta \leq \alpha$

Region 4: $\alpha < \beta \leq \pi/2 - \gamma$

Region 5: $3\pi/2 - \gamma < \beta \leq 3\pi/2$

Region 1: A previously verified cutting force model is used in this shearing zone. From [1], it is shown that the tangential cutting force (F_t) can be expressed as a function of the uncut chip thickness (h) and a flank component (h^*). The radial force (F_r) on the edge of the tool is proportional to the tangential cutting force component, see Fig.3.6.

$$\left.\begin{aligned} F_t &= K_s a(h + h^*) \\ F_r &= K_s a(r_1 h + r_2 h^*) \end{aligned}\right\} \tag{3.64}$$

(K_s), (h^*), (r_1) and (r_2) are experimentally determined cutting force constants for a cutter-workpiece pair. Full immersion fly cutting (single tooth) of 7075-T6 aluminum with a rigid end mill was used to determine the cutting model parameters. The tool used was a 50.8 *mm* diameter carbide tipped face mill. A single insert was used to eliminate runout effects. The axial depth of cut was 5.1 *mm* and the spindle speed was 128 *rpm*. Several feedrates were used to vary the mean uncut chip thickness. Cutting forces were measured with a Kistler 9275A dynamometer. The forces were recorded using a PC based data aquisition system with a Data Translation DT2801 board and internally developed software. The system was trigerred by a 64 slot external encoder mounted to the milling machine spindle.

The average force is defined as the mean value applied to the tool in a given direction during one tooth period. The average experimental cutting forces in the (x) and (y) directions, (F_{ax}) and (F_{ay}) respectively, are plotted against the feedrate in Fig.3.7. The results are linear except at very low feeds, and are fit to Eqns. 3.65 and 3.66 using linear regression.

$$F_{ax} = \zeta_{1x}c + \zeta_{2x} \tag{3.65}$$

$$F_{ay} = \zeta_{1y}c + \zeta_{2y} \tag{3.66}$$

(c) is the feed per tooth. Values obtained for the constants are:

$$\zeta_{1x} = 657$$

$$\zeta_{2x} = 103$$

$$\zeta_{1y} = 1500$$

$$\zeta_{2y} = 20$$

From [1] it is shown that the cutting parameters can be calculated as:

$$K_s = 4\zeta_{1y}/aZ$$

$$r_1 = 4\zeta_{1x}/K_s aZ$$

$$h^* = \pi\zeta_{2y}/4\zeta_{1y}$$

$$r_2 = \pi r_1 \zeta_{2x}/4h^*\zeta_{1x}$$

From the above results, for the experimental case considered here, the following values of the cutting parameters are obtained:

$$K_s = 1185(N/mm^2)$$

$$r_1 = 0.437$$

$$h^* = 0.0105(mm)$$

$$r_2 = 5.1$$

These parameters are used throughout this chapter.

Previous researchers have approximated the uncut chip thickness as:

$$h = c\sin(\psi)$$

where (c) is the feed per tooth and (ψ) is the instantaneous immersion angle. Although the approximation does not produce significant errors in general milling analyses, it does not represent the tool motion accurately enough for precision surface prediction under vibratory conditions. The chip thickness is calculated in discrete time from the instantaneous positions of the tool edge and the workpiece surface where the edge is in contact. The radial position (R_t) of the tooth is found from Eq. 3.53.

$$R_t = \sqrt{x_t^2 + y_t^2} \tag{3.67}$$

The surface coordinates of the workpiece in discrete time are given by:

$$\left.\begin{aligned} x_p &= SURF(i,1,k) \\ y_p &= SURF(i,2,k) \end{aligned}\right\} \tag{3.68}$$

The radial position of the workpiece (R_p) relative to the spindle center is,

$$R_p = \sqrt{x_p^2 + y_p^2} \tag{3.69}$$

The uncut chip thickness is measured as the distance between the outer surface of the workpiece and the edge-workpiece contact point,

$$h \approx R_t - R_p \tag{3.70}$$

Since the discretization error of the surface can be made very small by decreasing the integration time step, the approximation of Eq.3.70 can also be reduced to an insignificant level. Note that the cutting force is zero when there is no tool-workpiece contact (i.e. $F_t = F_r = 0 \leftarrow R_t \leq R_p$). Thus, the nonlinearity in chatter is taken into account [40]. The cutting forces contributed by each tooth in Region 1 are:

$$\left.\begin{aligned} F_{xi} &= F_{ti}\cos\psi_i + F_{ri}\sin\psi_i \\ F_{yi} &= -F_{ti}\sin\psi_i + F_{ri}\cos\psi_i \end{aligned}\right\} \tag{3.71}$$

Region 2: The tool edge looses its contact with the workpiece in this region, therefore the cutting forces are taken as zero.

Region 3: In this region the tool flank face tries to penetrate into the workpiece. Contact between the tool and workpiece is occuring on the flank face only. The clearance face may interfere with the workpiece when the flank is worn (i.e. creating zero clearance angle), or when vibratory cutting is present which is the case considered here. Due to the elliptical motion of the tool during chatter vibrations, the clearance face may rub into the workpiece material in regions 3 and 4. The possibility of motion in this region has been either neglected in previous metal cutting models, or approximated by dynamic cutting force coefficients [37]. A recent paper written by Wu [50] proposes a ploughing model which is based on a previous friction analysis done by Bailey [3] in machining.

A different ploughing model, from friction analysis [12], is used to estimate the forces here. The ploughing analysis is an approximation and requires further investigation. The geometry of motion is given in Fig.3.8, the tool travels from point 1 to point 2 in direction $(\vec{v}_{t/p})$. The material in area 1-2-3 is displaced by the tool flank face. The length of contact projected in direction $(\vec{v}_{t/p})$, when the tool is at point 2, is (l_1). The length of contact projected perpendicular to direction $(\vec{v}_{t/p})$, when the tool is at point 2, is (l_2). When the axial depth of cut is (a), the corresponding areas of contact are given by :

$$\left.\begin{aligned} A_1 &= l_1 a \\ A_2 &= l_2 a \end{aligned}\right\} \tag{3.72}$$

The coordinates of the edge at points 1 and 2 (Fig.3.8) are calculated from Eq. 3.53 as (x_{t1}, y_{t1}) and (x_{t2}, y_{t2}). The distances (l_1) and (l_2) are found from the geometry as:

$$\begin{aligned} R_m &= \sqrt{(y_{t2} - y_{t1})^2 + (x_{t2} - x_{t1})^2} \\ l_1 &= R_m \frac{cos\beta}{\sin\gamma} cos(\gamma - \beta) \\ l_2 &= R_m \frac{cos\beta}{\sin\gamma} sin(\gamma - \beta) \end{aligned}$$

From ploughing analysis [12] the shearing and normal forces, (F_s) and (F_n) respectively, are approximated as:

$$\left.\begin{aligned} F_s &= p_o A_1 \\ F_n &= p_o A_2 \end{aligned}\right\} \tag{3.73}$$

where (p_0) is the workpiece yield pressure. The cutting forces contributed by ploughing when the edge is in Region 3 are:

$$\left.\begin{aligned} F_{xi} &= -F_{si} sin\eta_i + F_{ni} cos\eta_i \\ F_{yi} &= -F_{si} cos\eta_i - F_{ni} sin\eta_i \end{aligned}\right\} \tag{3.74}$$

Region 4: The rake face and the flank face are both in contact with the workpiece here. The model of region 1 is used on the rake face. The model of region 3 is used on the flank face. The forces from both models are calculated and added vectorially to find the force on the tooth.

Region 5: The force model used in this region is ploughing. If no contact is present the forces are taken as zero.

The forces contributed by all teeth are summed at discrete time intervals to find the instantaneous cutting forces on the cutter and the workpiece.

$$\left.\begin{aligned} F_X &= \Sigma_{i=1}^{Z}(F_{xi}) \\ F_Y &= \Sigma_{i=1}^{Z}(F_{yi}) \end{aligned}\right\} \tag{3.75}$$

3.4 Cutting Model Verification

The proposed cutting model has been coded in FORTRAN for simulation. The input data to the program is the tool geometry, workpice dimensions, difference equations which represent the tool and workpiece dynamics, spindle speed, feeding velocity, axial depth of cut, immersion angles, cutting force constants (K_s, r_1, r_2, h^*), workpiece yield pressure and the duration in time of the simulation. The integration time interval is chosen to capture the highest vibration frequency. The program iterates through time calculating cutting forces and updating the finished surface geometry. Output from the simulation includes: cutting forces, workpiece and tool deflections and an (xy) profile of the cut surface. Since each tooth of the cutter is defined by its radial length from the spindle center, the radial run-outs on the teeth are automatically accounted for.

As a first test, milling with a rigid tool-rigid workpiece system has been considered. Since the exact motion of the cutter is modelled, the feed marks obtained from the

simulation are expected to match the analytical result presented by Martellotti [22] as:

$$h_f = \frac{c^2}{8[R + cZ/\pi]} \tag{3.76}$$

The surface finish obtained from cutting with a four tooth cutter is shown in Fig. 3.9. A feedmark wave amplitude of 0.0127mm was obtained from the simulation which is comparable to the 0.0116 mm value given by Eq. 3.76.

In order to further verify the model, two controlled cutting experiments have been carried out on an in house retrofitted vertical CNC milling machine. Full immersion cutting experiments were carried out using a rigid $50.8mm$ diameter double positive face milling cutter with one insert. The radial rake and the clearance angles of the tool are 5 and 3 degrees respectively. The workpiece material was $7075 - T6$ aluminum alloy with a yield pressure of $p_o = 500MPa$. The cutting constants were identified ($K_s = 1185N/mm^2, h^* = 0.0105mm, r_1 = 0.437, r_2 = 5.09$) from a series of cutting experiments as explained earlier. A spindle speed of 2.3 rev/s and a feeding velocity of $0.8125mm/s$ ($0.352mm/tooth$) were used. The axial depth of cut was $a = 5.08mm$. The workpiece was rigidly clamped onto a table dynamometer and the feeding (F_X) and normal (F_Y) cutting forces were sampled at $1ms$ intervals, see Fig.3.10. The four slotted spindle encoder signal is recorded to syncronise the simulation with the experiments.

The first milling experiment was carried out to test cutting with a rigid tool and rigid workpiece system. The simulation cutting forces are shown in Fig.3.11 and the corresponding experimentally measured forces are shown in Fig.3.12. A more detailed view of the cutting forces is given in Fig.3.13 for a single tooth period. The forces are in very close agreement. One difference is the high frequency component of the experimentally obtained forces which is due to the neglected tool-workpiece dynamics for this case. From these results it can be said that the uncut chip thickness calculation and the cutting force model of region 1 are satisfactory, and that the experimentally

determined cutting force parameters are also acceptable.

The second experiment was carried out under the same cutting conditions as the first one except that the $y-axis$ is vibrating. The vibration was produced by feeding a function generator's sinusoidal output signal to the dc servo motor amplifier of the $y-axis$ feed drive, see Fig.3.14. The bandwidth of the feed drive servo is about $65Hz$ and the table is vibrated at $18Hz$. The limitation of the equipment to impose higher frequency oscillations is unfortunate, since the experiment will not verify the model's capability of handling ploughing during high frequency dynamic cutting. However, the controlled workpiece vibration allows verification of the proposed kinematics of chip thickness variation, force generation and surface generation. If these mechanisms are verified the results obtained for machining with the presence of actual structural vibrations can be relied upon. The imposed vibration in the (y) direction corresponds to the following normal displacement of the workpiece which is used in Eqn.3.58 for tracking the finished surface.

$$y_p(t) = 0.109\sin(112.3t) \tag{3.77}$$

Vibratory cutting was experimented and simulated. The simulation cutting forces are shown in Fig.3.15 and the corresponding experimentally measured forces are shown in Fig.3.16. A more detailed view of the cutting forces for a single revolution is given in Fig.3.17. The milled surface was measured on a Talysurf instrumented with a PC based data acquisition system. A three dimensional view of the wavy finished surface segment is shown in Fig.3.18 (a) for $3mm$ wide and $2mm$ deep. The remaining part of the surface finish is similar. The (x), (y) and (z) axes represent the feeding direction, the surface normal and the axial direction respectively. Since the helix angle is zero, the vibratory surface has the same profile along the axial depth of cut or $z-$axis. A $1.8mm$ long $xy-$plane view of the simulated and experimentally measured workpiece surface is

shown in Fig.3.18 (b). The results indicate that the milling model accurately simulates both the cutting forces and the finished surface geometry.

The result obtained for the surface finish is rather interesting. The dominant marks left on the surface are of a frequency which is significantly smaller than that which would be expected by either of the cutting or vibration motions separately. This phenomena will be termed *washboarding* in this thesis. As shown in Fig.3.19 (a) for a rigid tool the path of a single tooth is circular. In (b) the $y - axis$ vibration of the workpiece and the y-coordinate of the cutting edge are shown. As was noted by Smith and Tlusty [33], the surface finish is being generated only when the tooth is at point A. This results in a flat surface finish (by simulation) when the rotational and vibrational frequencies are equal [33], or infact when they may be divided without any fractional remainder, with the vibration frequency being faster. In the case of Fig.3.19 , the frequencies don't divide evenly and the resultant surface generated in time is given in (c). The physical surface finish is shown in (d). The spindle (or tooth) period is $T_c = 0.433\,s$ and the period of workpiece vibration is $T_v = 0.0559\,s$. The workpiece is moving at a feedrate of $f = 0.813\,mm/s$. Since from Fig.3.18 the washboarding wavelength (λ) is $1.45mm$, the washboarding period is $T_{wb} = \lambda/vw = 1.78\,sec$ which is greater than both of (T_c) and (T_v). The ratio of process periods is $r = T_c/T_v = 7.75$. That is there are 7.75 vibration oscillations in a single tooth period. The aliasing period is $T_a = NT_c$ where:

$$\left.\begin{array}{rcll} N & = & [frac(r)]^{-1} & frac(r) \leq 0.5 \\ N & = & [1 - frac(r)]^{-1} & frac(r) > 0.5 \end{array}\right\} \tag{3.78}$$

where ($frac(r)$) is the fractional component of (r). In our case $N = 4.0$ and the aliasing period is $T_a = NT_c = 1.73\,sec$. This is in good agreement with the washboarding period obtained from the simulation.

Notice that if ($frac(r)$) is exactly zero then the aliasing perion will be infinite. This implies that if the rotational period is an integer multiple of the vibration period there

will be a theoretically smooth surface finish on the workpiece even though it is vibrating.

3.5 Conclusions

A comprehensive dynamic milling model, which gives accurate prediction of cutting forces and the finished surface of the workpiece, has been developed. The model considers the mechanics of cutting in the normal shearing and ploughing zones. The uncut chip thickness is found by accurate modelling of cutter and workpiece geometry and kinematics. Vibrations of both the workpiece and the milling cutter are incorporated.

The experimental and simulation results show that the model is able to simulate low frequency dynamic milling correctly. Surface generation in milling as a function of tooth passing and vibration frequencies is simulated, experimentally verified and analytically explained. The results should help in selecting spindle speeds to obtain a smoother surface finish when the dominant vibration frequencies are known.

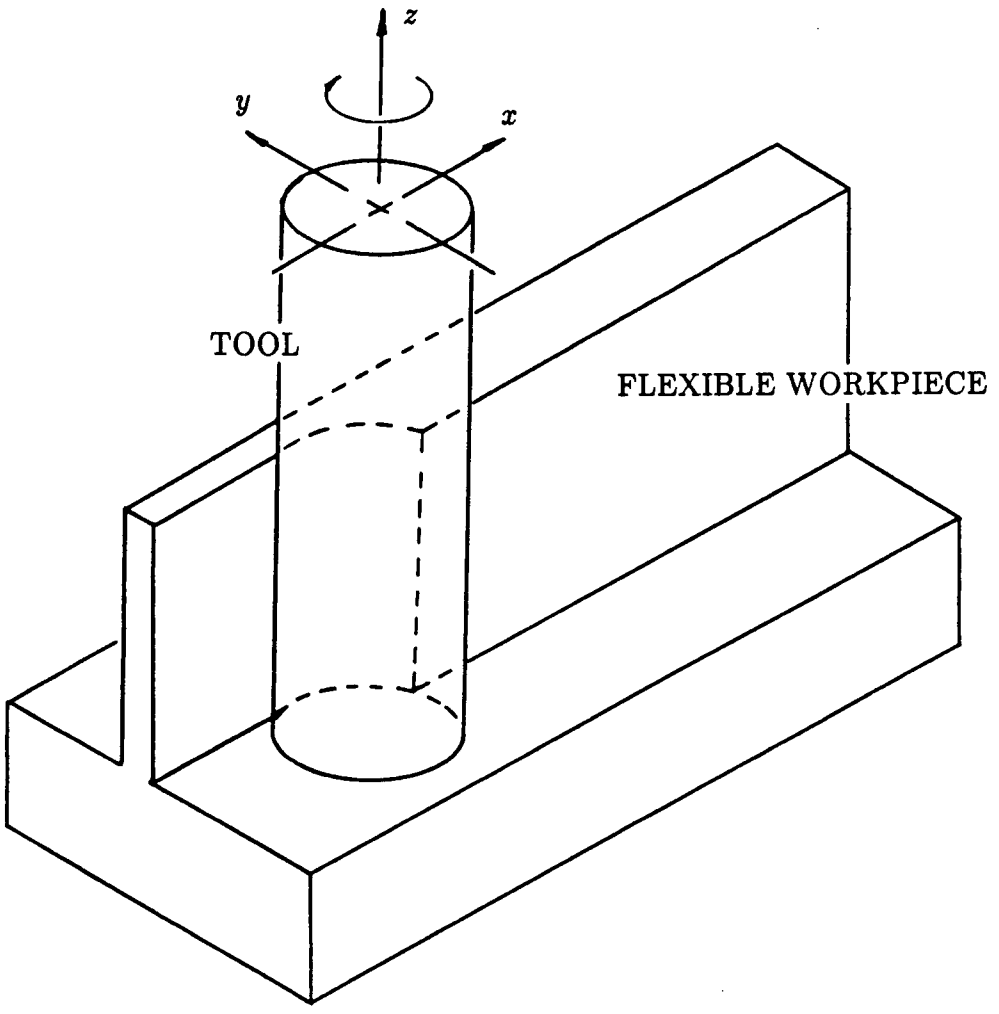

Figure 3.1: Peripheral milling of a flexible workpiece.

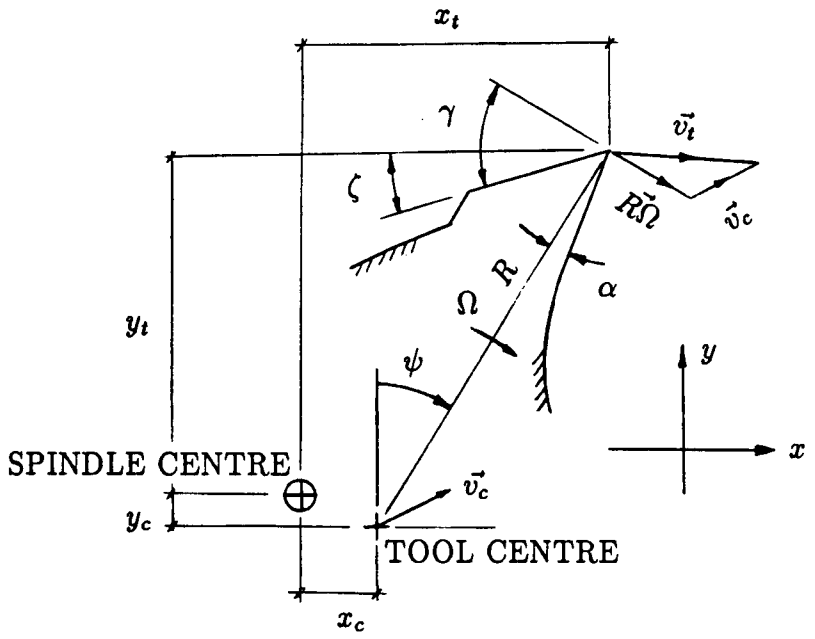

Figure 3.2: The geometry of tool motion.

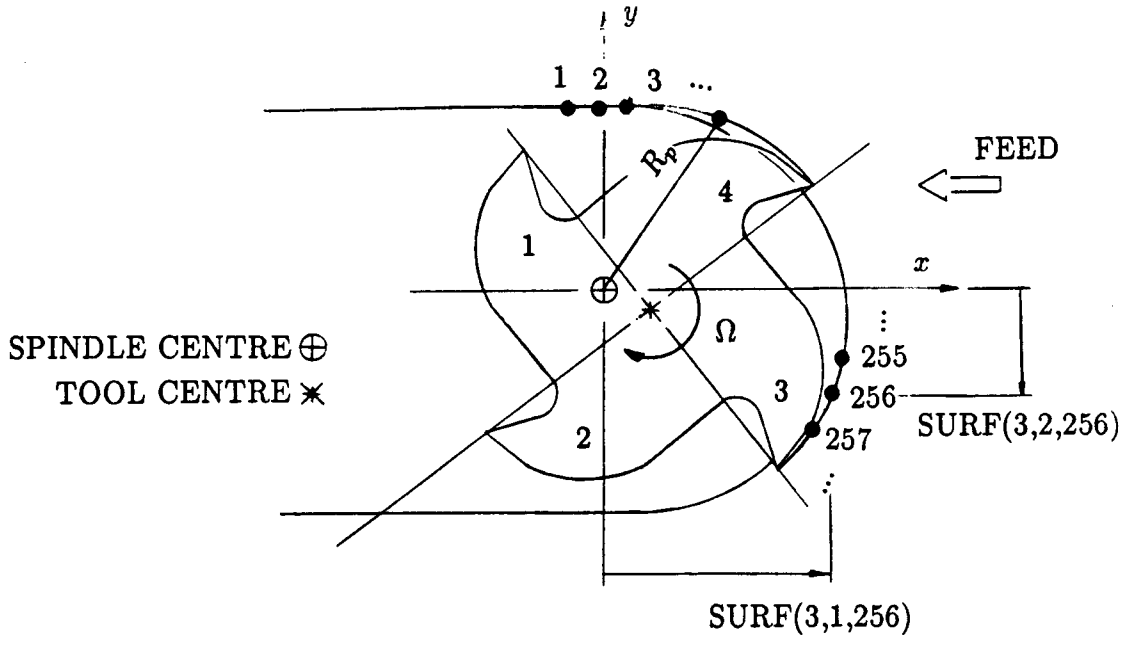

Figure 3.3: The geometry of workpiece motion.

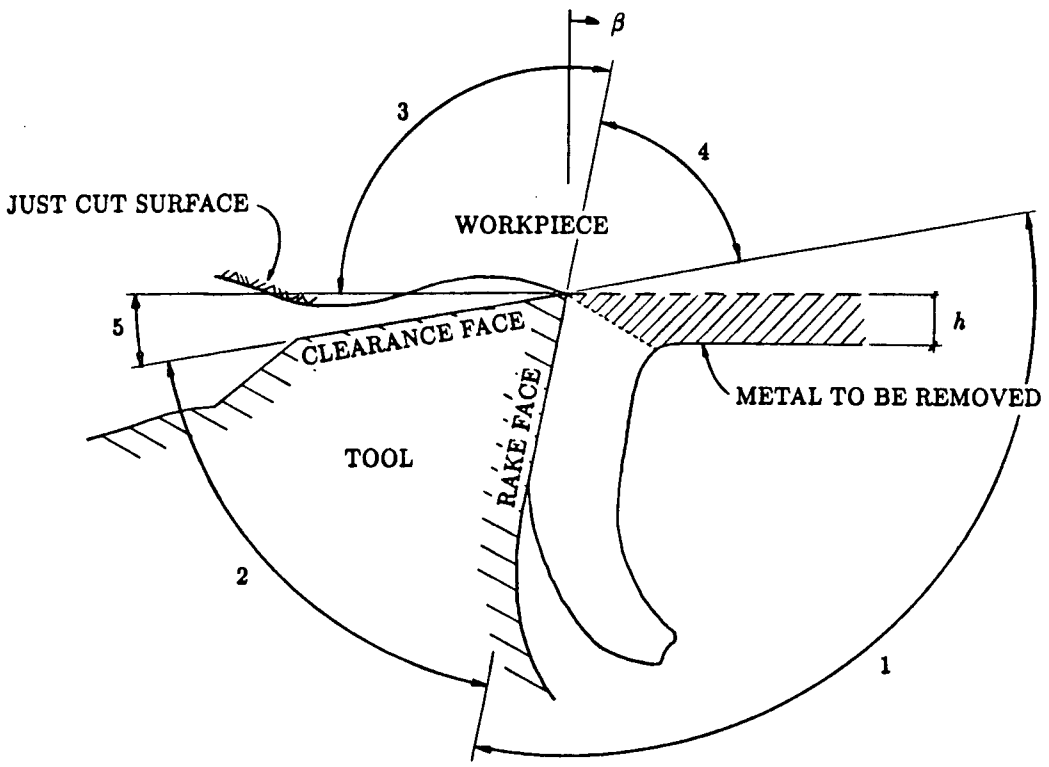

Figure 3.4: Five zone metal cutting model.

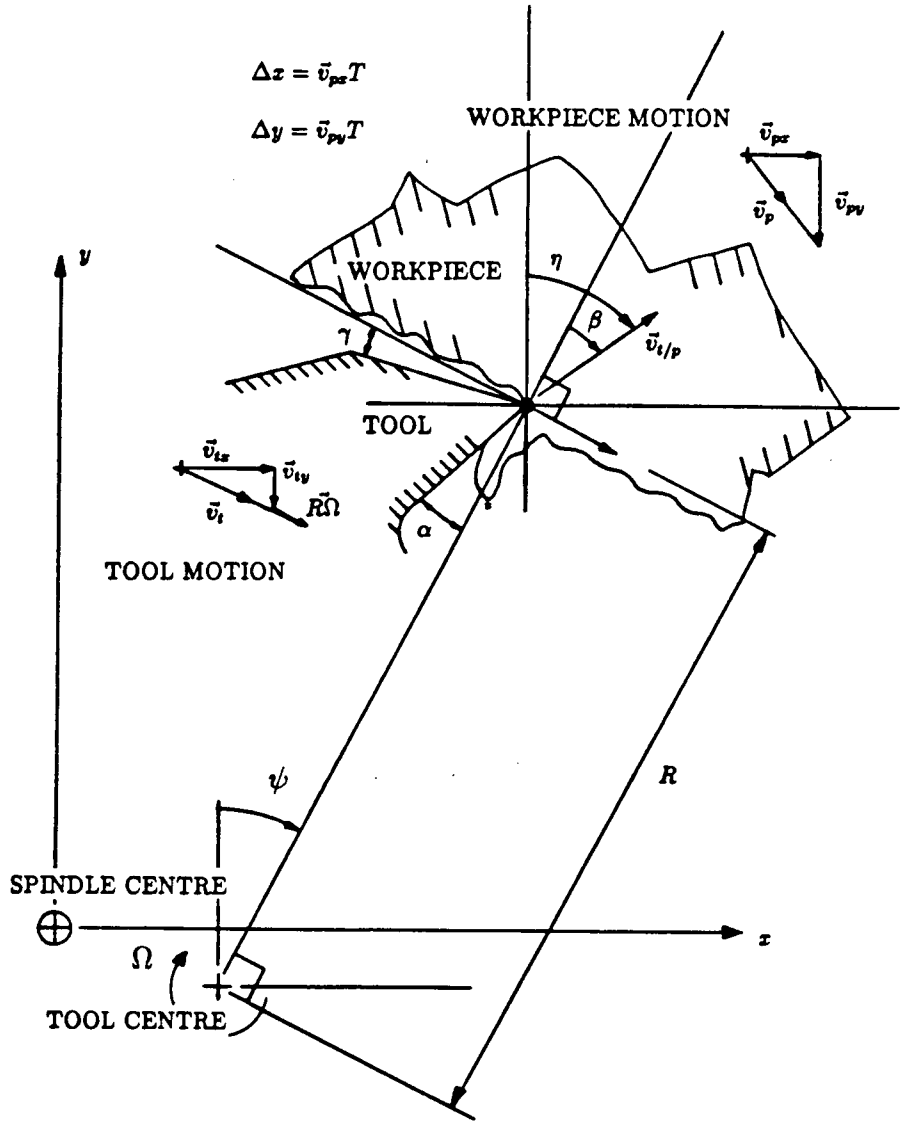

Figure 3.5: Geometry of the relative motion between the tool and the workpiece.

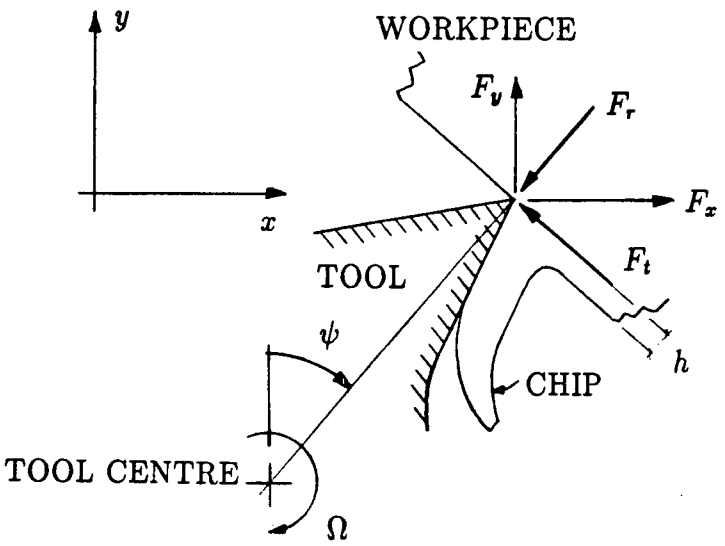

Figure 3.6: The geometry of shearing motion in region 1.

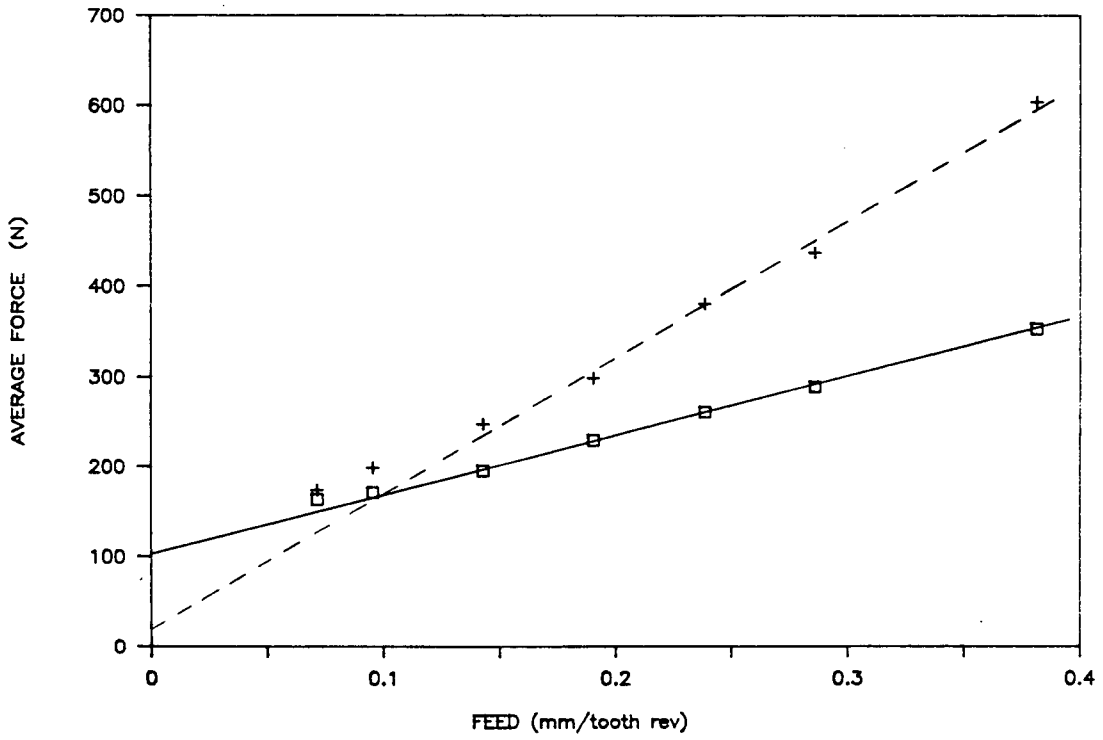

Figure 3.7: Average cutting force vs. feed per tooth in milling.

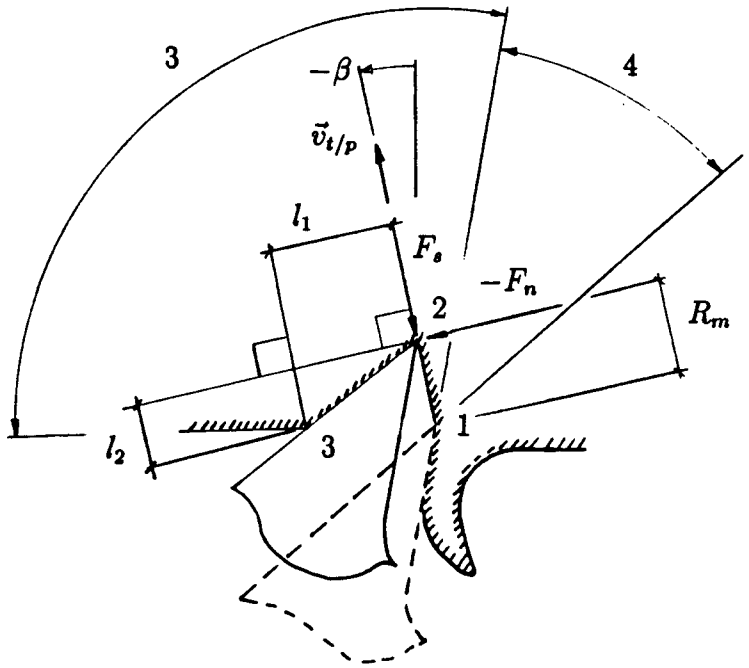

Figure 3.8: Geometry of ploughing motion.

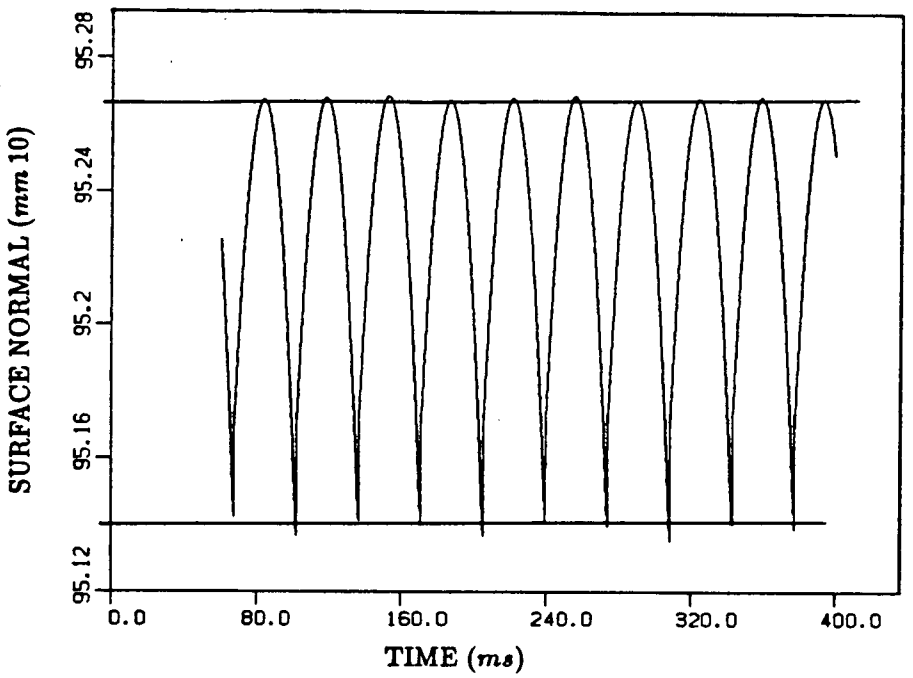

Figure 3.9: Simulation result for feed marks in milling with a rigid system.

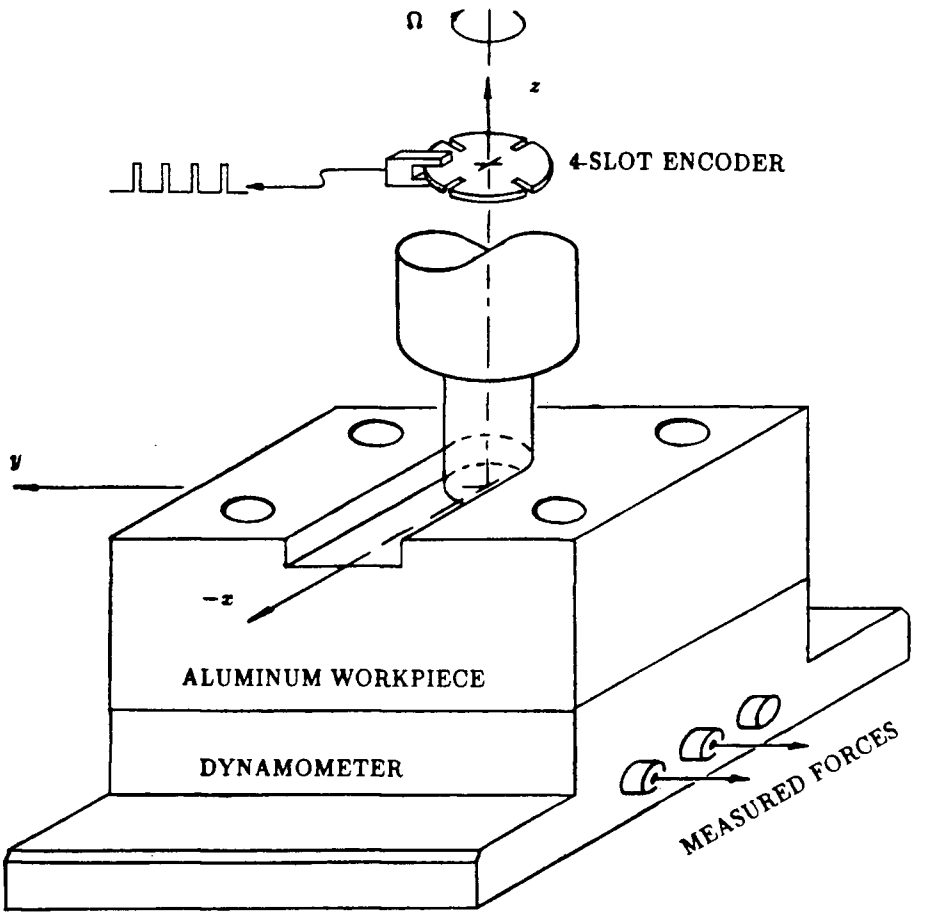

Figure 3.10: Experimental workpiece setup for milling force measurement.

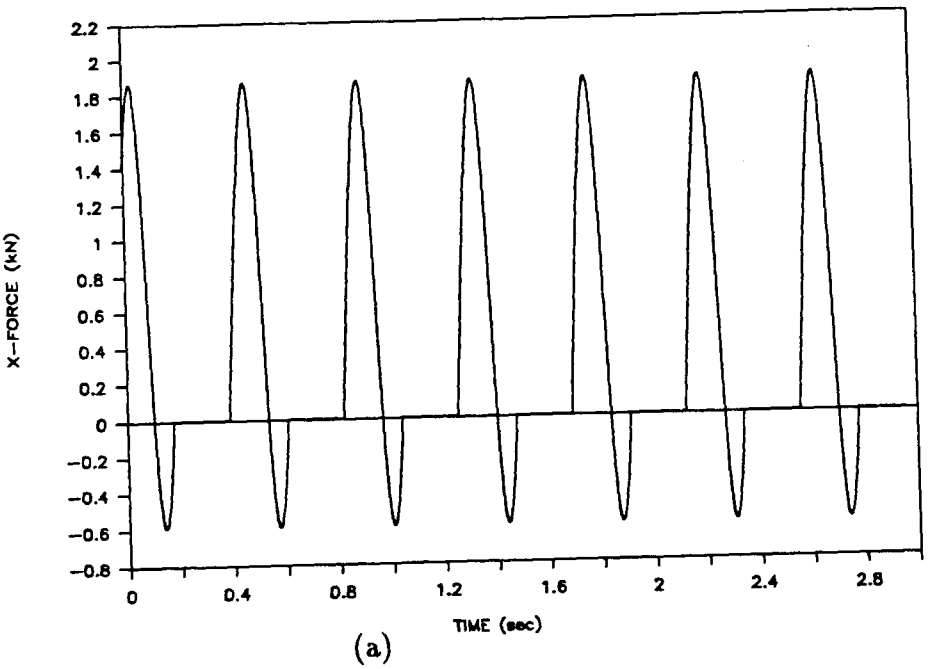

(a)

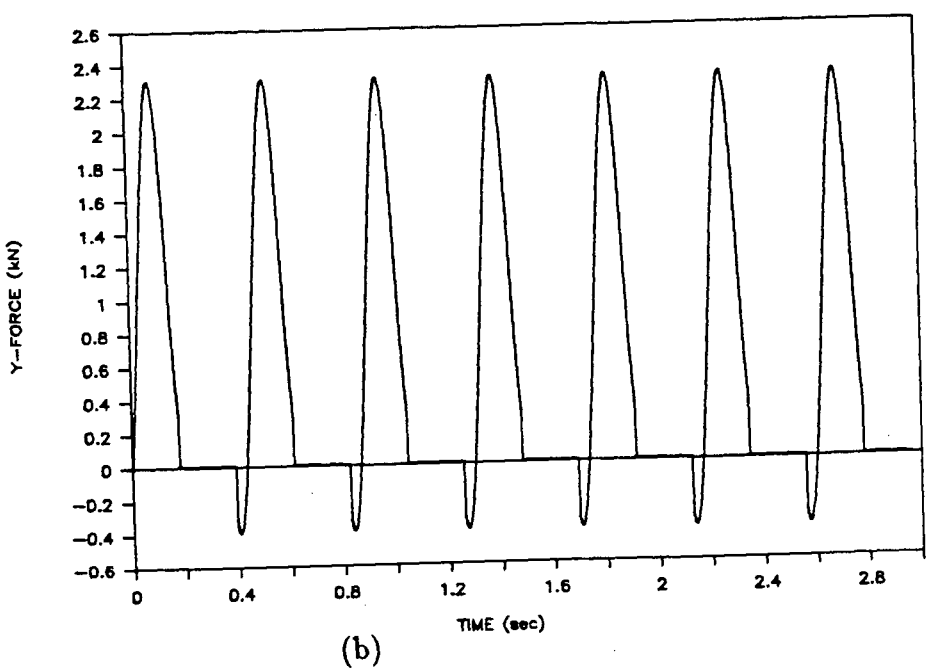

(b)

Figure 3.11: Simulation cutting forces for a rigid tool-workpiece system.

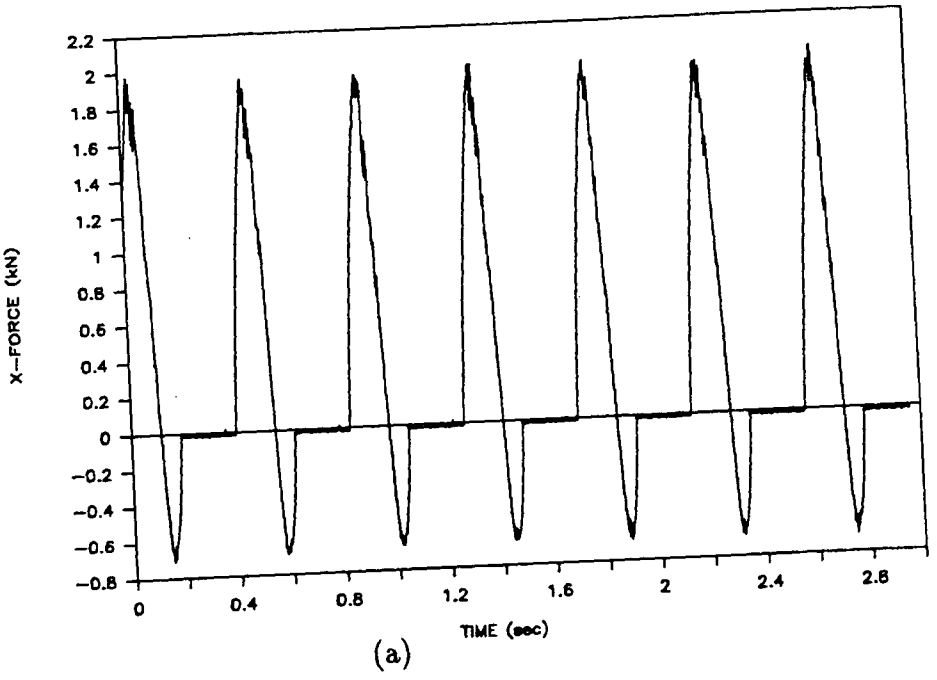

(a)

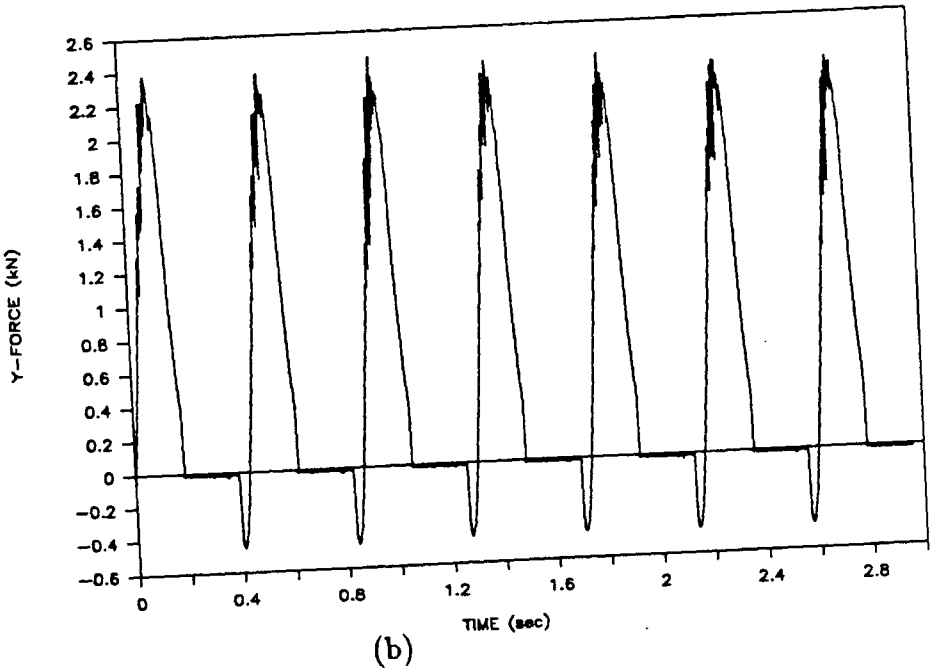

(b)

Figure 3.12: Experimental cutting forces for a rigid tool-workpiece system.

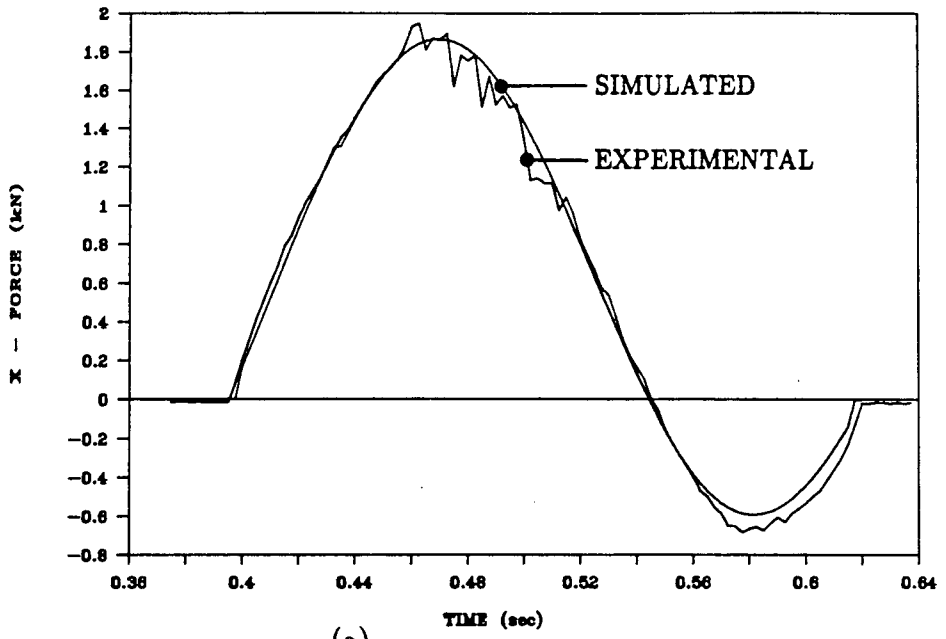

(a)

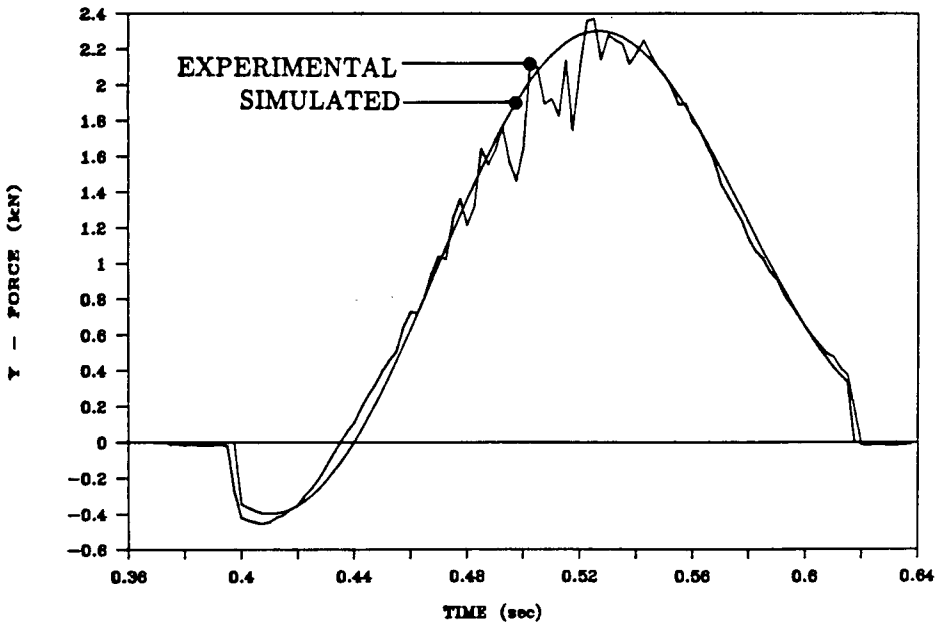

(b)

Figure 3.13: Detailed cutting forces for a rigid tool-workpiece system.

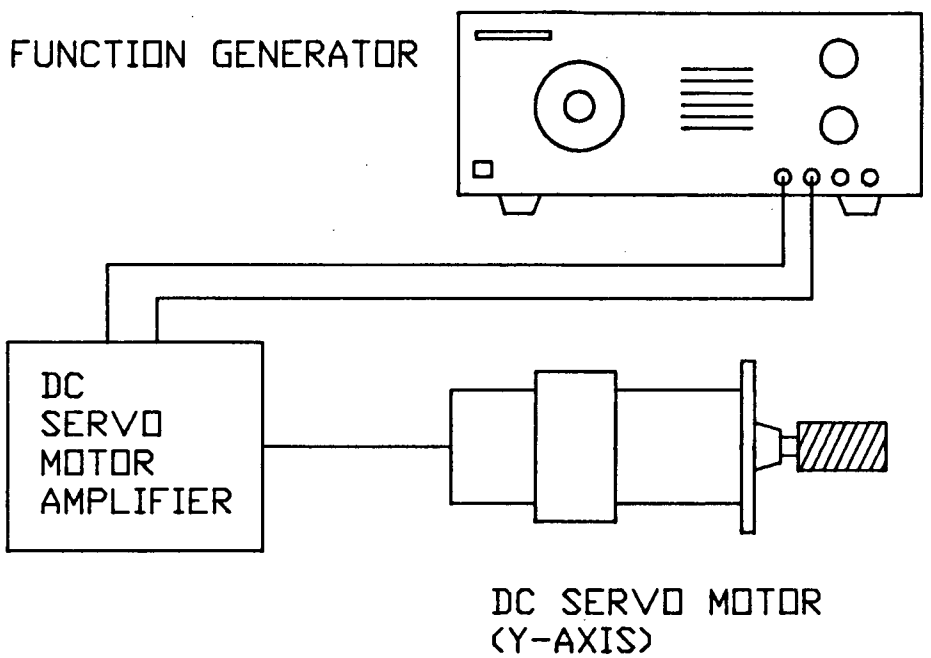

Figure 3.14: Experimental set-up for vibratory milling experiment.

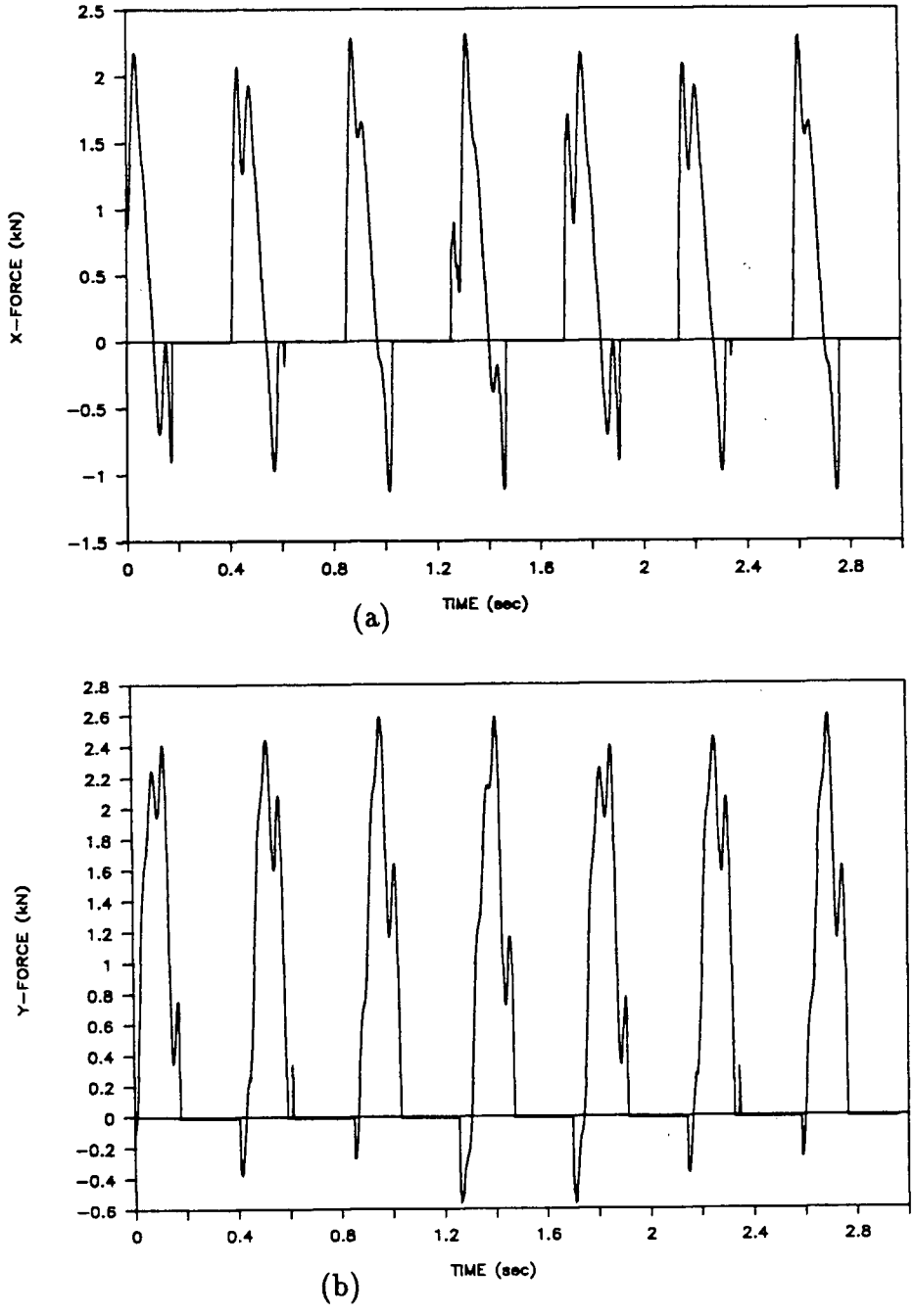

Figure 3.15: Simulation cutting forces for a vibrating tool-workpiece system.

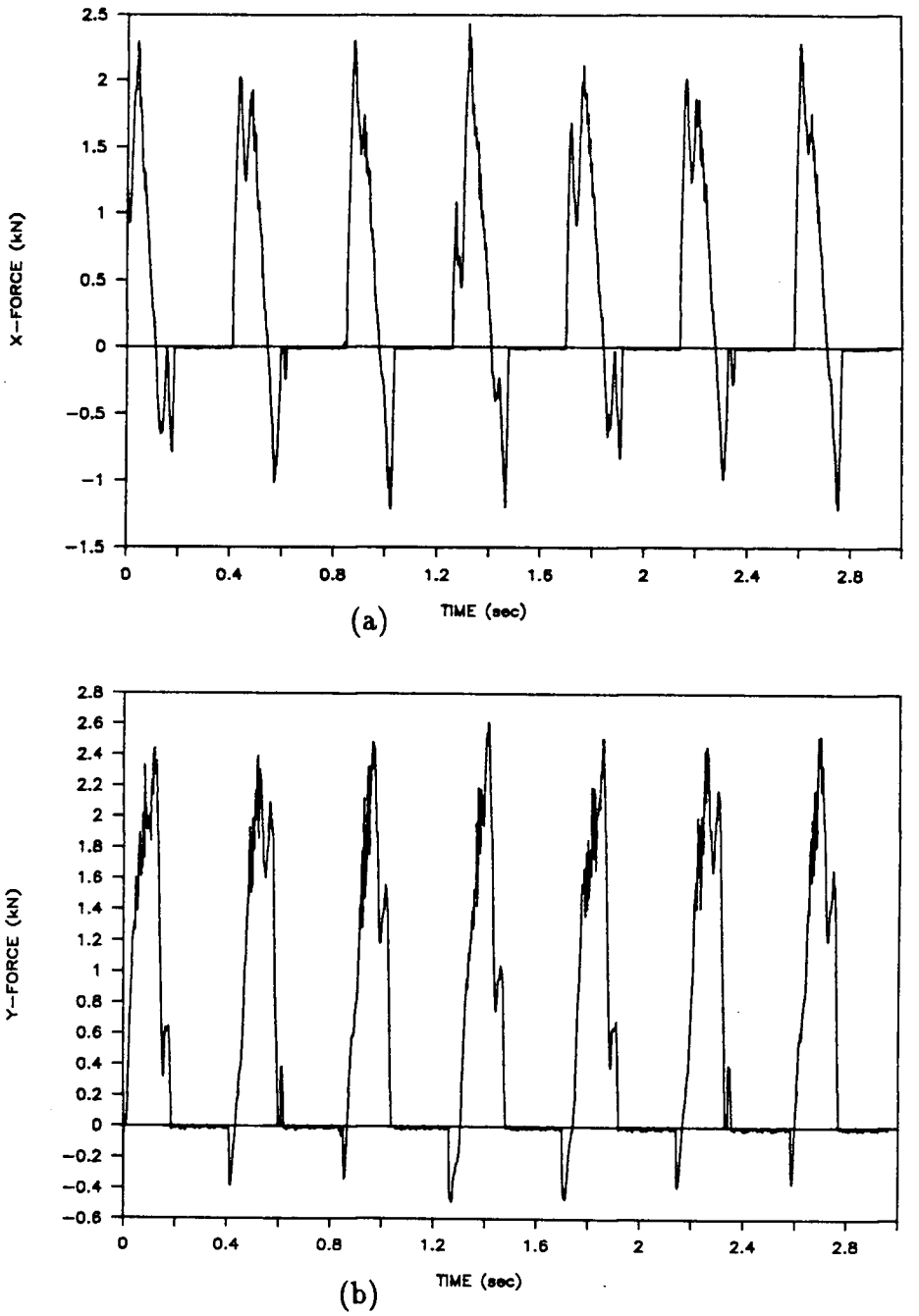

Figure 3.16: Measured cutting forces for a vibrating tool-workpiece system.

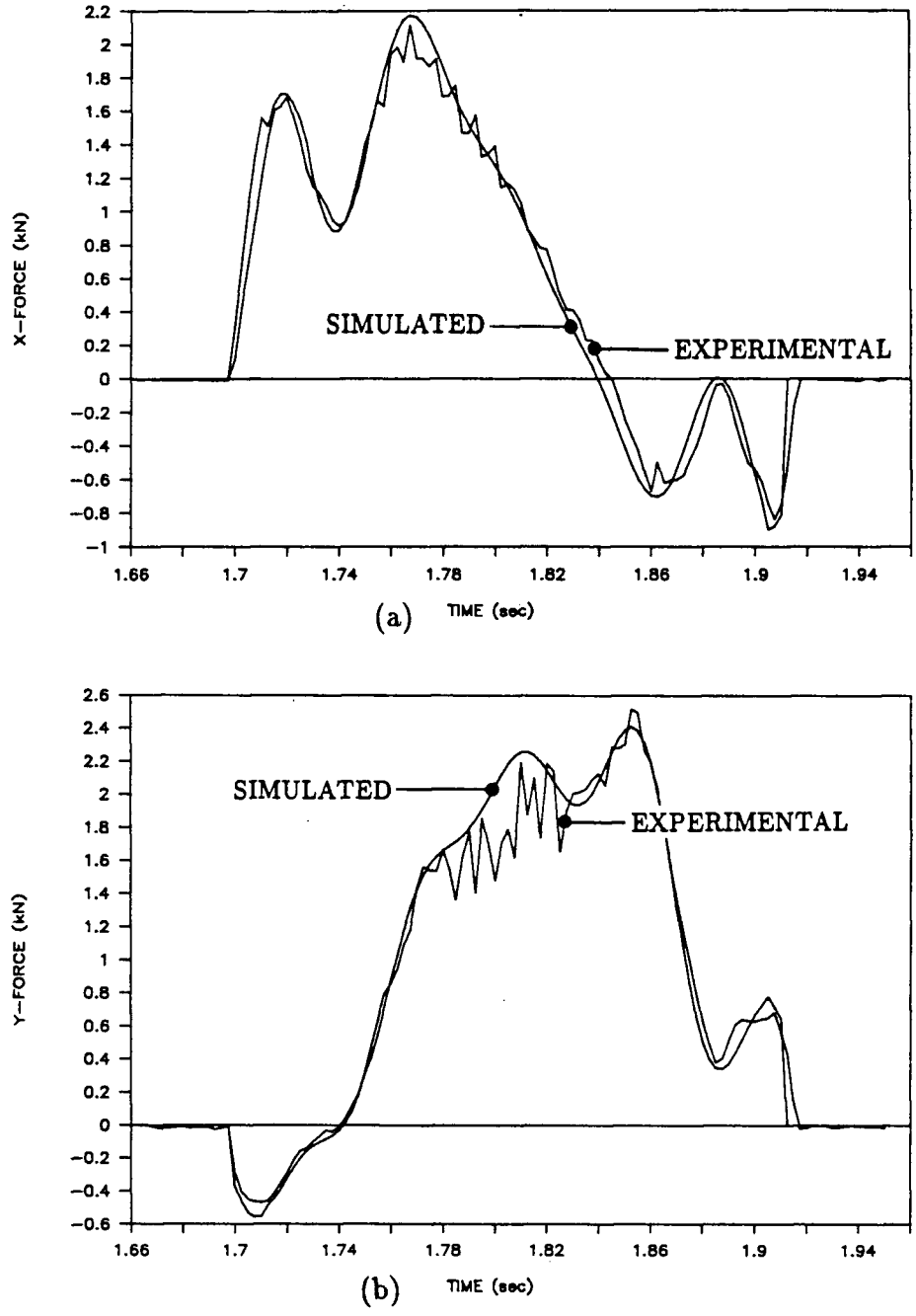

Figure 3.17: Detailed cutting forces for a vibrating tool-workpiece system.

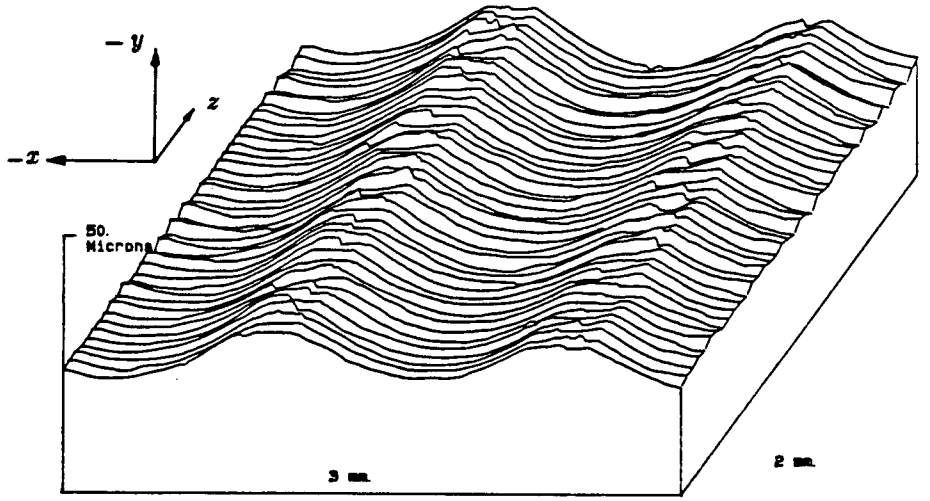

(a)

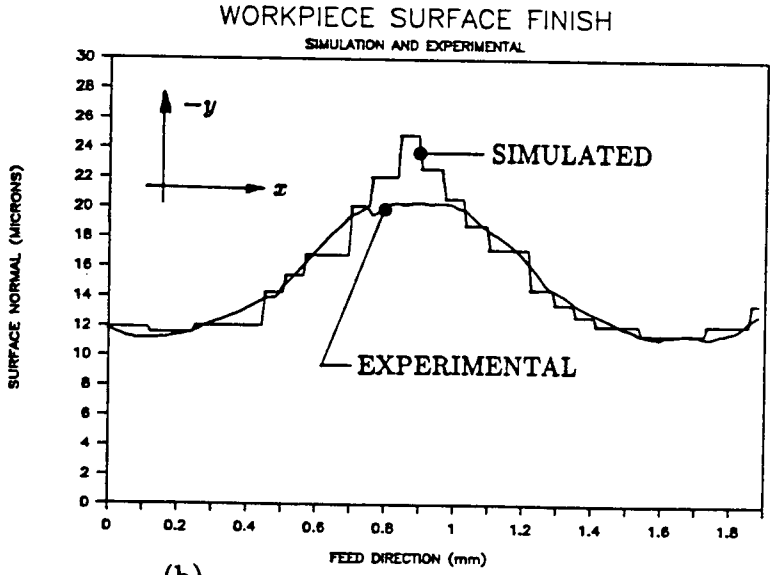

(b)

Figure 3.18: Microscopic surface finish machined during vibratory milling.

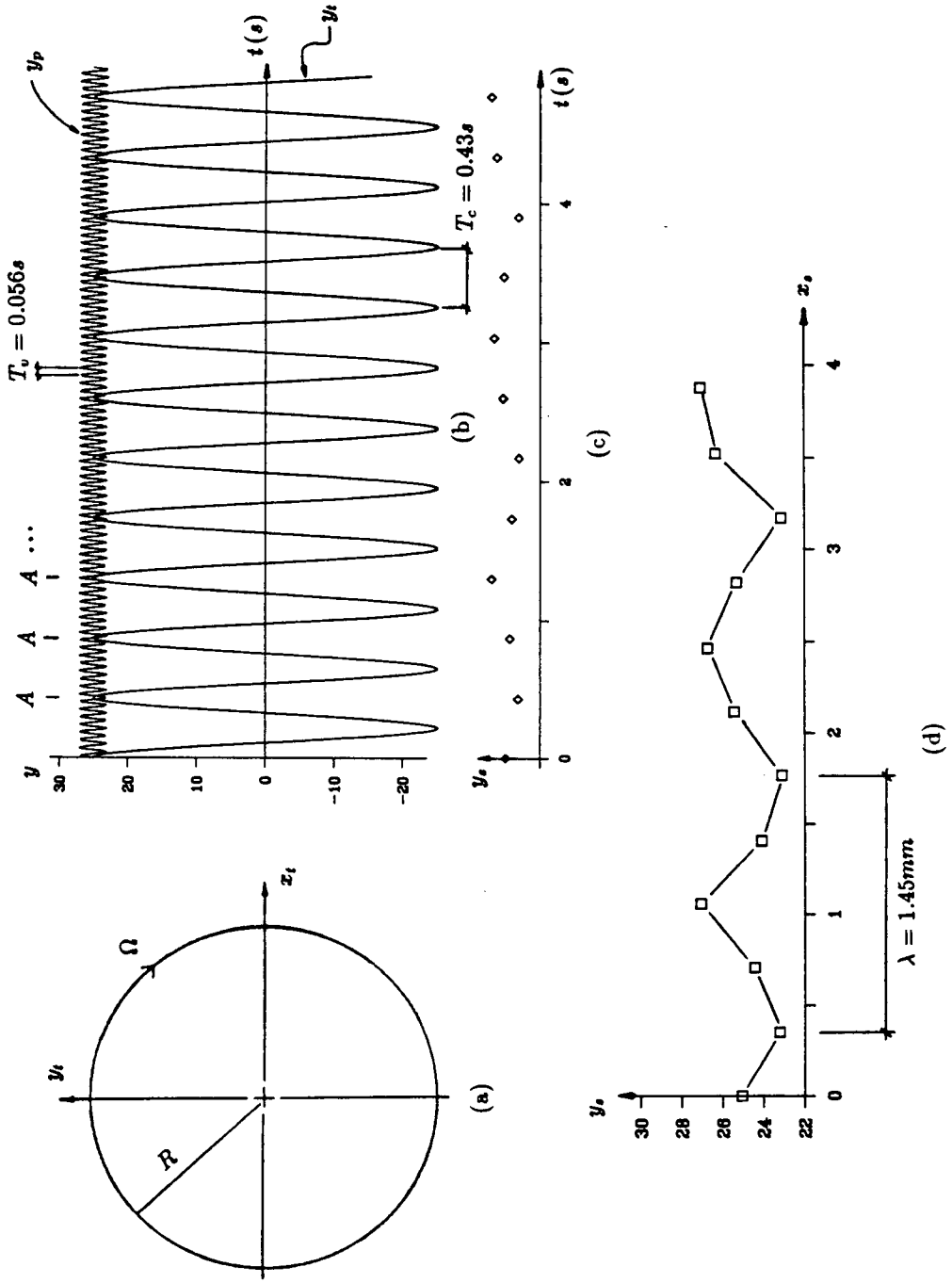

Figure 3.19: Illustration of surface finish generation in vibratory milling.

Chapter 4

Plate Dynamics

4.1 Introduction

The workpiece considered in this research is a square cantilevered-free-free- free (CFFF) plate as shown in Fig.4.1. The workpiece is referred to as a plate although it does not satisfy the formal definition of a plate due to its discontinuity in thickness. The material used is 7075-T6 aluminum with the following mechanical properties:

- E = elastic modulus = $70[kN/mm^2]$
- γ = density = $0.277(10)^{-8}[Ns^2/mm^4]$
- ν = Poisson's ratio = 0.33
- σ_o = yield strength = $490[MPa]$

The following discussion considers the physics of the plate from a structural dynamic perspective. The cutting tool and machine structure are assumed to be rigid as compared to the plate. The discontinuity in thickness of the plate requires that the structure be considered as a three dimensional object, at least in the region of the discontinuity. This discontinuity is a result of the metal removal process and indicates the position of the cutting tool. Factors in the dynamic analysis of the plate which are considered here are:

- loading conditions and response
- finite element modelling and reduction

- experimental modal analysis
- forced response of the plate

4.2 Loading Conditions and Response

The milling process generates metal removal forces in the cutting zone as shown in Fig.4.2. Forces may be applied to the plate anywhere in the cutting zone but not out of the cutting zone. Since chip removal, regeneration of waviness and surface finish generation are occurring in the cutting zone only, the response of the entire plate is not required to model the machining of such a workpiece. Only the dynamics of the plate in the cutting zone therefore are of interest in this analysis. The plate is considered first as a static structure and second as a dynamic structure.

From a static approach the plate flexibility is greatest in the out of plane direction. The following results are derived in Appendix A. Consider the constant thickness plate as loaded in Fig.4.3. Each load acts independently and results in some static deflection of the plate. The maximum deflection resulting from $F_x = 1$ (N) is calculated using beam bending theory as $3/E$ (m) in the (x) direction at the point of application. The maximum deflection resulting from $M = F_x(t/2) = .0013$ (Nm) is calculated as $77/E$ (m) in the (y) direction at the extreme edge of the plate (ie. away from the cutting zone). The maximum deflection resulting from $F_y = 1$ (N) calculated for a CCCF plate is $3600/E$ (m) in the (y) direction at the point of aplication. This result is conservative since a CCCF plate is much more rigid than a CFFF plate of equivalent dimensions. Clearly from these results the plate can be considered as rigid to in plane loads (in the static case) unless they are extremely large.

Approximate dynamic characteristics of the plate can be obtained by studying constant thickness cantilevered plates. The natural frequencies are determined using the

following equation [13]:

$$\omega_{ni} = K_i[\frac{Dg}{\gamma t l^4}]^{1/2}$$

where,

$$D = \frac{Et^3}{12(1-\nu^2)}$$

and (ν), (γ), (g) and (K_i) are Poisson's ratio, the weight density, the acceleration due to gravity ($g = 9.81\ m/s^2$) and a modal scaling factor respectively (K_i = 3.5, 8.5, 21, 27 and 31 for the first five modes).

The first five natural frequencies of a 2.5x2.5x0.05 (in.) (63.5x63.5x1.27 mm) CFFF 7075-T6 aluminum plate are: 135, 330, 828, 1069 and 1204 (Hz). The first five natural frequencies of a 2.5x2.5x0.1 (in.) (63.5x63.5x2.54 mm) CFFF 7075-T6 aluminum plate are: 540, 1319, 3313, 4275 and 4817 (Hz). The frequencies increase with the square of the plate thickness. The first five mode shapes are: first horizontal bending, first torsional, second horizontal bending, first vertical bending and the second torsional mode.

For a plate of variable thickness there is no simple relationship to obtain the modal characteristics of the structure. The overall mass and stiffness properties will vary depending on where the material has been removed. This will also vary for different modes of the system. Material removed from locations of large deflection will mostly decrease the mass, while material removed from locations of high strain will mostly decrease the stiffness. The dynamic characteristics of the plate will be considered more thoroughly in Sections 4.3 and 4.4.

Another consideration is that the plate dynamics will be varying continuously while the machining operation is taking place. That is, since metal is being removed from the plate its mass and stiffness must be changing. Since the material is being removed slowly

the dynamics should also be changing slowly. This factor is neglected in this work and only one location of the cutting zone is considered.

4.3 Finite Element Analysis of the Stepped Plate

A dynamic finite element (FE) model has been developed for the plate considered in Section 4.1, see Fig.4.1. The undeformed FE grid is shown in Fig.4.4. The software used to generate the model was the Vibration and Strength Analysis Program (VAST) [48] used by the Defence Research Establishment Atlantic in Canada. The plate was modelled using 20 node brick elements with three translational dof per node, see Fig.4.5. The total model size was 1594 dof. Material properties used in the analysis are the same as those given in Section 3.1 for 7075-T6 aluminum. The computations were carried out on a Vax 11/750 computer.

Output from VAST includes global mass and stiffness matrices with mode shapes and natural frequencies for the first five vibrational modes. The modal characteristics are shown graphically in Fig.4.6. The first five natural frequencies calculated for the stepped plate are: 476, 1058, 2499, 2933 and 3687 (Hz). These values predicted by VAST are within the theoretically expected range for flat plates calculated earlier, see Fig.4.7. In this figure VAST was used to generate the frequencies for the stepped plate, and the theory of Section 4.2 was used to determine the frequencies of the flat (50 and 100 THOU) plates. The mode shapes are also of the same type for each of the first five modes as those predicted for flat plates of similar dimensions.

The purpose of modelling the plate with the finite element method is to obtain an analytical solution for the response of the plate to forces acting in the cutting zone. Since the response is only required over a small percentage of the plates surface the FE model is reduced using the system equivalent reduction expansion process (SEREP) outlined in

the Literature Survey of this work. Using this process the 1594 dof FE model is reduced to a 27 dof SEREP model of the plate dynamics in the cutting zone, see Fig.4.8. The SEREP process extracts points from the FE model on the surface of the plate in the cutting zone. The reduced model is more suitable for forced response analyses such as machining of flexible structures.

Several computer programs are listed in Appendix B which are used in the model reduction process and to verify the model. Functions carried out by the computer programs include :

- Reading VAST mass, stiffness and eigensolution files and rewriting them into formatted files for further processing (Courtesy of James Yang).

- Perform SEREP reduction process on FEA files for specified dof. SEREP is outlined in Chapter 2 as Eqs.2.33 to 2.42. The algorithm is general and can be used with any specified dofs.

- Calculate the point receptance frequency response function (FRF) of the reduced dynamic model at a specified dof. This is accomplished by first reducing the 27 dof SEREP equation of motion (see Eq.4.79) to five modal equations of motion (see Eqs.4.80 to 4.84). The FRF is determined for each mode using Eq.2.27. Each of the modal FRF's are added to obtain the local FRF of the plate at any specified node. The eigenvectors must be normalized to the desired dof before this procedure is done.

- Calculate a forced response of the reduced dynamic model by numerical integration. This is accomplished by first reducing the 27 dof SEREP equation of motion (see Eq.4.79) to five modal equations of motion (see Eqs.4.80 to 4.84). The response of each modal equation of motion is calculated using Eq.2.25. Each of the modal

responses is transformed to the local coordinate system using Eq.4.85. The total response of the plate is determined by adding the individual modal responses in the local coordinates.

- Determine the frequency content of output data files using the Fast Fourier Transform method. This program uses a standard procedure [30].

The modal properties of the reduced dynamic model of the stepped plate are presented in Table 4.1. Using experimentally determined values for the viscous damping coefficient of each mode (see Section 4.4), receptance FRF plots for three points in the cutting zone are presented in Fig.4.9. The plots show that the first mode is dominant at the top of the plate while the contributions of other modes become more significant towards the cantilevered edge of the plate. Also the plate is much more rigid at its base than near its tip as expected. Detailed study of the mode shapes obtained directly from VAST has shown that in-plane values of the modes are small relative to the values in the y-direction. The appearance of antiresonances between resonance peaks is required and can be seen on the plots. The model of the plate seems reasonable and is expected to match well with experimental results.

4.4 Experimental Modal Testing of Stepped Plate

The purpose of this section is to experimentally determine some of the dynamic characteristics of the plate in order to verify the results of the finite element analysis and reduction process presented in the previous section. An impact hammer is used to excite the plate with the deflection being measured by a proximitor probe. The process consisted of impacting the plate several times with the hammer at several locations and recording the frequency response on a dual spectrum analyzer. The setup is shown in Fig.4.10. Equipment used in the experiments included: Bruel & Kjaer dual spectrum

analyzer, Nicolet oscilliscope, analog filters, Bruel & Kjaer charge amplifiers, impact hammer, PC based data aquisition system, Bentley Nevada proximitor and probe and the plate mounting bracket.

Several FRF data plots were recorded to give a good indication of the plate's dynamic characteristics in the cutting zone. The plots are presented as Fig.4.11 and are discussed here.

Plot a) is a direct receptance FRF measured at node 5 of the plate. Plot b) shows the low frequency detail of plot a). The static flexibility is taken directly from plot b) as 3 (THOU/LB) . Plot c) is the coherence of the measurements taken to produce plot b). The determined coherence value close to unity gives a high level of confidence in the measurements taken. The value of the coherence is very low near 60 (Hz) due to the line frequency of the instrumentation power supply. This phenomenon is seen on other graphs and should be recognized and neglected. Plot a) shows a clear resonance at 494 (Hz) with no other modes being easily detected. Several comparisons can be drawn between the measured and estimated (see Fig.4.9) FRF's. The static flexibilities are equal at 3 (THOU/LB). The magnitude of the 494 (Hz) resonant peak is also very close for both plots. The higher modes are not apparent on the measured FRF because the impact hammer cannot excite very high frequencies when used with such a flexible structure. Also the second mode is dominated by the mass of the first mode as seen on the theoretical plot and results in poor definition of the second mode on the experimental FRF.

Plot d) is a direct receptance FRF measured at point 14 on the plate. Two resonant frequencies were detected at 494 and 1056 (Hz) corresponding to the first bending and torsional modes respectively. Frequencies above 2000 (Hz) were not excited by the impact hammer and useful results could not be obtained in this range. The theoretical and measured static flexibilities are both 0.6 (THOU/LB). The magnitude of the first mode

is consistent between theory and experiment but the magnitude of the second mode is off by a factor of two. This is probably due to the the closeness of the excitation point to a nodal line of this mode.

Plot e) is a direct receptance FRF measured at point 23 on the plate. The first five vibrational modes are clearly seen at 487, 1056, 2495, 2915, and 3639 (Hz). These values correspond well with the theoretically predicted values using the finite element method (see Fig.4.6). The measured static flexibility is 0.04 (THOU/LB) and the predicted value is 0.004 (THOU/LB), so there is an order of magnitude discrepancy. This is probably due to two separate factors. First the location of the measurement is close to nodal lines for all of the modes and therefore the stiffness gradient is large so that experimental errors could become significant. Second the experimental setup consists of a clamping mechanism which may introduce some added flexibility to the plate which wouldn't have been noticeable away from the base of the plate. The peak amplitudes of each mode are consistent with the predicted values considering the experimental errors previously discussed. Other modes at higher frequencies may also be significant. These higher modes are not included in the analytical model and will be assumed to be unimportant for the remainder of this work. The expected antiresonances between modes are not present for most cases which probably indicates [10] "poor measurement quality because of inadequate vibration levels resulting in poor definition of the antiresonance regions."

Plots f) to j) are detailed direct receptance FRF's of each resonance taken at point 23 on the plate. These plots are used to estimate the viscous damping ratios used to generate the theoretical model of the plate whose FRF's are given in Fig.4.9. The half power (bandwith) method [8] is used to obtain the following modal damping ratios:

$$\zeta_1 = 0.001$$

$$\zeta_2 = 0.001$$

$$\zeta_3 = 0.001$$

$$\zeta_4 = 0.0003$$

$$\zeta_5 = 0.0004$$

Point 23 was chosen as the location for taking the measurements used to obtain the damping ratios because the impact hammer was able to excite all five modes there. Errors involved with estimation of the damping ratios include:

- noisy signals at higher modes resulting in difficulty finding the bandwidth at the half power points
- effect of nonliniearities (ie. mounting assembly)
- influence of other modes (this is probably small due to the relatively large distance between the modes)

Plots k), l) and m) are the magnitude, real and imaginary parts respectively of the FRF for the first vibrational mode taken at point 14. The damping ratio obtained from these plots is $\zeta_1 = 0.001$ which is equal to those obtained from the bandwidth method. This result gives further confidence in the damping ratios obtained for the other modes.

Time domain plots are also presented for the force and deflection of the plate during free vibration, see Fig.4.12. The plate vibration is measured at node 14. These graphs may be used to obtain an estimate of the effect of vibration on forces transmitted to the dynamometer during cutting experiments. The amplitude of the transmitted forces is 20 (N) and the vibration amplitude is 0.06 (mm). The equivalent stiffness of the plate from

Fig.4.12 c) is k_{eq} =310 (N/mm), and the vibration frequency of the plate is 488(Hz). The equivalent mass of the plate at node 14 is then $m_{eq} = k_{eq}/4\pi^2\omega_n^2 = 0.033$ (kg). The transmitted force measured here is large enough to significantly affect measured cutting forces if the vibration of the plate is large.

The experimental results presented in this section compare favourably with those obtained from the finite element modelling process. Several possible error sources have been indicated which could result in those discrepancies which have been encountered. Other sources of error are:

- The glue and steel reflectors mounted on the plate would affect the plate dynamic characteristics
- Geometric differences in the physical plate and the FE model
- Statistical variations in the level and location of the impact.

The effects of these factors are difficult to quantify and it will suffice here to simply note that they exist. The result of these experiments is that the reduced analytical model of the plate can be used without modification to simulate the plate dynamics in the peripheral milling of flexible structures.

4.5 Dynamic Solution of Reduced Plate Model

The plate dynamic response to a known disturbance is considered here. The reduced dynamic model results in a 27 dof equation of motion :

$$M\ddot{x} + C\dot{x} + Kx = F \tag{4.79}$$

where: $(M[27,27])$, $(C[27,27])$, $(K[27,27])$, $(F[27])$ and $(x[27])$ are the mass, damping, stiffness, applied force and displacement of the system in local coordinates. The

eigenvalues (λ_i) and eigenvectors ($\phi_i[27,1]$) of the reduced system are also known for the first five modes. Eq.4.79 is uncoupled using the modal analysis procedure where mode i is represented by:

$$m_i\ddot{x}_i + c_i\dot{x}_i + k_i x_i = f_i \tag{4.80}$$

where,

$$m_i = \phi_i^T M \phi_i \tag{4.81}$$

$$c_i = \phi_i^T C \phi_i \tag{4.82}$$

$$k_i = \phi_i^T K \phi_i \tag{4.83}$$

$$f_i = \phi_i^T F \tag{4.84}$$

$$x = \phi_i x_i \tag{4.85}$$

If the input force (F) is known then the modal forces ($f_i[1,1]$) can be calculated using Eq.4.84. ($m_i[1,1]$), ($c_i[1,1]$) and ($k_i[1,1]$) are the modal mass, damping and stiffness respectively and are constants. The modal responses ($x_i[1,1]$) can be determined using a discrete-time solution of a SDOF system (see Eq.2.25). The response of the plate in local coordinates, including the first n modes, is calculated as: $x = \sum_{i=1}^{n} \phi_i x_i$.

The response of the plate to a unit step input applied at node 23 is given in Fig.4.13. The damping factors used are those from the experimental modal testing of the previous section. The result is consistent with a multiple degree of freedom lightly damped dynamic structure.

The distribution of cutting forces on the grid points is an important factor in carrying out a forced response of the plate. Consider the simple grid shown in Fig.4.14. with forces applied as shown. In plane loads and applied moments are not considered here. Three rules are used to distribute the forces onto the grid:

1. The total force applied to the structure is equal to the sum of the forces applied to the individual nodes.

2. Forces are applied only to those nodes directly neighbouring the point of force application.

3. The fraction of an applied force which is distributed onto a particular node is inversely proportional to its distance from that node.

For the example of Fig.4.14 the following force distributions would apply:

$$FA \qquad F_1 = F_A$$

$$FB \qquad F_1 = (\frac{b - l_{y1}}{b})FB$$
$$F_4 = FB - F_1$$

$$FC \qquad F_1 = (\frac{a - l_{x1}}{a})(\frac{b - l_{y1}}{b})FC$$
$$F_2 = (\frac{a - l_{x2}}{a})(\frac{b - l_{y2}}{b})FC$$
$$F_3 = (\frac{a - l_{x3}}{a})(\frac{b - l_{y3}}{b})FC$$
$$F_4 = (\frac{a - l_{x4}}{a})(\frac{b - l_{y4}}{b})FC$$

$$FD \qquad F_3 = (\frac{a - l_{x4}}{a})FD$$
$$F_4 = FD - F_3$$

This example considers all possibilities which might be encountered in a more complex problem, and may be applied directly to in plane forces if required.

A general solution for calculating the force applied at node i is:

$$F_i = (\frac{a - l_{xi}}{a})(\frac{b - l_{yi}}{b})F \tag{4.86}$$

where: (F), (F_i), (a), (b), (l_{xi}) and (l_{yi}) are the applied force, nodal force due to (F), x-coordinate grid width, y-coordinate grid width, distance from node (i) to the applied force in the x-direction and the distance from node (i) to the applied force in the y-direction. Eq.4.86 is used for each applied force according to the three aforementioned rules.

4.6 Conclusions

In this section the dynamic characteristics of the stepped plate have been thoroughly investigated. Since the largest deflections are expected to occur at the top of the plate in the out of plane directions any in plane loads and moments can be safely neglected from the analysis. Use of the 27 dof SEREP reduced model of the plate has been successfully used to model the forced response and frequency response of the plate. This implies that the finite element model used can be modified to model the dynamics of the plate at other locations of the cutting zone in future studies. This same model will be used to simulate the plate response to cutting forces during the dynamic milling process in the following chapter.

	MODE No.				
	1	2	3	4	5
NODE #	MODE SHAPES				
1	0.89	0.15	-0.61	-0.27	-0.24
2	0.87	4.93E-02	-0.53	-0.28	-0.37
3	0.86	-4.33E-02	-0.45	-0.25	-0.47
4	0.74	0.17	-0.34	-0.25	-3.18E-02
5	0.72	8.17E-02	-0.29	-0.26	-0.10
6	0.71	-4.43E-03	-0.25	-0.23	-0.17
7	0.59	0.18	-7.68E-02	-0.26	0.12
8	0.57	9.97E-02	-7.38E-02	-0.25	0.10
9	0.56	2.34E-02	-5.83E-02	-0.22	8.75E-02
10	0.44	0.17	0.13	-0.26	0.21
11	0.43	0.10	0.10	-0.25	0.24
12	0.42	3.90E-02	9.00E-02	-0.21	0.26
13	0.30	0.14	0.24	-0.24	0.23
14	0.30	9.25E-02	0.19	-0.22	0.29
15	0.29	4.32E-02	0.16	-0.19	0.32
16	0.18	0.10	0.24	-0.19	0.18
17	0.17	7.04E-02	0.19	-0.17	0.24
18	0.17	3.71E-02	0.16	-0.14	0.28
19	8.31E-02	5.97E-02	0.15	-0.11	0.10
20	8.35E-02	4.16E-02	0.12	-0.10	0.14
21	8.36E-02	2.39E-02	0.10	-8.67E-02	0.17
22	2.00E-02	1.80E-02	4.79E-02	-3.61E-02	2.79E-02
23	2.08E-02	1.34E-02	4.02E-02	-3.23E-02	4.24E-02
24	2.16E-02	8.30E-03	3.45E-02	-2.75E-02	5.41E-02
25	0.00	0.00	0.00	0.00	0.00
26	0.00	0.00	0.00	0.00	0.00
27	0.00	0.00	0.00	0.00	0.00
	FREQUENCIES (Hz)				
	476	1058	2499	2933	3687

Table 4.1: Modal Data for the Stepped Plate

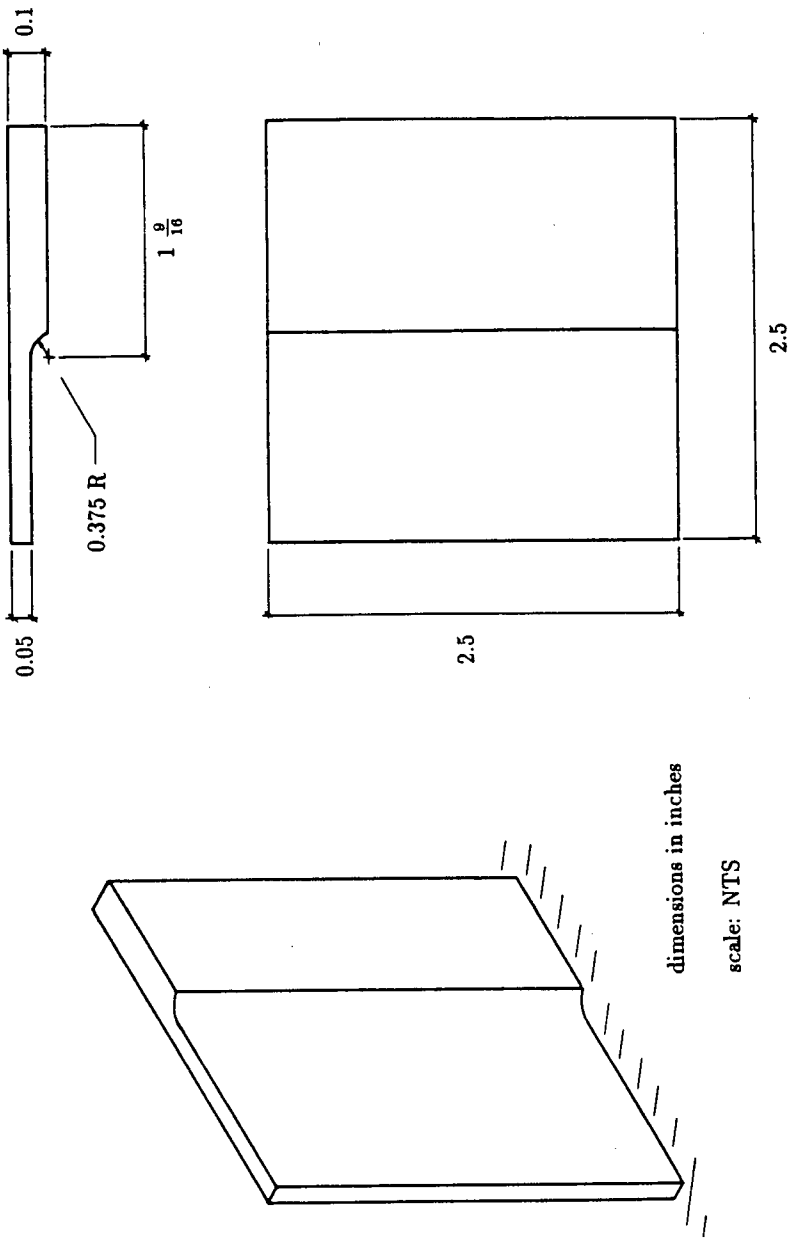

Figure 4.1: Stepped, square cantilevered plate.

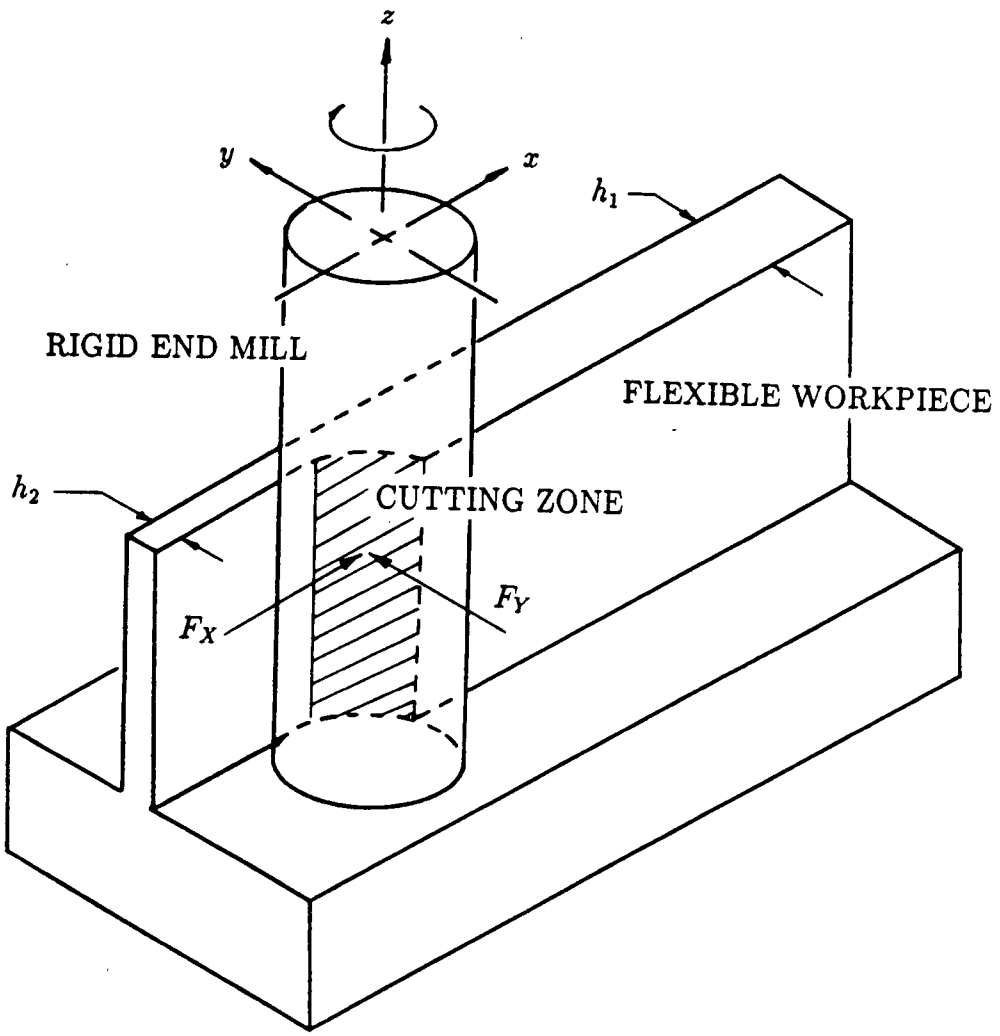

Figure 4.2: Plate machining forces and cutting zone.

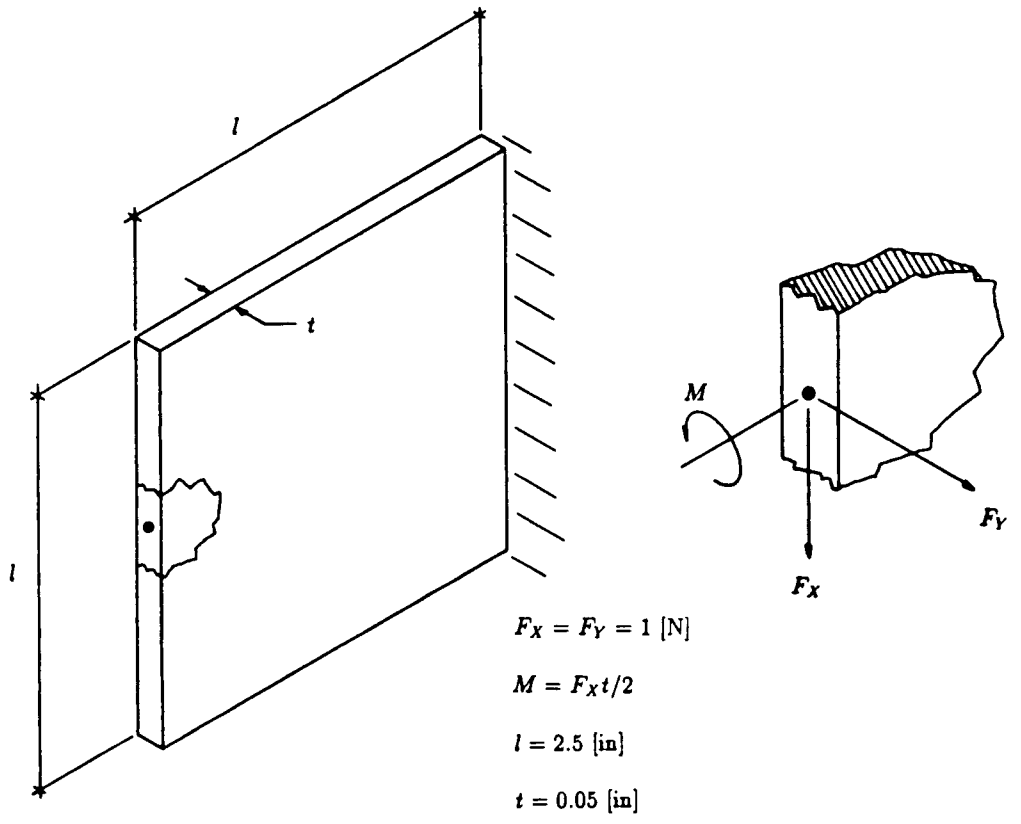

Figure 4.3: Static loads on a cantilever plate.

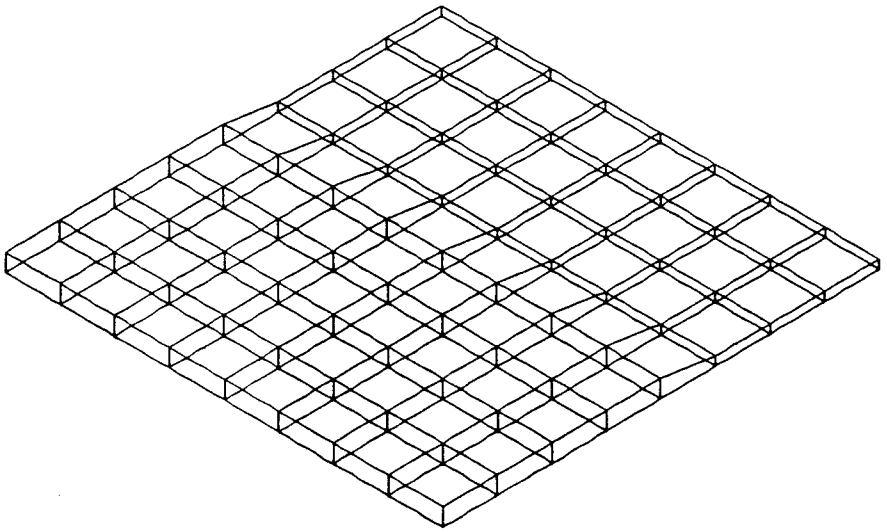

Figure 4.4: Undeformed finite element grid.

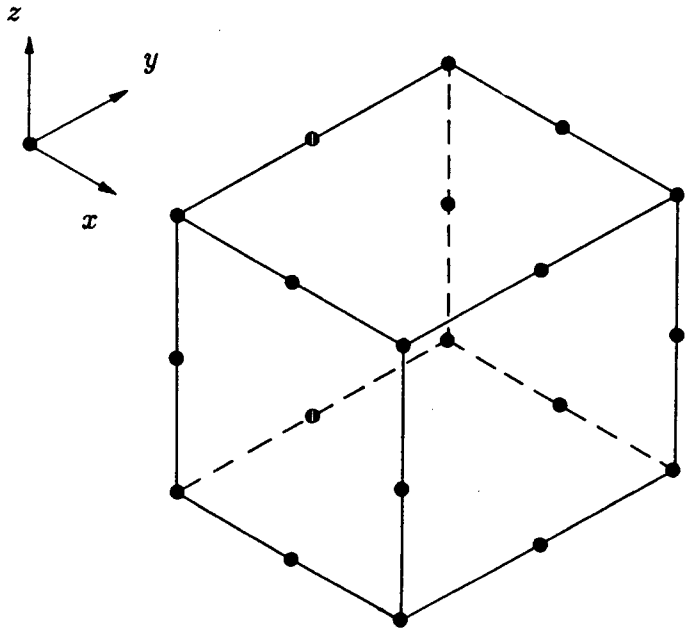

Figure 4.5: 20-node, 60-dof brick element.

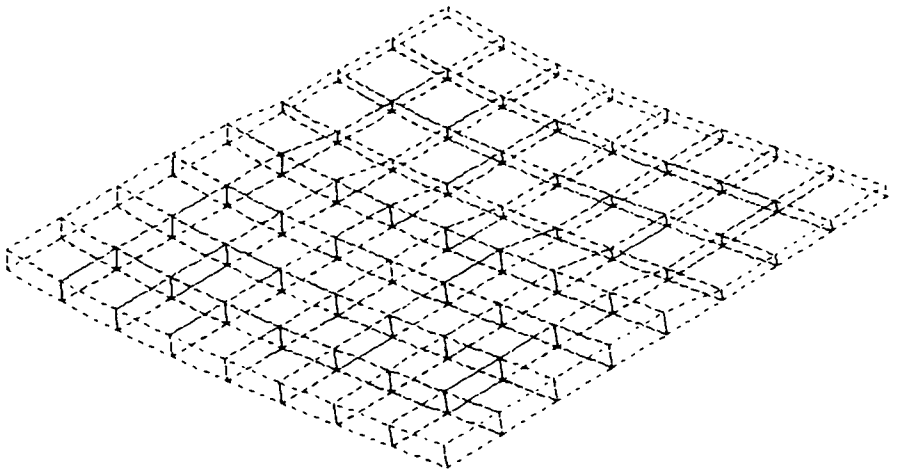

MODE No. 1

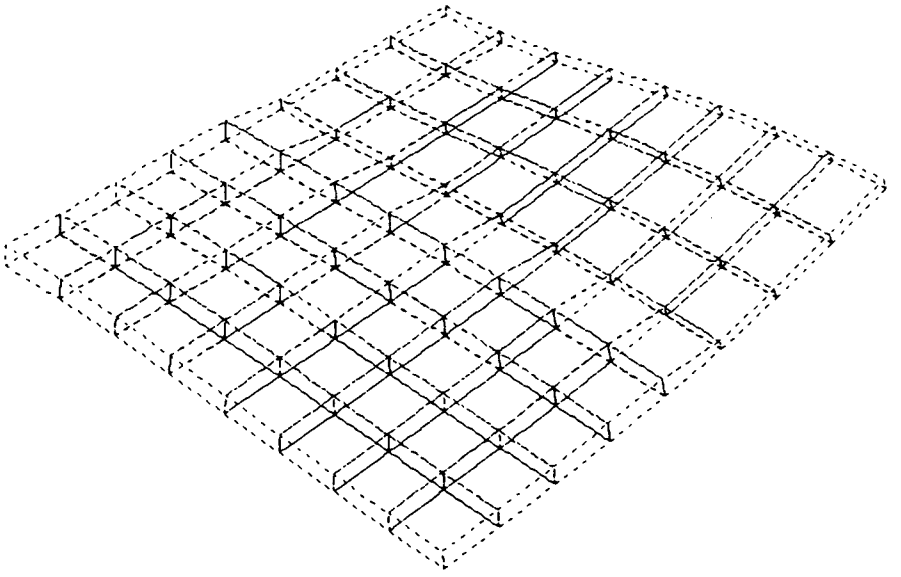

MODE No. 2

Figure 4.6: First five mode shapes for the stepped plate.

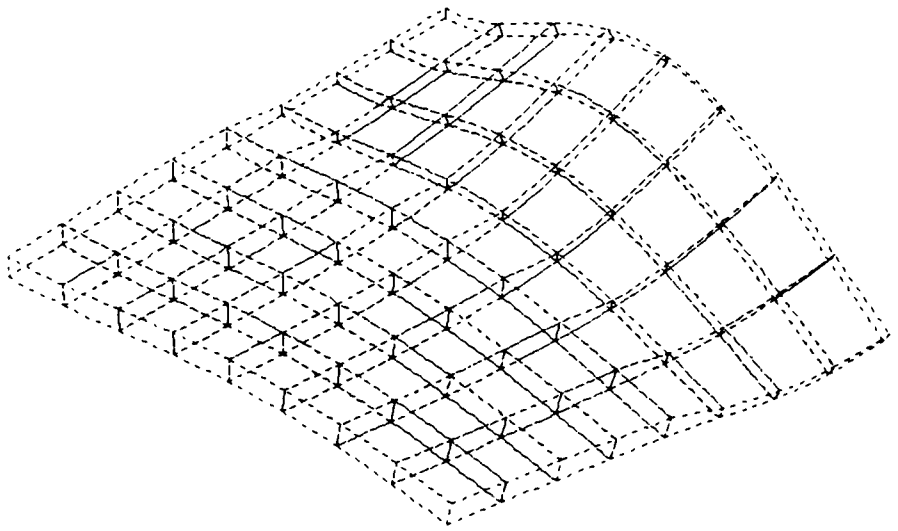

MODE No. 3

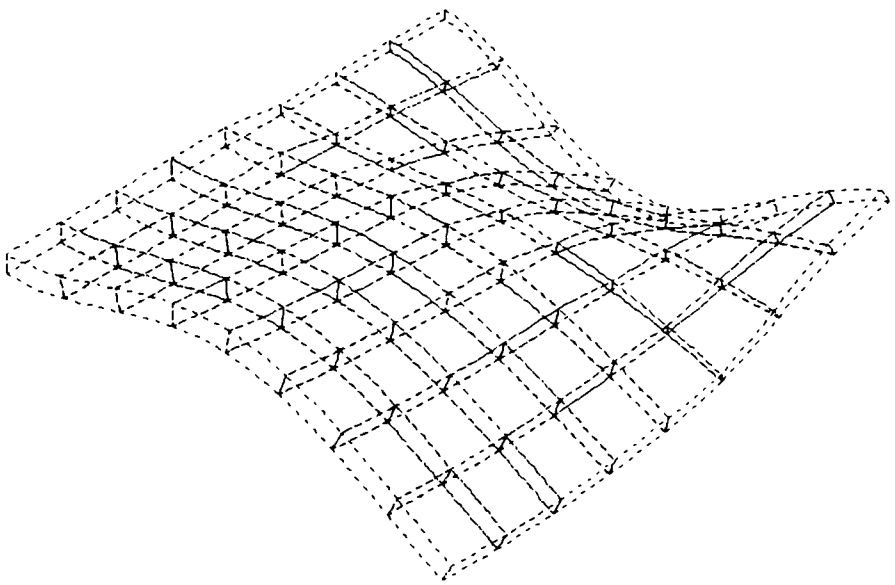

MODE No. 4

Figure 4.6: First five mode shapes for the stepped plate.

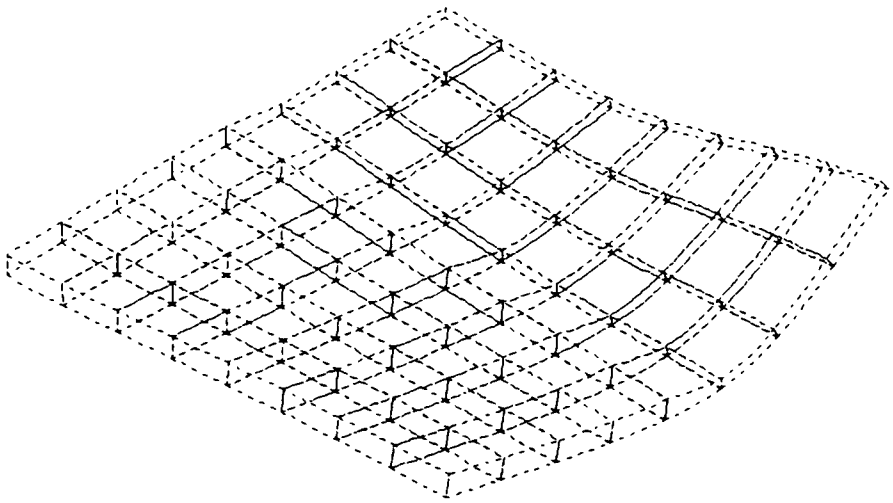

MODE No. 5

Figure 4.6: First five mode shapes for the stepped plate.

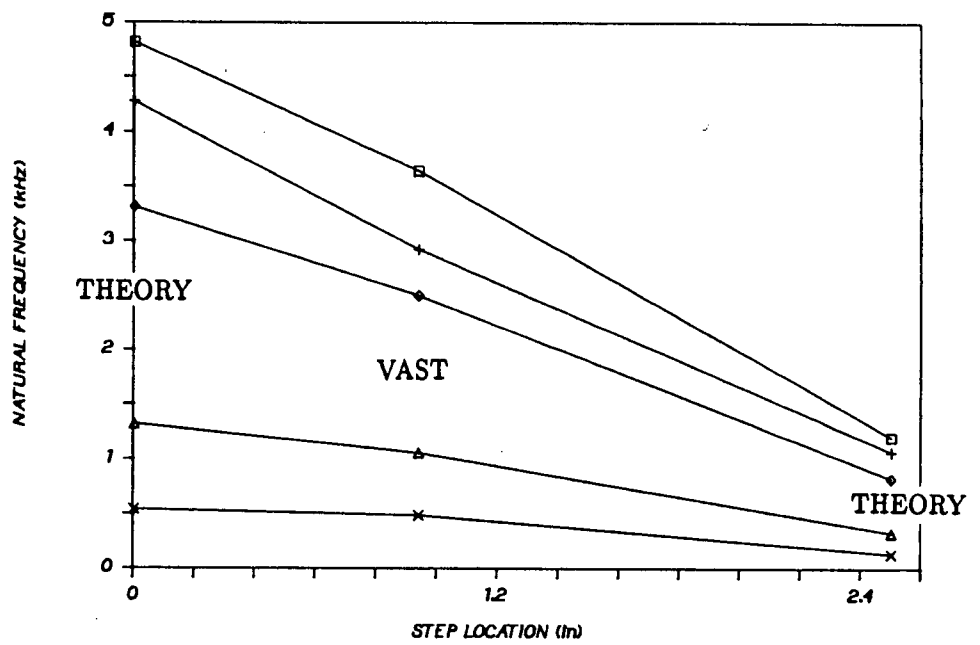

Figure 4.7: Natural frequency variation for various cutting zone locations.

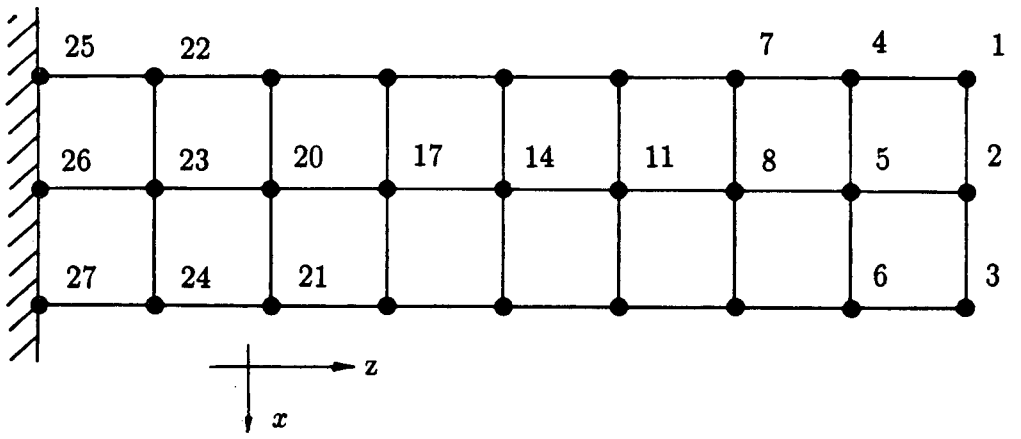

Figure 4.8: Reduced 27-dof SEREP model of the stepped plate.

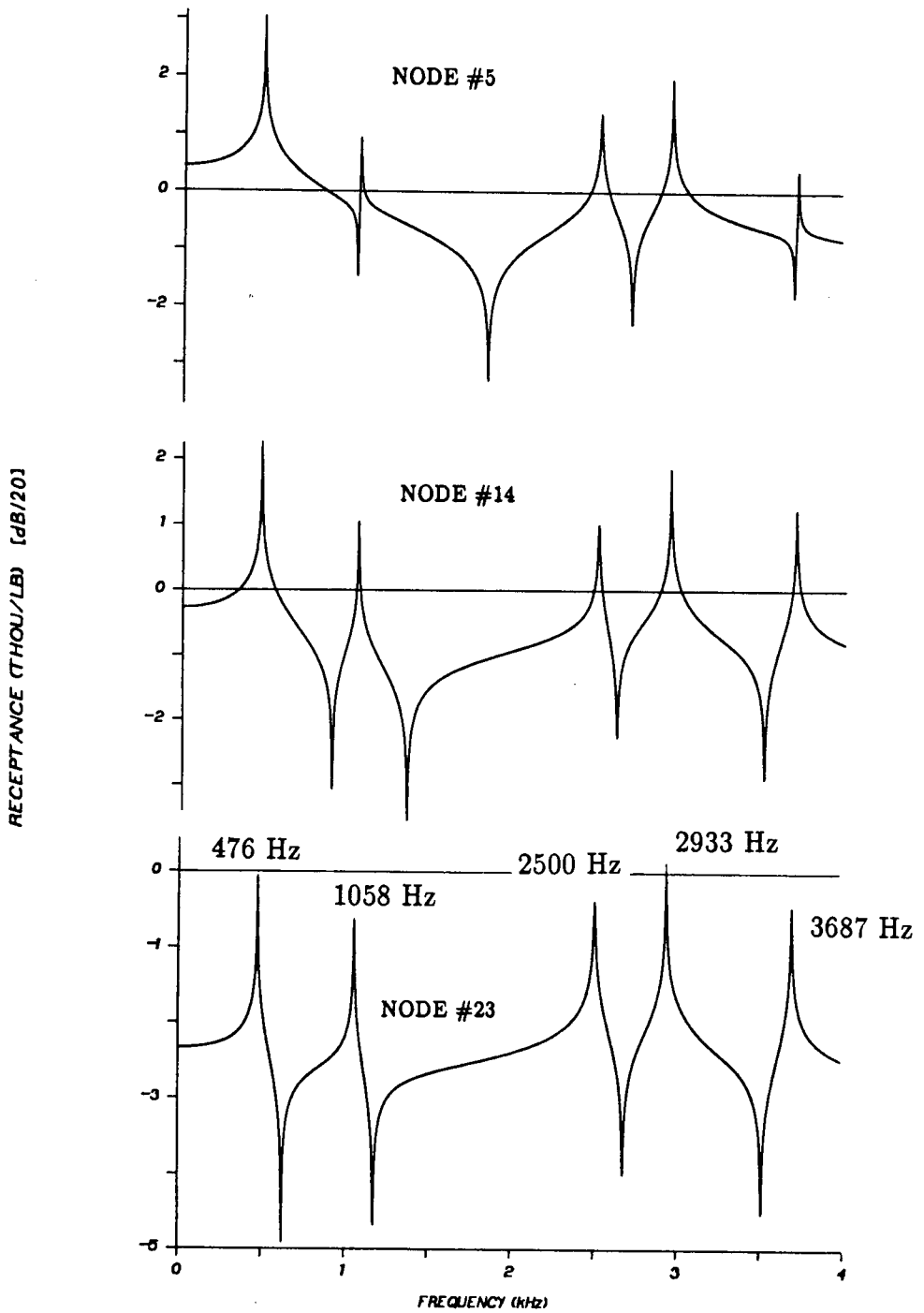

Figure 4.9: Reduced model receptance FRF plots.

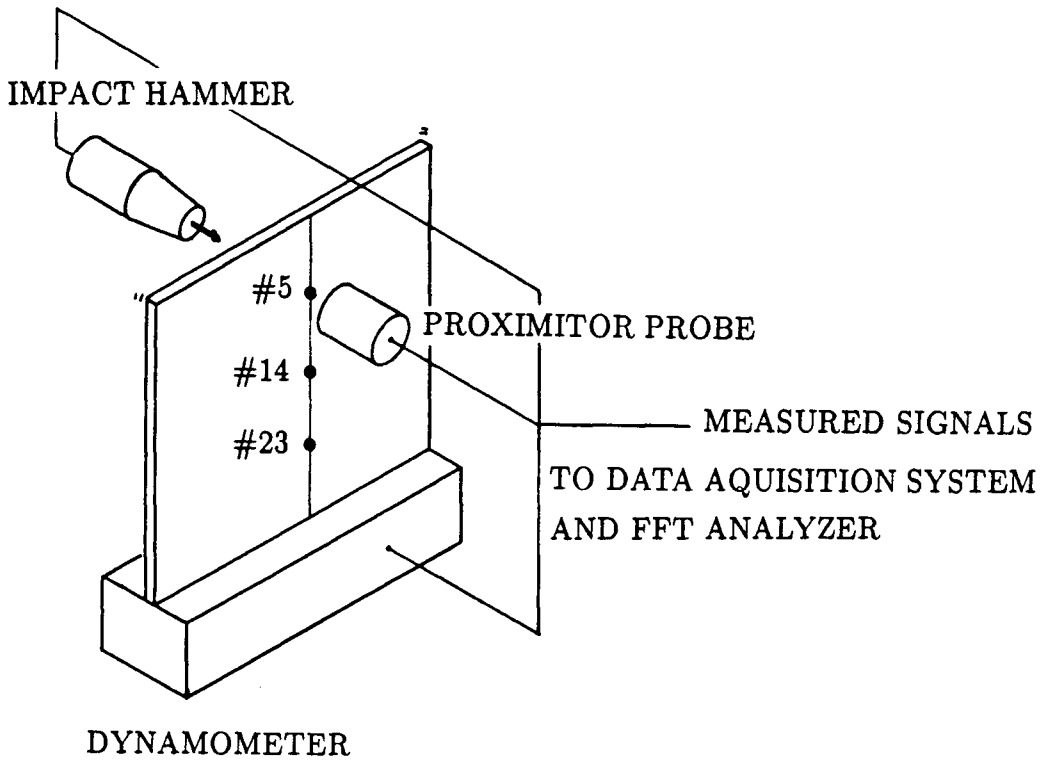

Figure 4.10: Experimental set-up for determining modal characteristics of the stepped plate.

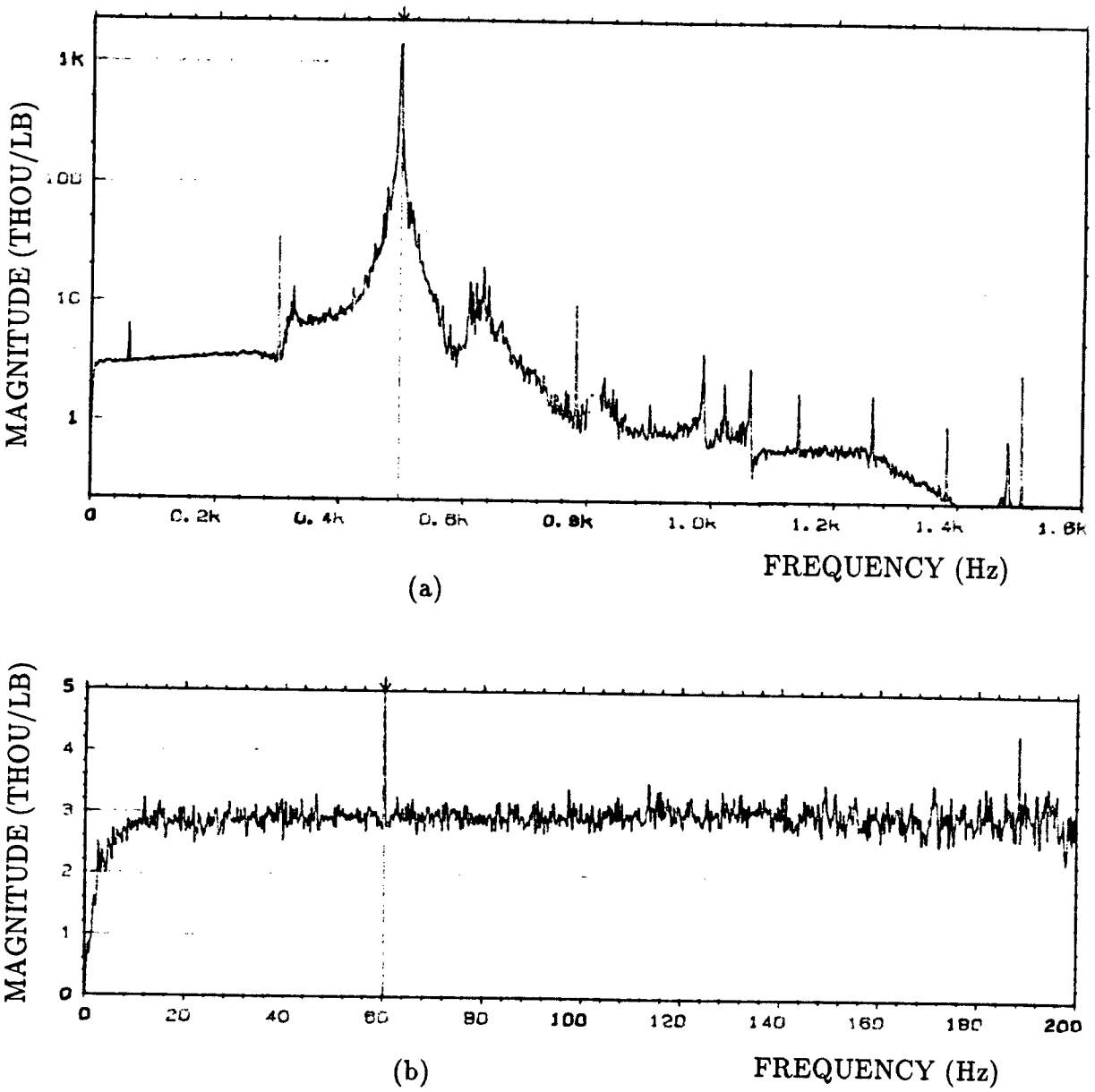

Figure 4.11: Experimentally measured receptance FRF plots.

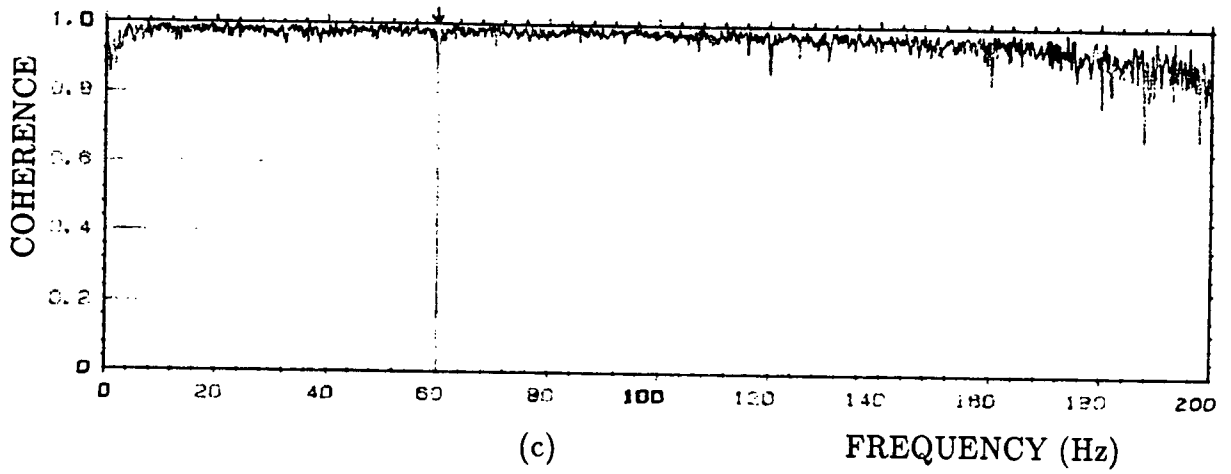

(c)

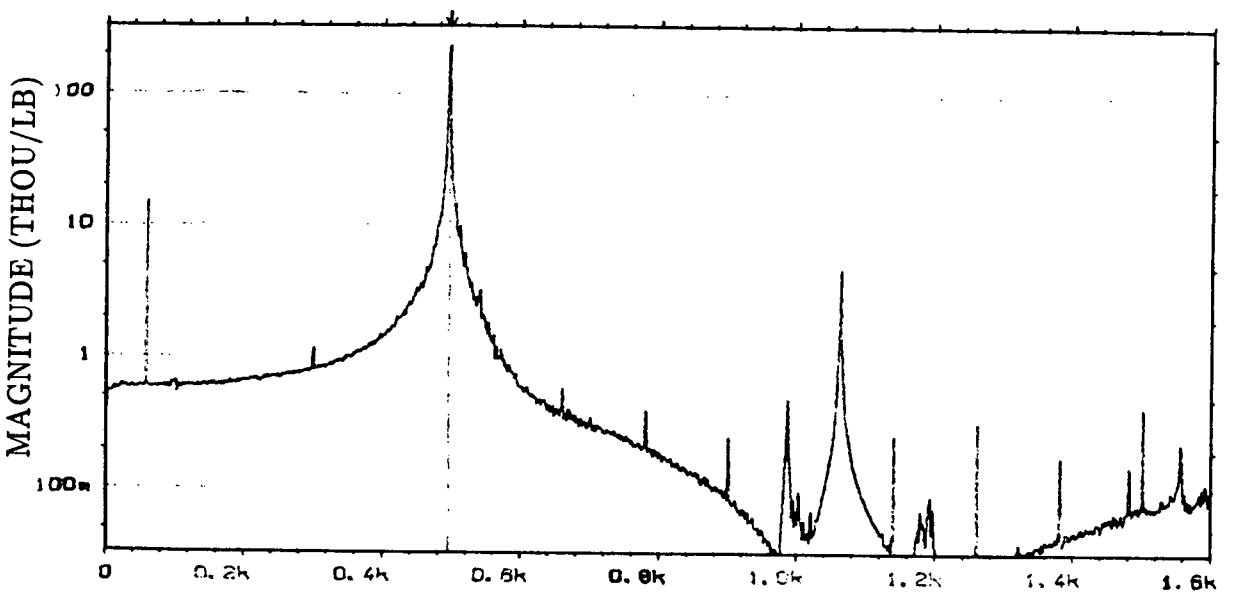

(d)

Figure 4.11: Experimentally measured receptance FRF plots.

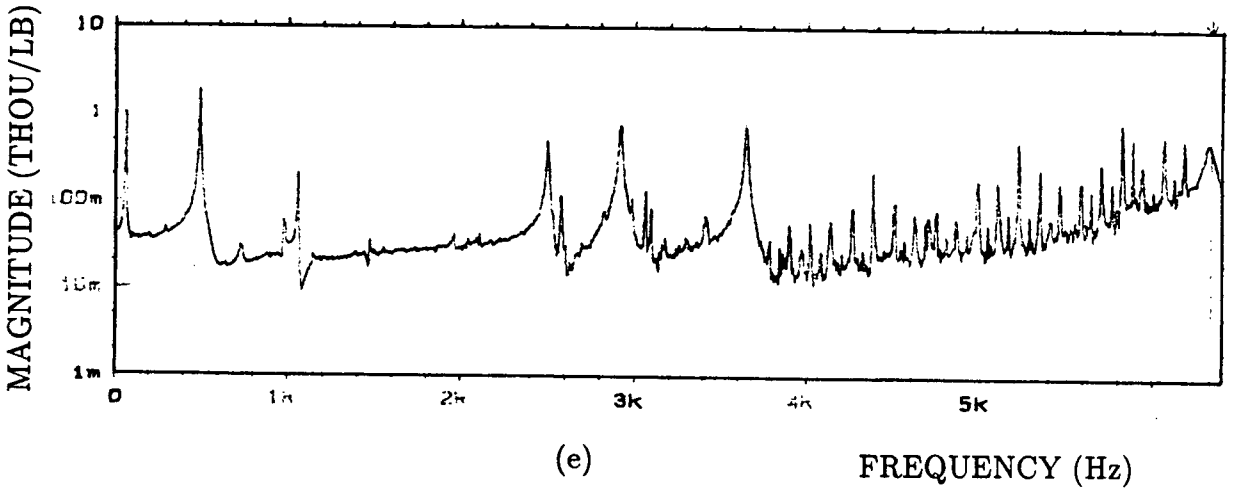

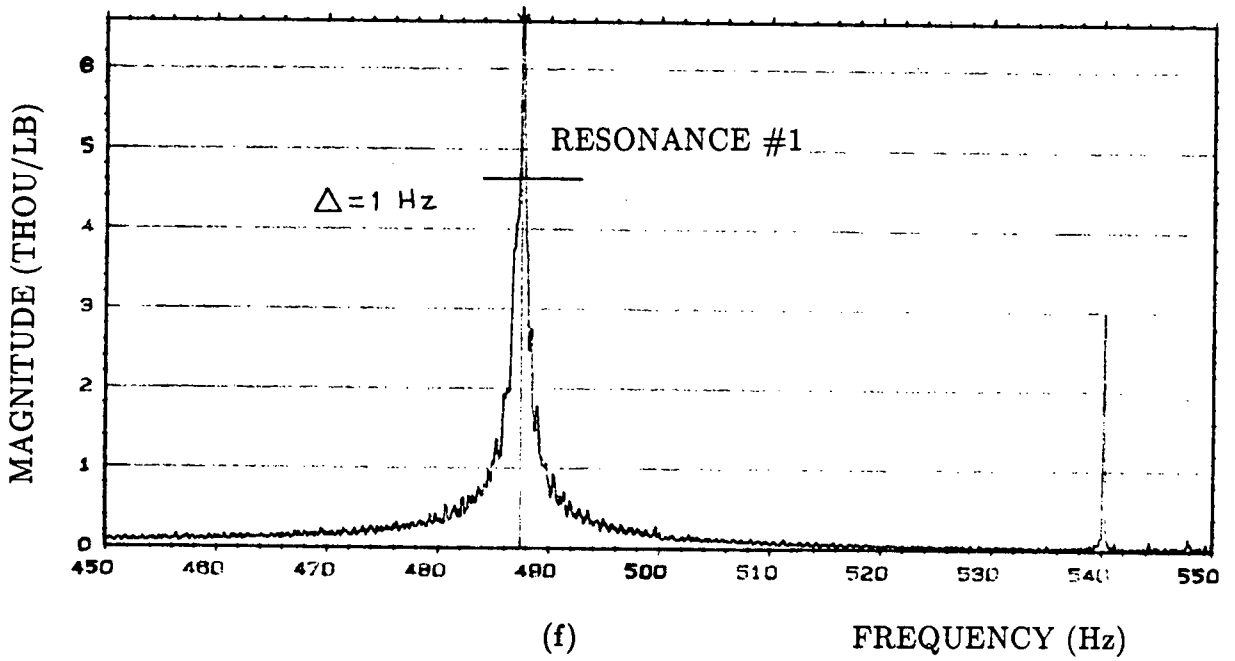

Figure 4.11: Experimentally measured receptance FRF plots.

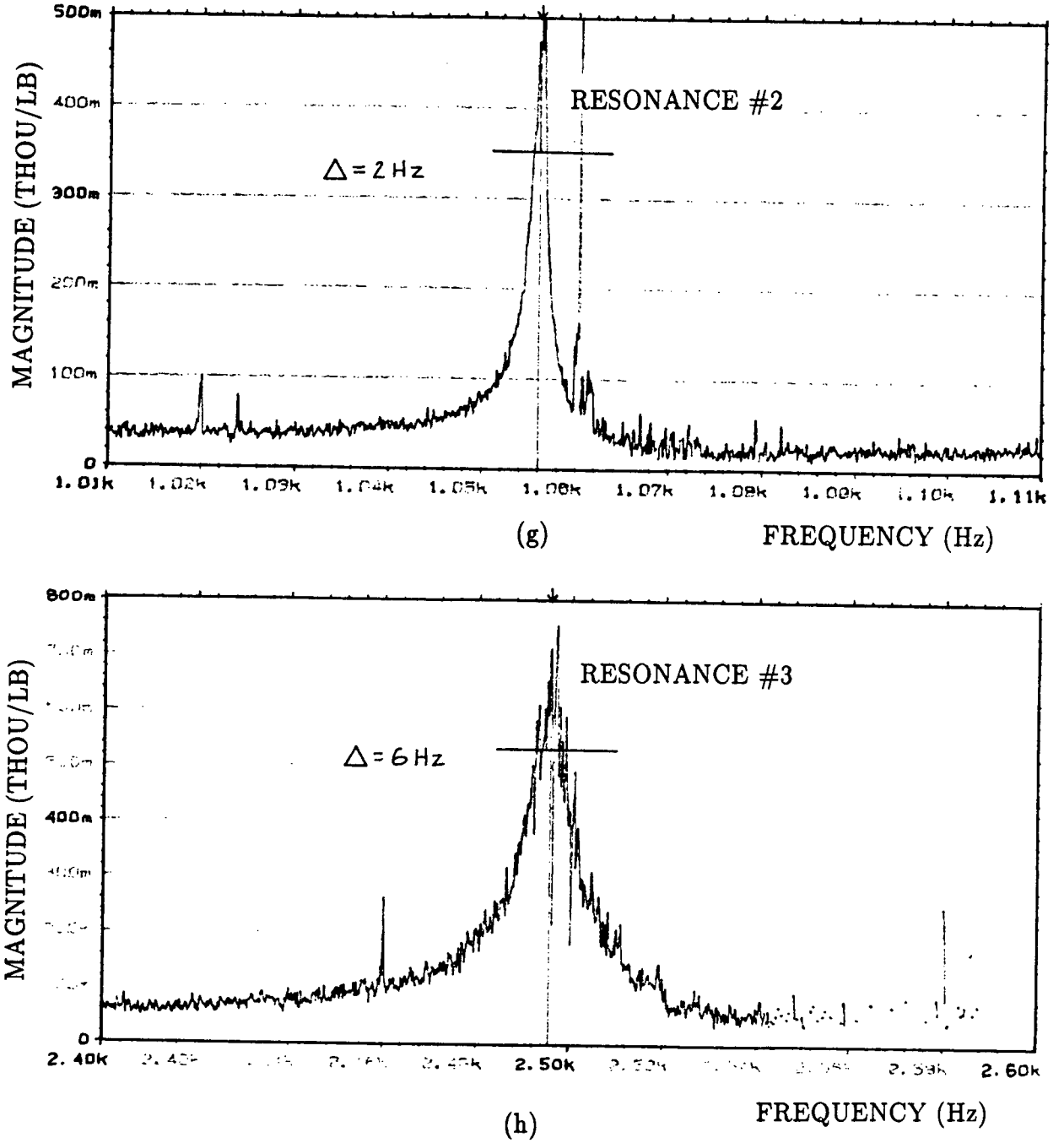

Figure 4.11: Experimentally measured receptance FRF plots.

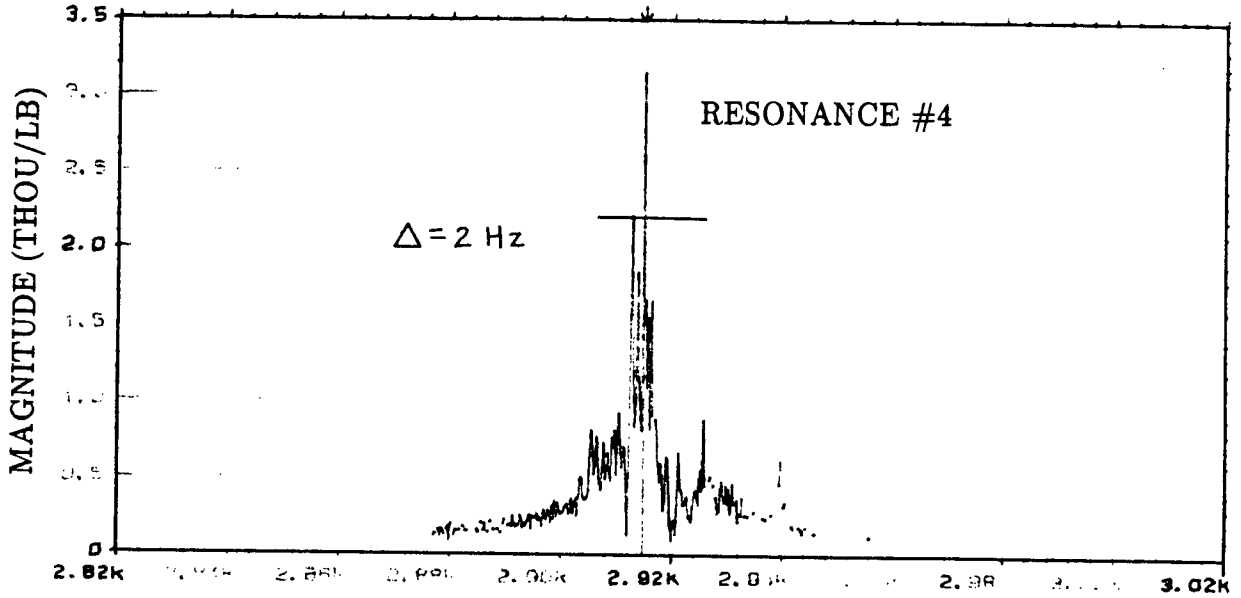

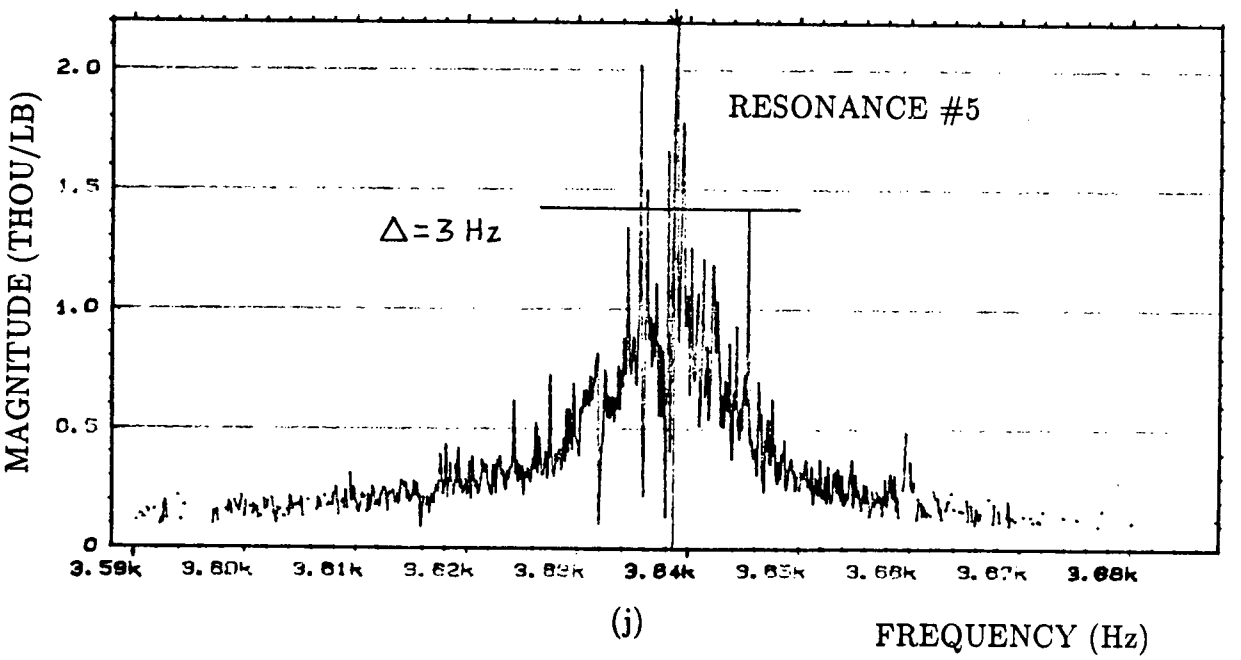

Figure 4.11: Experimentally measured receptance FRF plots.

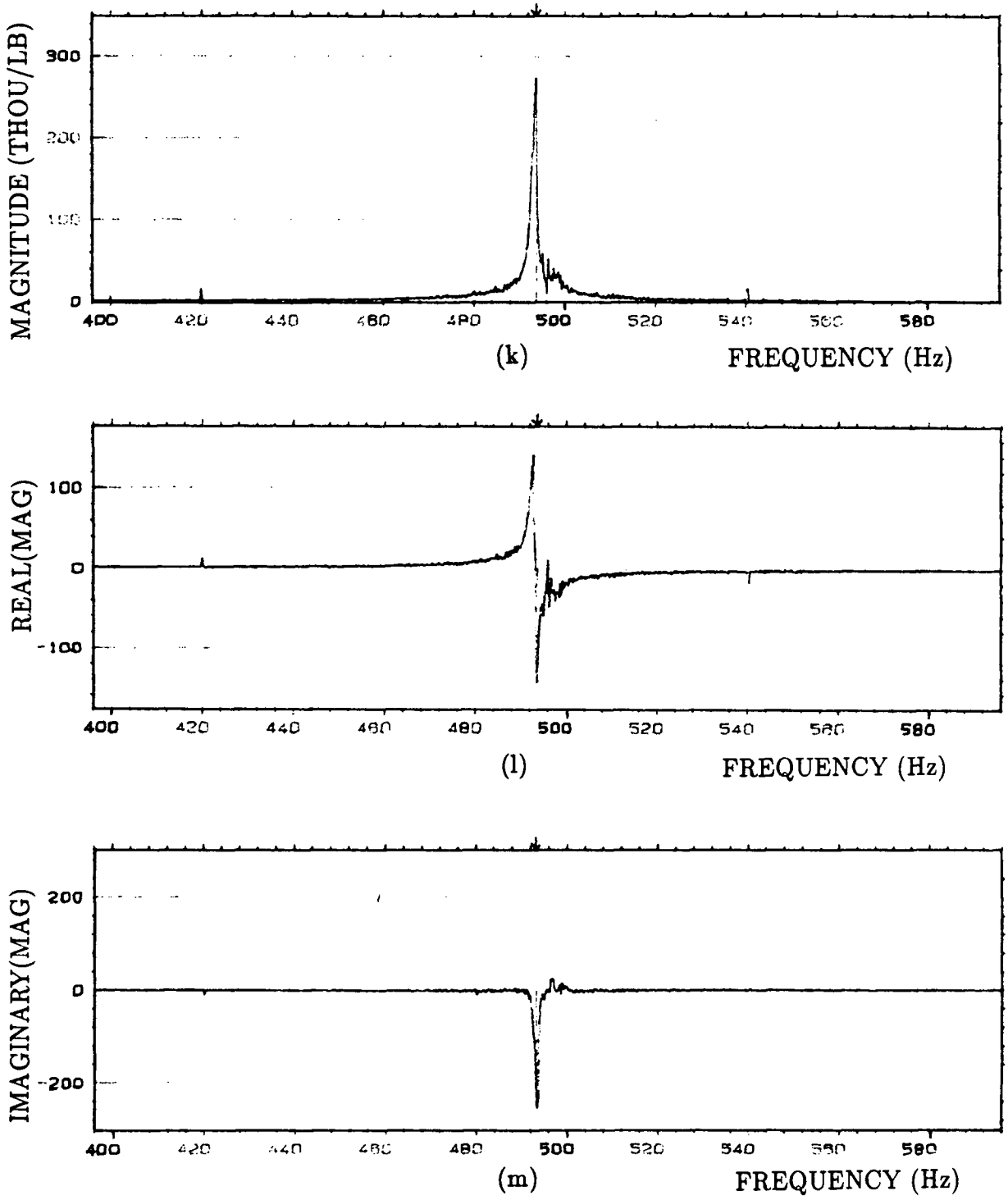

Figure 4.11: Experimentally measured receptance FRF plots.

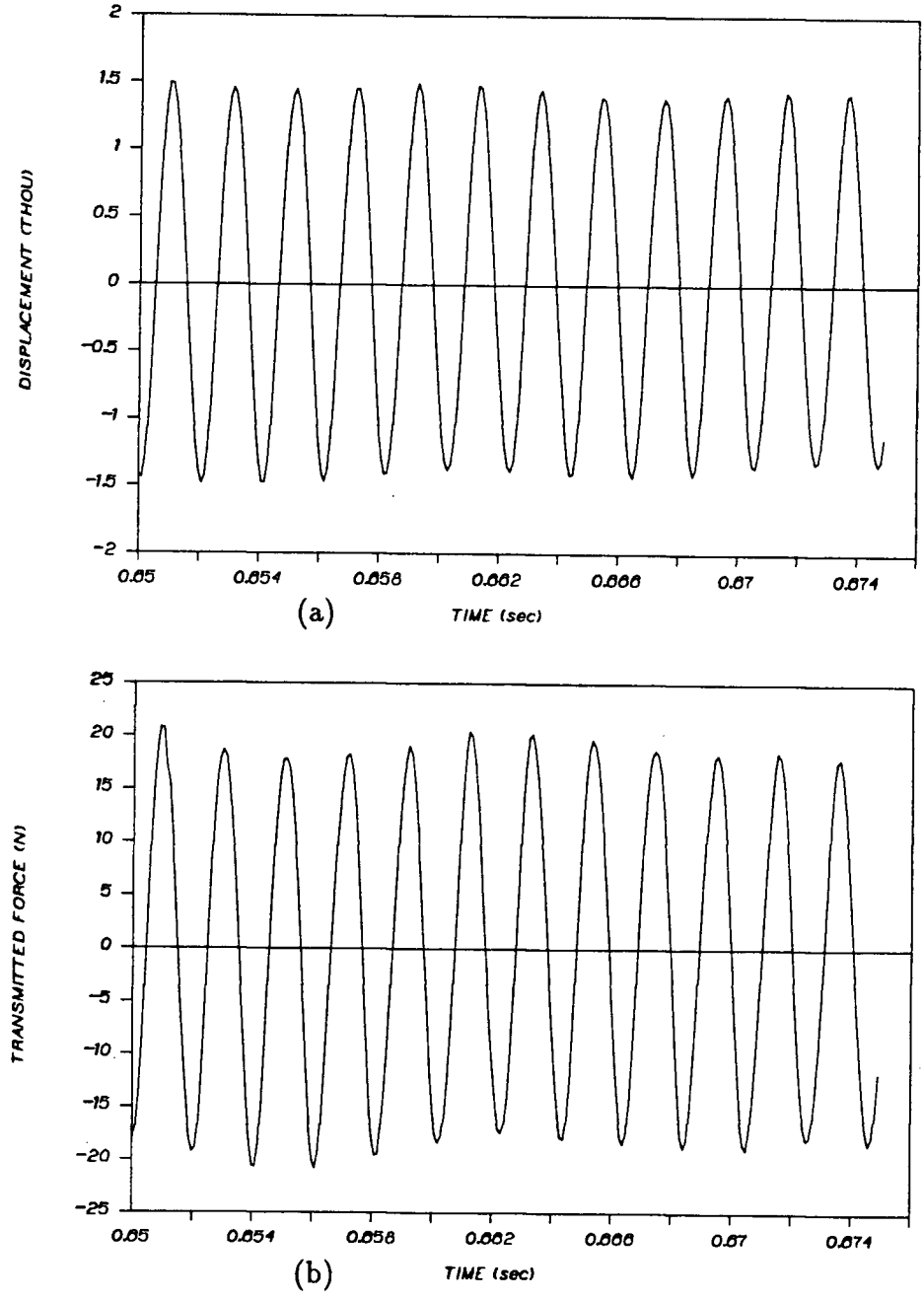

Figure 4.12: Experimental plate response, free vibration.

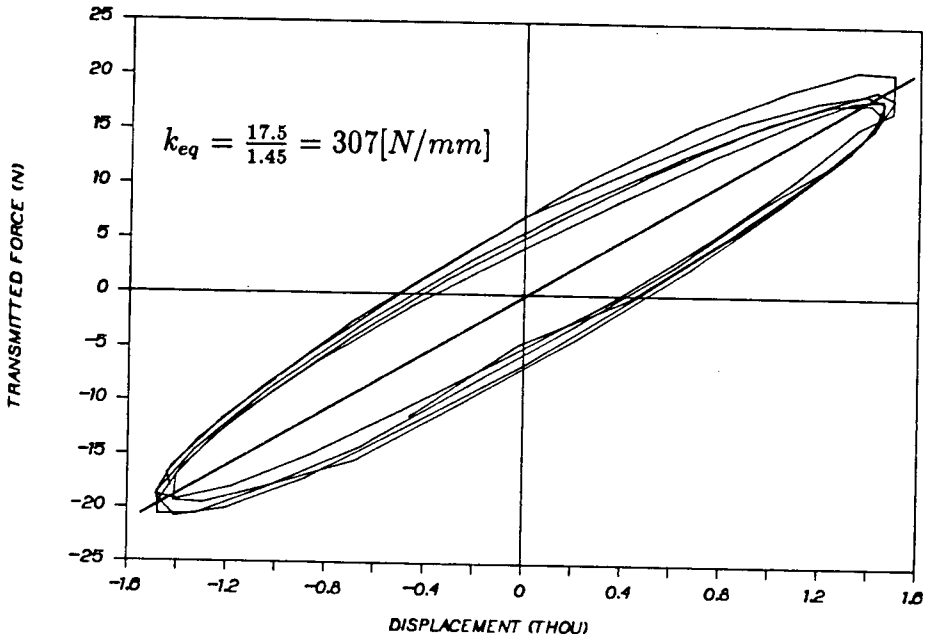

(c)

Figure 4.12: Experimental plate response, free vibration.

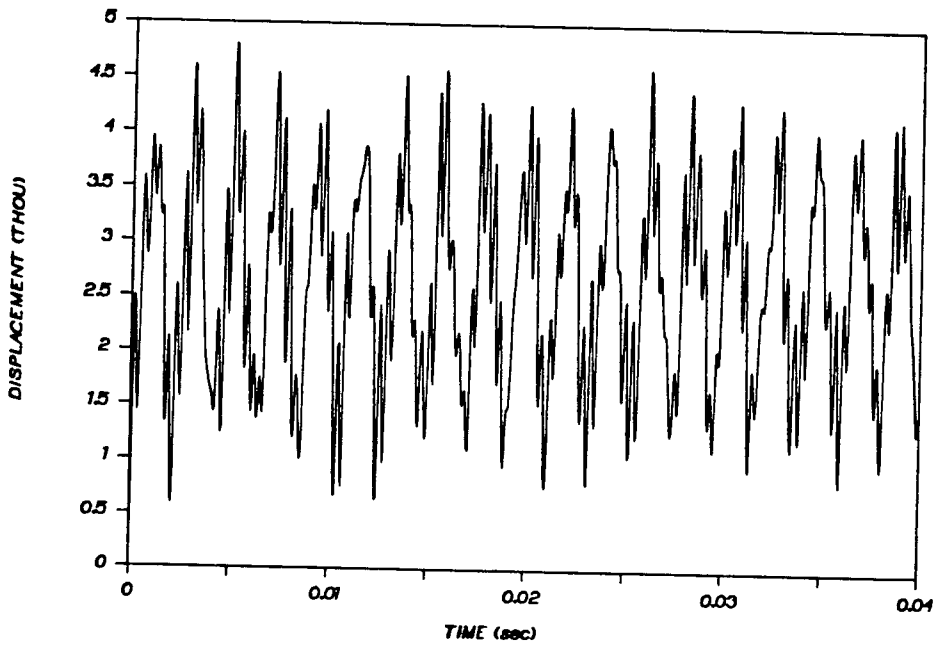

Figure 4.13: Simulated plate response to a unit step input.

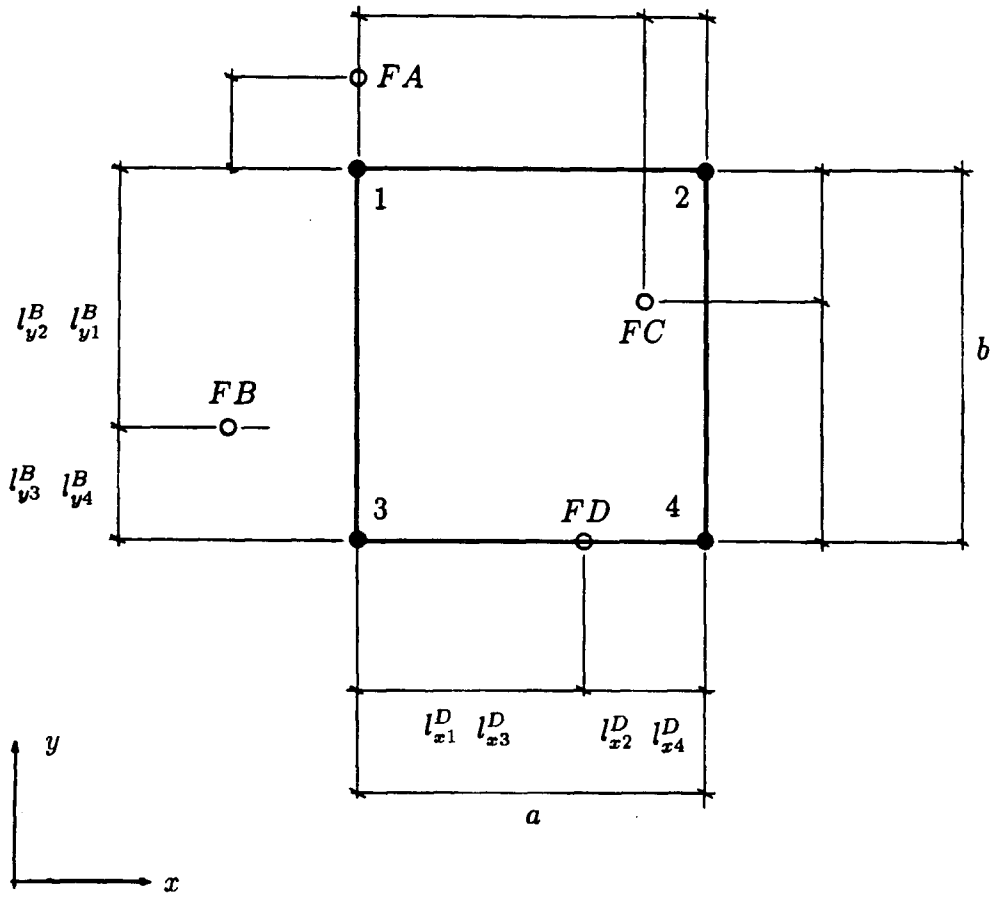

Figure 4.14: Example of forces distributed on a simple grid.

Chapter 5

Results of Plate Machining

5.1 Introduction

Machining of flat plates is analogous to many important industrial processes. The manufacture of jet engine impellers, microwave guideway systems, large turbine blades and many aircraft structural components are included in this classification. During machining operations these relatively flexible workpieces are subjected to periodically varying cutting forces of the milling process. These forces may result in both static and dynamic deflections of the workpiece and the machine tool. The relative motion between the workpiece and the tool also affect the cutting forces, making the process a closed loop dynamic system. An example of plate machining is given in Fig.5.1 which also shows the dynamic interaction between the tool and the workpiece. To model the machining of plates correctly several aspects of the process must be considered: kinematics and dynamics of the workpiece, cutter and machine tool, kinematics of milling and dynamic chip removal. These considerations have been discussed previously and are combined in this chapter. Simulation and experimental results for some cases of plate machining are presented. Recomendations for future work are given.

5.2 Simulation of Plate Machining

The previous two chapters have introduced discrete time methods for simulating dynamic milling and calculating the response of a stepped plate to known dynamic forces. To

model the machining of a flexible workpiece, both of these methods must be combined into a single integrated closed loop simulation approach. This is accomplished here by using the cutting forces to calculate the plates response which is then used to reevaluate the cutting forces in the following time step.

When applying this procedure to flexible workpiece machining several characteristics of the entire process must be considered. The kinematic, dynamic and metal cutting models must describe their respective systems accurately without causing problems elsewhere in the global simulation.

First consider the discretized system kinematics described in Chapter 3. It has been shown that the method used for describing the geometry of the tool and the workpiece can accurately define the chip removal and surface generation of low frequency dynamic milling. When machining flexible structures the discretization time step must be chosen small enough to capture any dynamic modes, to give a clear view of microscopic surface finish details and to accurately define any system changes due to nonlinearities of the cutting process. All of these conditions are quite complex. In considering the plate dynamic modes, it must also be noted that the cutting process stiffness and damping will influence the vibration frequencies encountered. Generally these frequencies will be increased but it is difficult to predict by how much. This makes the choice of the simulation time step difficult. In order to capture details of the microscopic surface finish it is necessary to know the maximum relative velocity between the plate and the tool, which is also difficult without first carrying out experiments or simulations. Finally in vibratory milling the initial cutting force (due possibly to both chip removal and ploughing) can be overestimated, thus setting up unrealistic transient vibrations, if the time step is too large. The time step must be chosen small enough so that these factors don't significantly affect the results.

Next consider the ability of the proposed dynamic model, presented in Chapter 4, to

accurately describe the motion of the workpiece. This model considers five vibrational modes and twenty-seven active degrees of freedom. The plate itself has an infinite number of both modes and degrees of freedom. A discrete method is used to model the plate because this would be the only realistic approach to the more complex geometry of jet engine impellers. The size of the discrete model was chosen as a compromise between computation time and satisfactory model definition.

Other considerations of the dynamic model are introduced due to the machining process. These include: continuously changing dynamics due to material removal, dynamic coupling of the tool and workpiece, the effect of a lubricant applied at the cutting zone, steadies placed behind the plate and the effective dynamic changes due to the cutting process stiffness and damping. Changes in the plate dynamics due to material removal are neglected here for simplicity. A possible approach to this problem is considered in Section 5.5. It is an assumption of this work that the plate is flexible and the tool is perfectly rigid. This assumption is made to simplify the current problem and could be overcome without difficulty if the tool dynamics were modelled. One problem which may occur if two frequencies of the coupled dynamic system are close is nonlinear behaviour which would be relatively difficult to model. A lubricant is used in many commercial machining operations. Because the plate mass is small, the effect of pouring a lubricant onto the cutting zone may significantly affect the dynamics of the plate. This would be difficult to quantify analytically and is neglected in this work, where no lubricant is used. Steadies placed behind the plate might be used to reduce vibrations. For the approach to be used most effectively the result of the steadies on the dynamics of the plate must be known. Modelling the ineraction between steadies and the plate is beyond the scope of this work, but is discussed briefly in Section 5.5. Process stiffness and damping are due to the nature of dynamic cutting. The result of these characteristics on the plate motion is similar to their structural counterparts. The process dynamics are inherently

defined in the metal removal model and are independent of the structural dynamics of the plate.

Finally consider the dynamic cutting process itself. The static cutting model was verified in Chapter 3, but estimation of the dynamic cutting forces due to flank interference and loss of contact between the tool and workpiece has not been tested. This is unfortunate because it increases the difficulty in comparing simulation and experimental results of plate machining. This limitation is necessary however, since there has not been an acceptable model for dynamic cutting presented to date in the literature. The model used here is sensitive to the time step used in the simulation. If the time step is too large the cutting forces can be grossly overestimated, depending on the relative velocity between the tool and the workpiece. Also if edge cutting forces are included in the cutting model (ie. $h^* \neq 0$ and $r_2 \neq 0$) unrealistic step inputs are applied to the plate's structural model. This results in false transient vibrations and therefore edge cutting forces are neglected in the following simulations. The cutting force calculation is strongly dependent on the accuracy of the kinematic representation of the tool and workpiece. Any approximations in the kinematics of the cutting process will be mirrored by errors in the calculated cutting forces.

Simulation results are presented in Section 5.4. The parameters considered are the resultant forces due to the cutting process, plate deflections and the generated surface finish. The effect of runout is neglected in all of the simulations.

5.3 Experimental Plate Machining

Results of four cases of plate machining are presented in Section 5.4. The process is represented in Fig.5.1 (a). The experiments were performed on a 3-axis vertical CNC milling machine. Measured data includes plate displacement and force transmitted to

the table dynamometer. Surface finish profiles were measured using dial gauges with end diameters of 0.4 mm. The plate material used was 7075-T6 aluminum and its geometry is given in Fig.5.2. Up milling was investigated in all cases. Several difficulties were encountered during the experimental phase of this work and these are discussed next.

Initial work included: choice of a plate material and geometry, design of a mounting bracket to fasten the plate onto the table dynamometer and fabrication of several plate specimens.

To facilitate experimental work a readily available and easily machined material was required. 7075-T6 aluminum satisfies these conditions. One overlooked difficulty with this choice was that the proximitor probe used to measure the plate displacement is insensitive to aluminum. This problem was overcome by glueing thin steel shims to the plate at sensor locations.

The size of the plate chosen for the experiments was 2.5 x 2.5 x 0.10 (in.) machined to 2.5 x 2.5 x 0.05 (in.) with a single pass of an end mill. These dimensions were chosen due to several considerations. The plate must have physical dimensions which can be easily mounted onto the table dynamometer. A square plate simplifies any analytical work. The plate must have regions where its stiffness is negligeble relative to the stiffness of the end mill so that the tool can be assumed to be rigid. The fundamental frequency of the plate should be as small as possible. Finally, in order to test the full capabilities of the simulation work, a process was desired where "unstable cutting" would be present.

A mounting bracket was designed to fasten the plate onto the dynamometer. Design requirements of the mounting bracket assembly included adequate stiffness, minimal influence on the plate dynamic response as measured on the table dynamometer, removeable from the dynamometer and the flexibility to hold many different plate sizes. The final design is shown in Fig.5.3 and satisfies the above requirements satisfactorily.

Several plate specimens were prepared for the experimental work. The stock material

used was 1/4 (in.) plate. The stock was machined to the shape shown in Fig.5.2. The ramp shown in Fig.5.2 was included for two reasons. The first reason was to reduce machining errors, and therefore errors in the plate dynamic model, prior to taking any measurements. The second reason is to eliminate the possibility of "catching" at the edge of the plate when the tool starts to cut at point B. This usually results in the destruction of the workpiece by plastic deformation. If the tool starts to cut at point A of Fig.5.2, the transition from non-cutting to cutting is smooth and catching doesn't occur.

With the workpiece setup established specifications of the end mill geometry, cutting conditions and data sampling frequency are required. Each of these specifications are given with the experimental cases. Two end mills, one with straight flutes and one with helical flutes, are used in the experiments. Some parameters considered in the choice of the end mills were: size, stiffness, availability, cost and cutting angles. Cutting conditions considered here are the feed per tooth and the spindle speed. The feed per tooth is chosen to give a desired maximum cutting force. Neglecting any deflections of the plate or tool, the cutting force can be estimated by:

$$F \approx K_s a h$$

Errors in this approximation due to plate deflections away from the tool will be conservative and overestimate the cutting force. The spindle speed is chosen to give a practical cutting speed and to decrease the overall experimental time. The sampling frequency is chosen to be as fast as possible in order to observe the maximum resolution of any high frequency activity.

Experimental results for four cases of plate machining are presented in the next section. Measured parameters considered are the transmitted force to the table dynamometer, plate deflections and the generated surface finish.

5.4 Discussion of Results

Results of four cases of plate machining are presented in this section. Both experimental and simulation results are considered and compared. The parameters for each case are sumarized in Table 5.1. A summary of the main results is given in Appencix C.

5.4.1 Case No.1

This case considers up milling with a 3/4 (in.) diameter, four fluted zero helix end mill. The spindle speed is 1500 (RPM) and the feedrate is 0.015 (in./s). The axial depth of cut is 2.5 (in.). Simulation cutting parameters used are $K_s = 1185$ (MPa) and $r = 1$; ploughing and edge cutting forces are neglected. All of the first five vibrational modes are included in the plate dynamic model. Structural damping is approximated as $\zeta = 0.05$ for all modes. The time step of the simulation is 10 (μ s). The simulation results are discussed first. Graphs showing simulated results for this case are shown in Figs. 5.4 to 5.10.

Fig. 5.4 shows the displacement of the plate at node 14 (near the middle of the plate) for the first 100 (ms) of the simulation. There are three characteristics to notice about this result. First, the response is growing, which indicates an unstable machining operation. Second, the frequency content of the displacement includes the tooth passing frequency (100 Hz), the first natural frequency of the plate (477 Hz) and some higher frequency signals. Third, the transient vibration between teeth is of a significant magnitude at the beginning of each cutting cycle. Fig.5.5 shows the displacement at node 14 after 800 (ms) and Fig.5.6 shows details of the deflection at nodes 5, 14 and 23 for a single tooth pass.

Figs.5.7 and 5.8 show the simulated cutting forces in the (x) and (y) directions respectively. Figs.5.9 and 5.10 show details of these cutting forces for a single tooth pass.

These forces are composed of a low frequency tooth passing component and a very high frequency (about 5 kHz) part present only during the cutting cycles. This would indicate that the plate is "bouncing" on the tool at a high frequency and that little "cutting" is taking place.

Comparing Figs.5.6 and 5.10 reveals an interesting result. The displacement due to cutting begins at 0.81 (s) while the cutting force doesn't become visible until about 0.8107 (s). Thus the displacement appears to lead the cutting force by 0.7 (ms). This isn't really the case. Since the top of the plate is extremely flexible (approximately 0.022 mm/N) virtually no metal cutting takes place there. For this reason the tool contacts the unmachined top of the plate first during each tooth pass. Since the plate is so flexible very little force is required to cause the initial displacement. This force isn't visible on the graph but it is present and as would be expected the force actually leads the displacement.

The experimental results for Case 1 are discussed next. Graphs showing experimental results for this case are shown in Figs.5.11 to 5.14.

Fig.5.11 shows the plate displacement measured at node 14. The corresponding plot from simulation studies is shown in Fig.5.5. The out of cut vibration frequency of the plate is high ($\approx$ 2 kHz) which may be due to excitation of one of the higher modes, or because the steel shim glued to the back of the plate became loose. The in cut vibration frequency is 900 (Hz) and corresponds well with the first mode component of the simulation results. The magnitude of in cut deflections correspond well.

The measured forces transmitted to the table dynamometer in the (x) and (y) directions are presented in Figs.5.12 and 5.13 respectively. The sign of the measured force in the (y) direction is opposite to that used in the simulation studies, this is a result of the measurement setup and is not an error. The corresponding simulation results are shown in Figs.5.7 and 5.8. First it should be noted that the measured force and the actual

cutting force are different. Inertial forces due to plate vibrations are also transmitted to the dynamometer and can contribute a significant amount to the measured results. Similarly to the simulation results, the measured forces have a strong component of a high frequency signal. Also the magnitudes of the measured and simulated forces are close.

A portion of the measured surface finish is shown in Fig.5.14. The mechanism of surface generation is explained in Section 5.4.3, and is a result of the plate vibration frequency and the cutting speed. The wavelength observed on the surface is 2.8 (mm). Theoretically, the resultant wavelength is $(R\Omega/f_{nc}) = 1.7$ (mm).

5.4.2 Case No.2

This case considers up milling with a 3/4 (in.) diameter, four fluted zero helix end mill. The spindle speed is 1157 (RPM) and the feedrate is 0.02 (in./s). The axial depth of cut is 2.5 (in.). Simulation cutting parameters used are $K_s = 1185$ (MPa) and $r = 1$; ploughing and edge cutting forces are neglected. All of the first five vibrational modes are included in the plate dynamic model. Three cases of structural damping are considered: $\zeta = 0.005$, $\zeta = 0.05$ and $\zeta = 0.5$ for all modes. The purpose of varying the damping ratio is to investigate the effect of process damping on plate machining. The time step of the simulation is 10 (μ s). The simulation results are discussed first. Graphs showing simulated results for this case are shown in Figs. 5.15 to 5.28.

$\zeta = 0.005$

Fig.5.15 shows the plate displacement at node 14 when $\zeta = 0.005$. Fig.5.16 shows the corresponding cutting force in the (y) direction. The process is strongly unstable and plate vibrations increase rapidly.

$\zeta = 0.05$

Fig.5.17 shows the initial displacement of the plate at node 5 and Fig.5.18 shows the corresponding vibration at node 14. There is a greater content of high frequency motion in the response at node 14. This is because the higher frequency modes are stronger at node 14 than at node 5.

Fig.5.19 shows the simulated displacement at node 14 from 800 to 900 (ms). A detailed view of the displacement for a single tooth pass is shown in Fig.5.20 for nodes 5, 14 and 23. Again, the higher frequency components are more visible at nodes 14 and 23. Considering the displacement at node 5 the fundamental vibration frequency is greater during cutting than during free vibrations. This is a result of the process stiffness increasing the equivalent structural stiffness and therefore increasing the vibration frequency. This is considered in more detail for simulation Case 3.

Cutting forces in the (x) and (y) directions are shown in Figs.5.21 and 5.22 respectively. Details of these cutting forces, for a single tooth pass, are given in Figs.5.23 and 5.24. These forces are composed of a low frequency tooth passing component and a very high frequency component present only during the cutting cycle.

$\zeta = 0.5$

Fig.5.25 shows the displacement of the plate at node 14 for the first 100 (ms) of the simulation. This result can be compared with Fig.5.18, where $\zeta = 0.05$. The rate of growth of the displacement when $\zeta = 0.5$ is much slower than the rate of growth when $\zeta = 0.05$. When $\zeta = 0.5$ the transient vibrations during non cutting are completely damped out between consecutive teeth. Also very little high frequency content is visible in Fig.5.25.

Fig.5.26 shows the plate displacement at node 14 after 800 (ms) and Fig.5.27 gives a

detailed view of the displacement for a single tooth pass at nodes 5, 14 and 23. Again the dominant vibration frequency is increased in cut, and the higher frequency modes are more visible at nodes 14 and 23.

Cutting forces in the (x) and (y) directions are given in Figs.5.28 and 5.29 respectively. Details of these forces are shown in Figs.5.9 and 5.10 for a single tooth pass. As before, the cutting forces consist primarily of the tooth passing frequency and some very high vibration frequency. The relative contribution of the high frequency forces indicates that most of the cutting is occuring at the bottom of the plate where the high frequency modes are more active.

From the three simulations of Case 2, an important result is that the stability increases as the structural damping ratio is increased.

Experimental results are considered next. Graphs showing experimental results for this case are shown in Figs.5.32 to 5.35.

Fig.5.32 shows the plate displacement measured at node 14. The corresponding simulation results are given in Figs.5.15, 5.19 and 5.26. The magnitudes of the simulated displacements don't predict the measured displacements accurately. The observed in cut vibration frequency is 860 (Hz) which corresponds well with the simulated value of 890 (Hz) measured from Fig.5.20. The experimental result has a sharp displacement between each of the tooth passes, which is the result of inadequate clearance behind the teeth. This is analogous to having short teeth with large negative rake angles between the cutting edges. This problem is eliminated for the experiments of Case 3.

Measured forces are given in Figs.5.33 and 5.34 for the (x) and (y) directions respectively. As with the simulated forces, a frequency component higher than the measured vibration frequency is strong. This is present because most of the cutting force is generated near the bottom of the plate where higher frequency modes are dominant. The static cutting force is larger for the measured forces than for the simulated forces. This

is because of an inadequate cutting force model. The inclusion of ploughing forces in the simulation is expected to reduce this discrepancy. This will be discussed in Case No. 3.

A portion of the measured surface finish is shown in Fig.5.35. The wavelength observed on the surface is about 2 (mm). Theoretically, the resultant wavelength is $(R\Omega/f_{nc}) = 1.3$ (mm).

5.4.3 Case No.3

This case considers up milling with a 3/4 (in.) diameter, four fluted zero helix end mill. The tool clearance angle is 10 deg with a primary land of 0.5 (mm) and the rake angle is 5 deg. The spindle speed is 1157 (RPM) and the feedrate is 0.394 (in./s). The axial depth of cut is 2.5 (in.). Simulation cutting parameters used are $K_s = 1185$ (MPa) and $r = 1$; edge cutting forces are neglected. Results of two simulations are presented. Ploughing forces are included in the second simulation where the yield strength is estimated as 496 (MPa). Only the first bending mode is included in the plate dynamic model. The purpose of this simplification in the dynamic model is to determine whether the higher frequency modes contribute significantly to the simulation results. A single mode approach also simplifies the plate motion which makes the surface generation mechanism easier to analyze. Structural damping is $\zeta = 0.5$. The time step of the simulation is 10 (μ s). Graphs showing simulated results for this case are shown in Figs. 5.36 to 5.44.

a) Zero Ploughing Forces

The first simulation doesn't consider ploughing forces on the tool flank face. Fig.5.36 shows the displacement of the plate at node 14 during steady state conditions. Four important characteristics of this graph should be noted.

First, none of the very high frequency ($\approx$ 5 kHz) vibrations are present which were seen in both of the previous two simulation cases. This is due to not including the four

higher vibrational modes in this simulation case.

Second, although the theoretical immersion angle is only 30 deg, the plate is deflected for about 66% of the time for each tooth pass. This is because the top of the plate isn't stiff enough to allow material to be removed from it. This results in the tool starting to cut at an immersion angle of -30 deg and finishing the cut at $+30$ deg. This accounts for 60 deg of tool-workpiece contact which corresponds to 66% of the cycle time. The inability to model this phenomenon is a limitation of other dynamic milling simulation methods.

Third, the vibration frequency during cutting ($\approx$ 1.3 kHz) is faster than the natural frequency of the plate (477 Hz). This is due to the influence of the process stiffness and process damping. A simplified analytical estimation of the effect of process stiffness on the cutting vibration frequency is as follows.

Assume that the plate is a SDOF dynamic structure with equivalent system parameters as calculated in Chapter 4 for node 14: $m = 0.033$ (kg), $k = 310$ (N/mm) and $\omega_n = 3056$ (RAD/s). A schematic representation of this simplified dynamic cutting process is given in Fig.5.37. The equation of motion for this system is:

$$m\ddot{y} + ky = K_s a(h_m - y)$$

or,

$$m\ddot{y} + (k + K_s a)y = K_s a h_m$$

The cutting vibration frequency is given simply as

$$f_{nc} = \frac{1}{2\pi}[(k + K_s a)/m]^{1/2}$$

If $K_s = 1185$ (MPa) and $a = 63.5$ (mm) then the cutting vibration frequency is $f_c = 7.6$ (kHz). This is a very simplified analysis and is not intended to give an accurate

estimate of (f_c). Factors neglected here are: process damping, regeneration, and the three dimensional geometry of both the plate and the milling process.

The fourth item to notice about Fig.5.36 is that the transient plate vibrations are very small at the start of each cutting cycle.

Figs.5.38 and 5.39 show the cutting forces in the (x) and (y) directions respectively. The high frequency component of the cutting force corresponds closely to the vibration frequency of the plate. This is because only one mode is present and the entire plate vibrates in phase at the same frequency. The static component of the cutting forces is more significant in this case due to the greatly increased feedrate.

The microscopic surface finish, generated by simulation, of the machined plate is shown in Fig.5.40. The graph shows how the surface varies in both the feed and axial directions. Three zones are identified on Fig.5.40. Zone 1 is a transient region dependent on the initial specifications of the plate geometry. Zone 2 is the steady state finished surface. Zone 3 shows the geometry of the workpiece material being fed into the tool. Several comments can be made about this surface profile.

In zone 2, surface errors are present which vary in both the feeding and axial directions. Variations in the feeding direction are present in the form of surface waves. The amplitude and static offset of these waves vary in the axial direction but the wavelength remains constant.

The wavelength is 1.6 (mm) measured from Fig.5.40. Two possible sources of these surface waves are investigated. First the washboarding phenomenon presented in Chapter 3 is considered. The tooth period is $T_c = (60/sZ) = 13$ (ms) and the period of workpiece vibration is $T_v = (1/f_{nc}) = 0.77$ (ms) where $f_{nc} = 1.3$ (kHz) is the plate vibration frequency during cutting. Following the analysis of Chapter 3 gives:

$$r = T_c/T_v = 16.854$$

$$N = (1 - 0.854)^{-1} = 6.85$$

$$T_a = NT_c = 89(ms)$$

This aliasing period (T_a) gives a surface wavelength of (fT_a) = 0.89 (mm) which corresponds to the simulated value of 1.6 (mm). This approach however is not satisfactory due to the uncertainty in estimating the parameter (r). Since the plate frequency in cut and out of cut are different, and only the in cut value was used in the calculations, some error must result. But it should also be noted that since the plate vibration between subsequent teeth is negligeble the out of cut vibration shouldn't have any effect on the cutting vibrations. Therefore since the tool has been seen to impact the workpiece at (-30 deg) immersion angle during each tooth pass, which initiates plate vibrations, the phase variation between the tooth motion and the workpiece vibration will be constant for subsequent teeth. This implies an infinite aliasing period, or a theoretically smooth surface. Since the workpiece surface is not smooth another mechanism must be responsible for generating the surface waves. This mechanism is the plate vibration superimposed onto the tool cutting motion. The cutting speed is ($R\Omega$) = 1154 (mm/s) and the plate vibration frequency is f_{nc} = 1300 (Hz). The resultant wavelength when the plate and tool motions are combined is ($R\Omega/f_{nc}$) = 0.9 (mm) which corresponds to the simulated value of 1.6 (mm). Clearly there isn't a close match between the theoretical and simulated frequencies. This is primarily due to the difficulty of estimating (f_{nc}) from the plate deflection.

Since the first bending mode only is used to estimate the plate motion, displacements will always increase towards the tip of the plate. For this reason both the static surface error and the amplitude of the waves increases towards the tip of the plate. This isn't

the case above the horizontal level where no cutting occurs, because the surface is flat there.

b) Ploughing Included

This simulation considers ploughing forces. Fig.5.41 shows the displacement of the plate at node 14. The result is similar to the displacement obtained when ploughing was neglected except that the in cut vibrations have been greatly reduced in amplitude. This is a result of increased process stiffness and damping. The in cut vibration frequency has risen to 1.5 (kHz) due to the increased process stiffness.

Figs.5.42 and 5.43 show the cutting forces in the (x) and (y) directions respectively.The dynamic component of the cutting forces has been decreased relative to the static component, in comparison with the cutting forces when ploughing was neglected.

The microscopic surface finish (of the machined plate) generated by simulation is shown in Fig.5.44. Three characteristics of the surface finish are discussed. The surface marks have a wavelength of 0.9 (mm) which is significantly less than the wavelength of the surface marks generated when ploughing forces were neglected. Theoretically, the resultant wavelength when the plate and tool motions are combined is $(R\Omega/f_{nc}) = 0.77$ (mm) which is close to the simulated value. The amplitude of the surface waves has decreased due to the corresponding decrease in plate vibrations. The static component of the surface error is close to that of the example which neglected ploughing.

Experimental results for Case 3 are presented next. Graphs showing the experimental results for this case are shown in Figs.5.45 to 5.48.

Fig.5.45 shows the plate displacement measured at node 14. Unfortunately the peaks of the curve were out of the range of the data aquisition system and are not shown in the figure. The measured displacement is comparable to both of the simulation results presented in Figs.5.36 and 5.41.

Figs.5.46 and 5.47 show the (x) and (y) measured forces respectively. The effect of tool runout can be clearly seen in these figures, where one tooth is dominant. The static component of the cutting force is strong in this case because of the increased feedrate used. The simulation results without ploughing (see Figs.5.38 and 5.39) overestimate the dynamic component of the cutting force. This is substantially improved when ploughing is included in the simulation (see Figs.5.42 and 5.43).

The measured surface finish is shown in Fig.5.48. The wavelength from this graph is 2 (mm). This is the same value of wavelength that was obtained in Case 2. This is expected since the cutting speeds and vibration frequencies are close for these two cases. The wavelength obtained for Case 1 was 2.8 (mm) which is larger corresponding to a faster cutting speed. This reinforces the proposed mechanism responsible for surface waviness. Fig.5.48 corresponds to zone 2 of Figs.5.40 and 5.44 whose wavelengths are 1.6 (mm) and 0.9 (mm) for the non-ploughing and ploughing simulations respectively. In the experimental case surface waves are present at the bottom of the plate which are 180 degrees out of phase with the waves elsewhere on the surface. This indicates that tool vibrations are significant and 180 degrees out of phase with the plate motion.

Two trends which are predicted correctly by the simulation results are that no cutting occurs at the top of the plate, and that surface waves are generated. These trends are significant and indicate the possibility of more accurate results with a refined simulation model.

5.4.4 Case No.4

This case considers up milling with a 1 (in.) diameter four fluted end mill with a 30 deg helix angle. The clearance angle is 5 deg with a primary land of 0.5 (mm) and the rake angle is 3 deg. The spindle speed is 1157 (RPM) and the feedrate is 0.394 (in./s). The axial depth of cut is 2.5 (in.). Simulation cutting parameters used are $K_s = 1185$ (MPa)

and $r = 1$; edge cutting forces are neglected. Ploughing forces are included where the yield strength is estimated as 496 (MPa). Only the first bending mode is included in the plate's dynamic model. Structural damping is $\zeta = 0.5$. The time step of the simulation is 10 (μ s). The simulation results are considered first. Graphs showing simulated results for this case are shown in Figs. 5.49 to 5.53.

Fig.5.49 shows the development of the plate motion at node 14 over one second. Both static and dynamic deflections are increasing with time. The graph clearly shows that chatter vibrations are strong for this machining operation. A high pitched loud noise was present during the cutting experiment. The steady state deflection is shown in Fig.5.50. The vibration frequency is about 1.35 (kHz) from the plot, which is less than 1.5 (kHz) which was the value when a zero helix tool was used. This is likely because of the reduced process stiffness from the helical tool geometry. The process stiffness is reduced because the instantaneous axial depth of cut is smaller when a helical tool is used.

Cutting forces in the (x) and (y) directions are given in Figs.5.51 and 5.52 respectively. These forces consist primarily of spikes corresponding to the plate vibration. The high frequency component is stronger in this case than in the previous cases when a zero helix tool was used.

The trend of the surface profile is shown in Fig.5.53. As for previous cases, the plate is not cut at its top and the amount of material increases towards the root of the plate. Only a few points are shown on the figure which make it difficult to discuss this result.

Experimental results for Case 4 are presented next. Graphs of the experimental results for this case are shown in Figs.5.54 to 5.57.

Fig.5.54 shows the plate displacement measured at point 14. The effect of runout is strong in this graph. Although the simulated result (see Fig.5.50) has a similar shape, the magnitude of the cutting forces is overpredicted. This error is the result of two seperate mechanisms. Since only a single mode solution is used in the dynamic modelling of the

plate, the deflection will be overpredicted near its top. The cutting mechanism is an oblique process when a helical tool is used, this may result in significant errors of the force prediction.

Measured forces in the (x) and (y) directions are shown in Fig.5.55 and 5.56 respectively. The forces have a strong dynamic component. The simulation overpredicts the magnitude of the cutting forces. This may be a result of inadequate modelling of the cutting process or excitation of the plate due to the discretization of the helix angle. Also since the dynamic model considers only a single mode, the deflection errors will be reflected in the cutting forces.

The measured surface profile in the axial direction is given in Fig.5.57. The trend of the simulated result (see Fig.5.53) is correct but significant errors are present due to inaccurate prediction of the plate displacement. The surface generation mechanism is significantly different when a helical tool is used. In this case the cutting edge first contacts the workpiece at its root rather than at its tip. Thus the transient vibrations resulting from the straight tooth impacting the tip of the plate are not present here. This is evident by the minimal variations of the plate surface in the feeding direction when a helical tool is used. More work must be done to achieve a clear understanding of the surface generation mechanism for plate machining with helical tools.

5.5 Future Work

It is clear from the results presented that some additional work must be carried out to fully model the milling of flexible workpieces. Considerations of several aspects of this work are discussed in this section.

5.5.1 Cutting Process

The method used to model the cutting process in this work is mostly the application of known procedures to a slightly different problem. Metal removal by the chip formation process has complex physics involving large plastic deformations, shearing, ploughing, adhesion, and significant heat flows. Due to this complexity the traditional approach in most practical studies has been to simplify the process and model it with a set of empirical rules. In the case of machining flexible structures considered here, the chip width is necessarily large with a correspondingly small chip thickness. The resultant chip shape is unusual and the physics which govern the removal of it are different from those for the removal of a more usually shaped chip. Also the influence of the bottom edges of the end mill will be less significant as the axial depth of cut is increased.

Since the metal cutting physics are different from those used to develop the current methods of force prediction, the introduction of a new cutting force model would be appropriate. This is a difficult task. For example, since the model would be used for applications with small feedrates, the edge cutting forces will be more significant than usual. Because these forces are strongly dependent on the geometry of the cutting edge some account of the tool wear may be required to obtain accurate results. Another difficulty arises due to ploughing encountered during the relatively large deflections. The plastic flow involved is very complex and any model of this mechanism should also account for changes in the cutting edge geometry.

5.5.2 Kinematics and Surface Generation

The kinematics of dynamic milling have been accurately modelled in this work. The purpose of this model is to generate chip loads and to produce detailed surface finishes. The approach taken here, as outlined in Chapter 3, is different from the method used by

other authors. Justification for taking this approach is to obtain accurate surface finish results and to model applications with relatively large workpiece deflections.

Although this model has proven adequate for the current application, four possible areas of investigation are given. The tool geometric parameters can be expanded to include a ball end and an improved runout model. Multi-axis machining geometry should be considered for milling parts with more complex shapes. Inefficient algorithms can be revised to decrease the time required for each simulation. Also the kinematics of surface generation for cutting plates with helical tools must be further investigated.

5.5.3 Dynamic Modelling of the Plate and Tool

In Chapter 4 the stepped plate was modelled satisfactorilly using the finite element method. It would also be advantageous to model the end mill dynamics in a similar manner. An alternative approach to modelling the dynamics of both the plate and the tool is by modal testing techniques and model construction from the measured frequency response functions. This method may be easier and more efficient if parts of more complex geometry are considered.

The effect of material removal on the dynamics of the workpiece should also be considered. If the workpiece is discretized into several cutting zone locations its dynamic model can be obtained for each location. When the cutting zone is between two of these models the workpiece dynamics can be interpolated to provide an accurate representation of its structural characteristics.

If steadies are used to reduce vibration when machining flexible workpieces, their interaction with the workpiece dynamics should be modelled.

5.5.4 Experimental Work

One difficulty with the experimental measurements taken while machining flexible plates in this work was the measurement of plate deflections. The deflections were large and of a high frequency. This resulted in several steel shims becoming loose and falling off the aluminum plates. For this reason it might be advantageous to machine steel plates if experiments such as these are attempted again. Also a more rigid plate should be used if deflection measurements are desired at the top of the plate.

5.5.5 Practical Solutions

Two solutions for reducing machining errors of flexible workpieces are presented. These methods are only intended to reduce the static errors and won't reduce the waves present on the machined surface.

The first solution involves machining a plate with the desired process parameters and measuring the surface errors. A new part is machined with the tool offset toward the workpiece an amount equal to the measured error. This method is itterative since the dynamics of the workpiece will change depending on machining errors.

The second method requires modelling the dynamics of the workpiece at several discrete cutting zones. The local stiffness of the plate is then used to determine the required offset of the tool. This method is more accurate and would be expected to give good results on the first attempt.

5.6 Conclusions

Four cases of machining flat plates have been examined in this chapter by both simulation and experimental studies. Although perfect matching between these results wasn't obtained, several important trends were predicted by simulation which were realized in

the experiments. These included: prediction of waves on the finished workpiece surface, lack of material removal at the top of the plate, an increased vibration frequency during cutting, high frequency components present in the cutting forces as a result of higher mode activity near the root of the plate and the reduction of dynamic cutting force amplitudes by the introduction of a ploughing force model. These trends suggest that highly realistic results could be obtained if a more accurate cutting force model is implemented. The tool dynamic response could also be included to improve the correlation between experimental and simulation results.

Conditions of Simulation and Experiments for Milling of Plates

Plate dimensions: 2.5 x 2.5 x 0.1 (in.) to 2.5 x 2.5 x 0.05 (in.)
63.5 x 63.5 x 2.54 (mm) to 63.5 x 63.5 x 1.27 (mm)

Common parameters for each case are:

Axial depth of cut	(2.5 in.)
Number of flutes on the cutter	(4)
Specific cutting pressure	(1185 MPa)
Cutting force ratio	(1)
Yield pressure	(496 MPa)

Specific parameters for each case are:

		CASE #1	CASE #2	CASE #3	CASE #4
Tool Diameter	(in.)	0.75	0.75	0.75	1
Helix Angle	(deg)	0	0	0	30
Rake Angle	(deg)	5	5	5	3
Clearance Angle	(deg)	10	10	10	5
Spindle Speed	(rpm)	1500	1157	1157	1157
Feed	(in./s)	0.015	0.02	0.4	0.4
Ploughing		no	no	a) no b) yes	yes

Table 5.1: Parameters for Four Cases of Plate Machining.

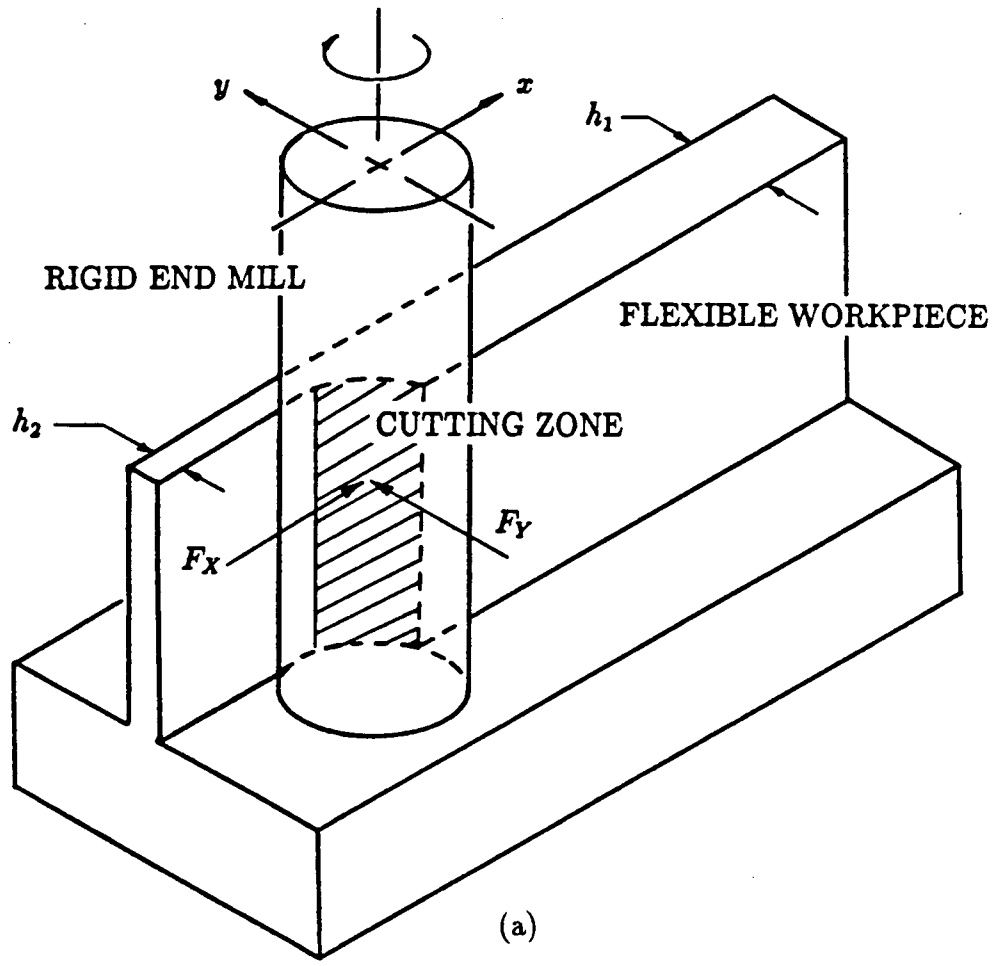

Figure 5.1: (a) Machining of a flexible workpiece and (b) Interaction between the tool and the workpiece.

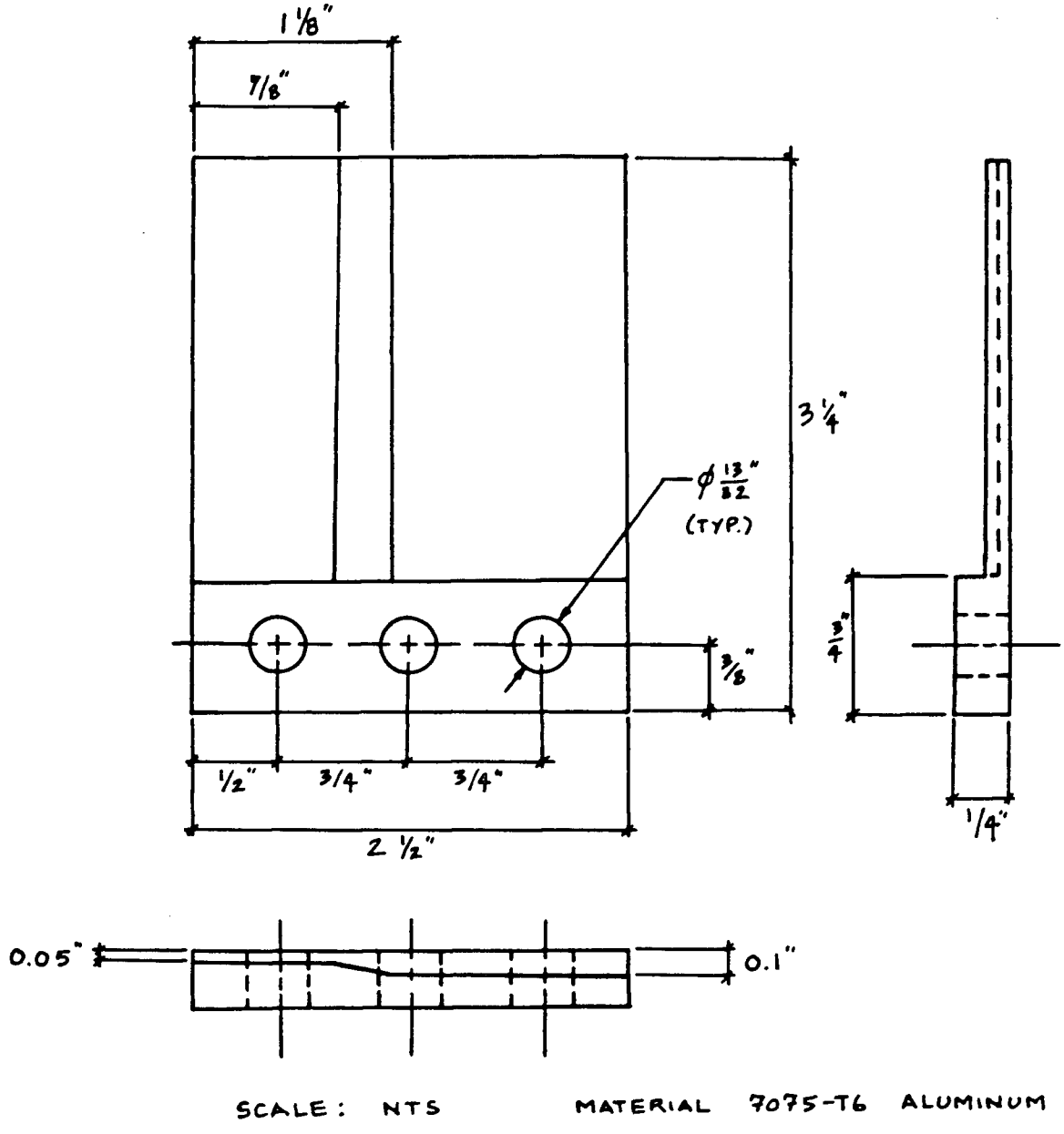

Figure 5.2: Shop drawing of plate for experimental work.

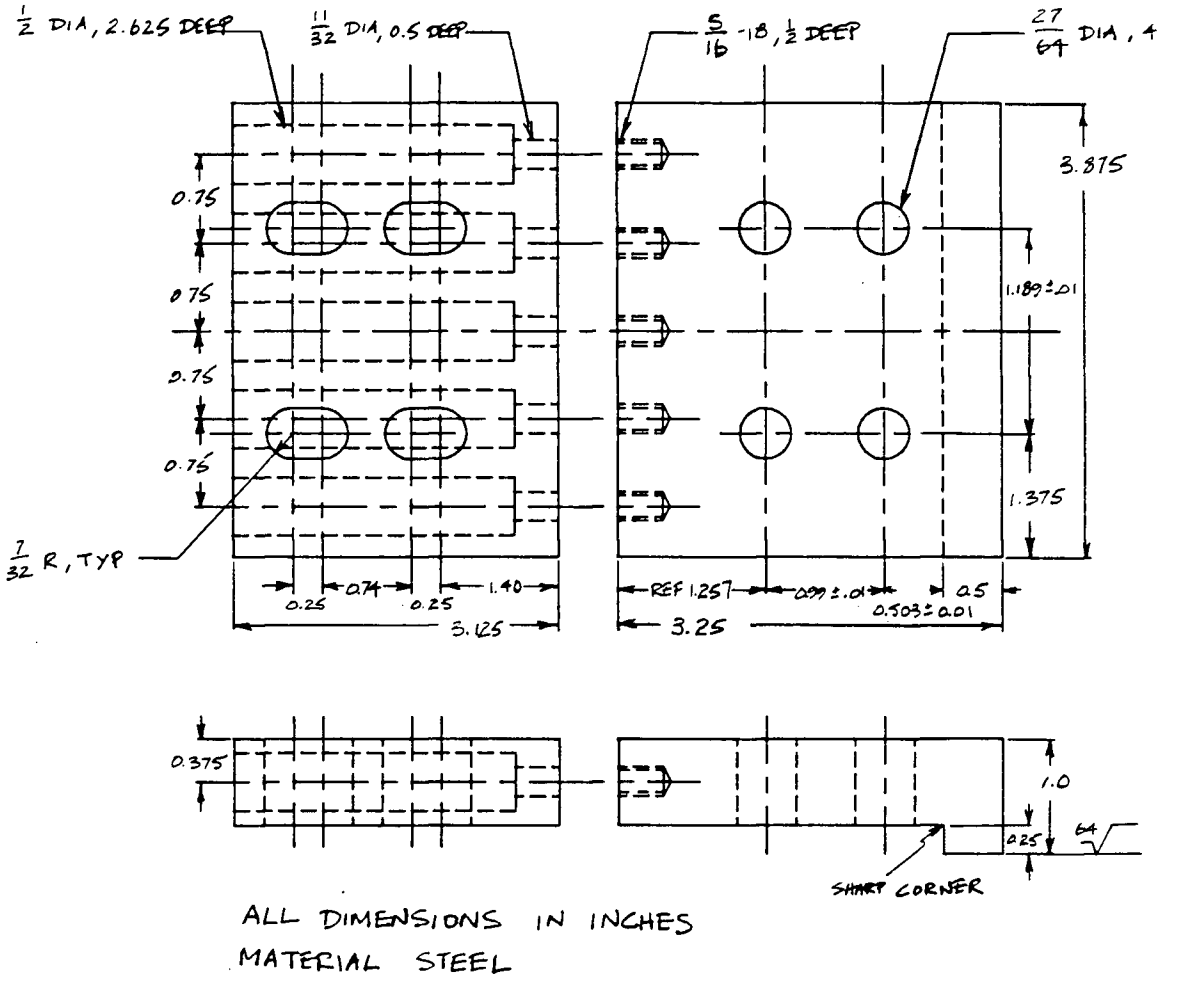

Figure 5.3: Mounting bracket for experimental plate machining.

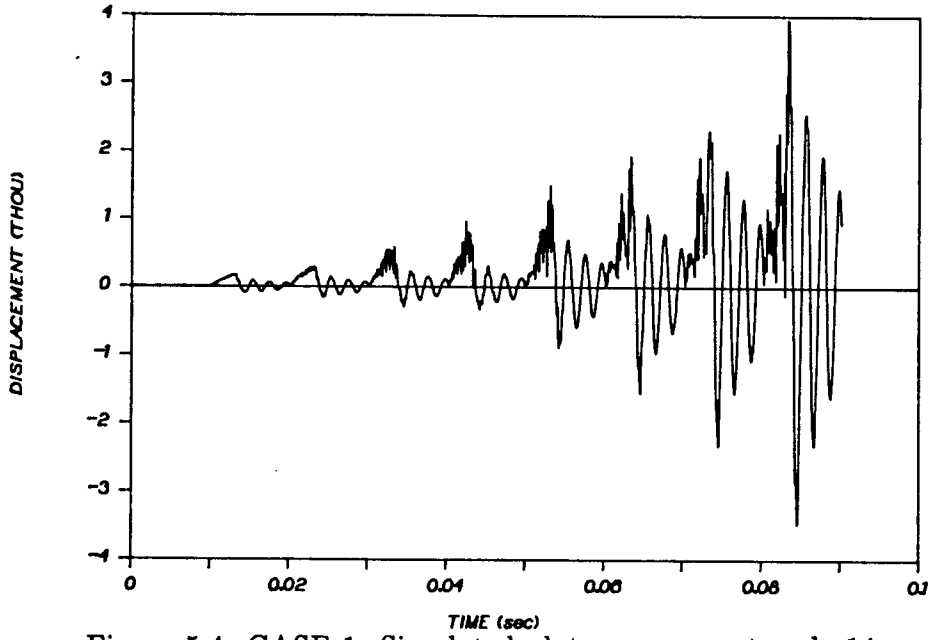

Figure 5.4: CASE 1: Simulated plate response at node 14.

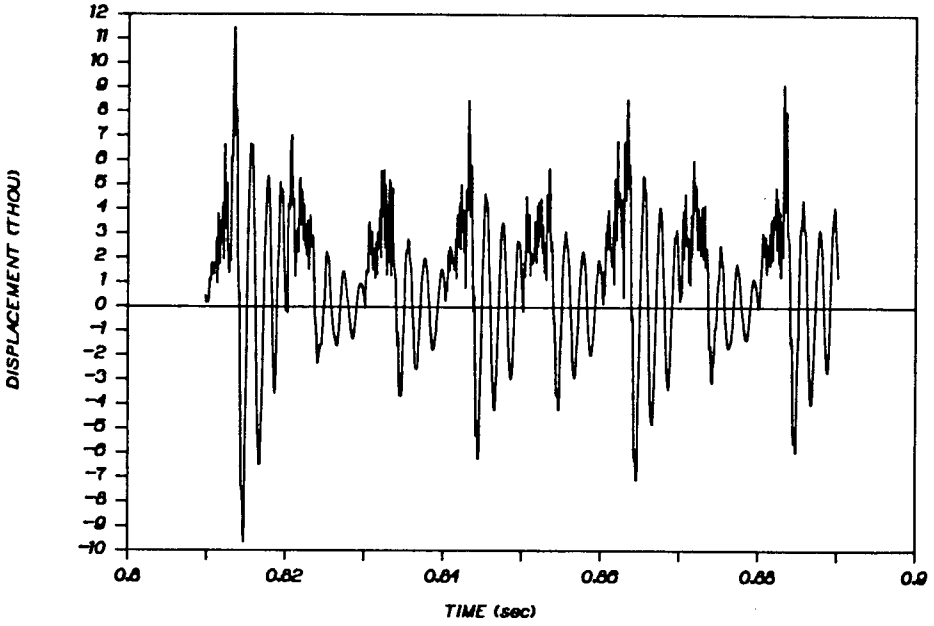

Figure 5.5: CASE 1: Simulated plate response at node 14.

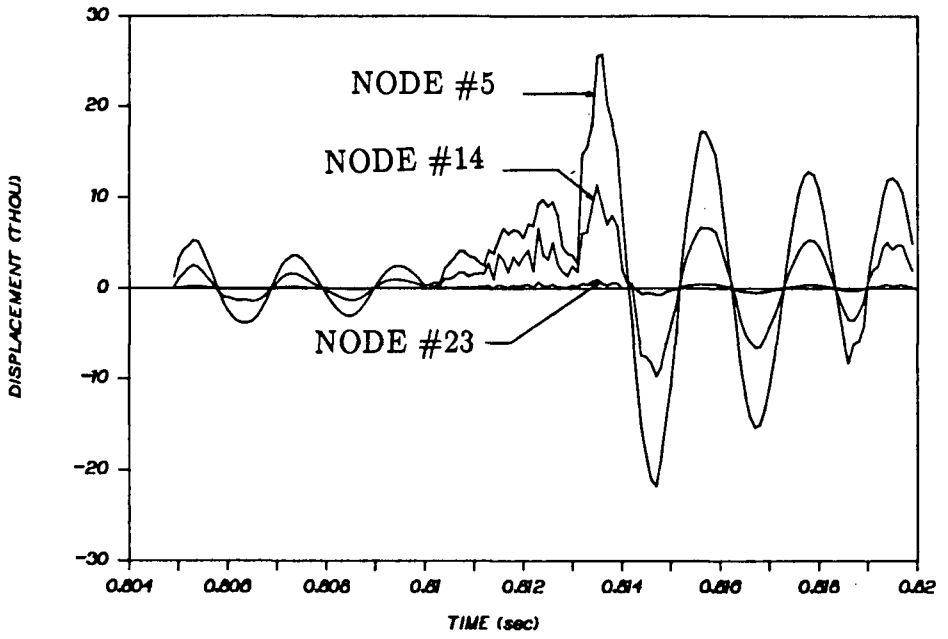

Figure 5.6: CASE 1: Simulated detailed plate response.

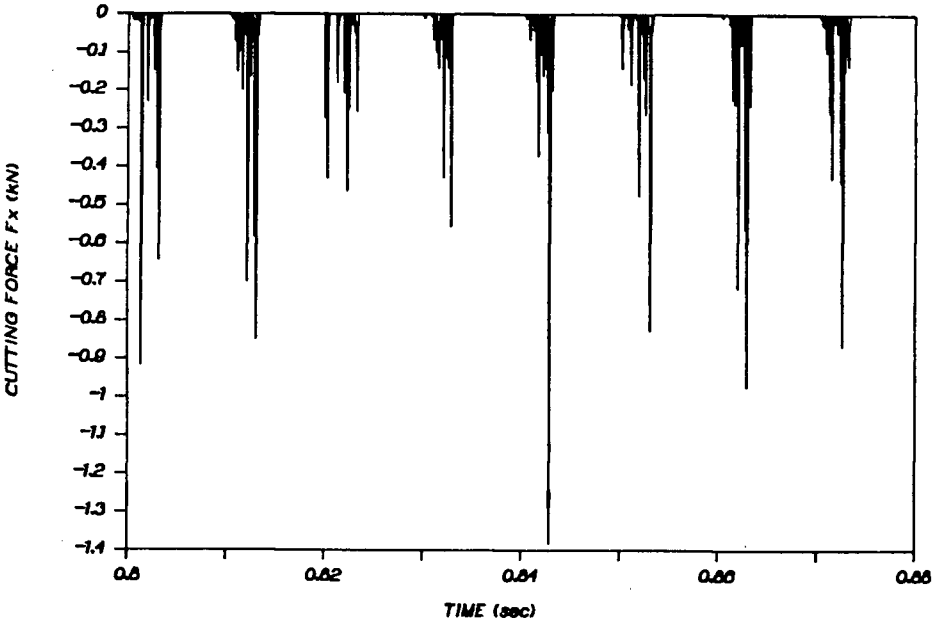

Figure 5.7: CASE 1: Simulated x-cutting force.

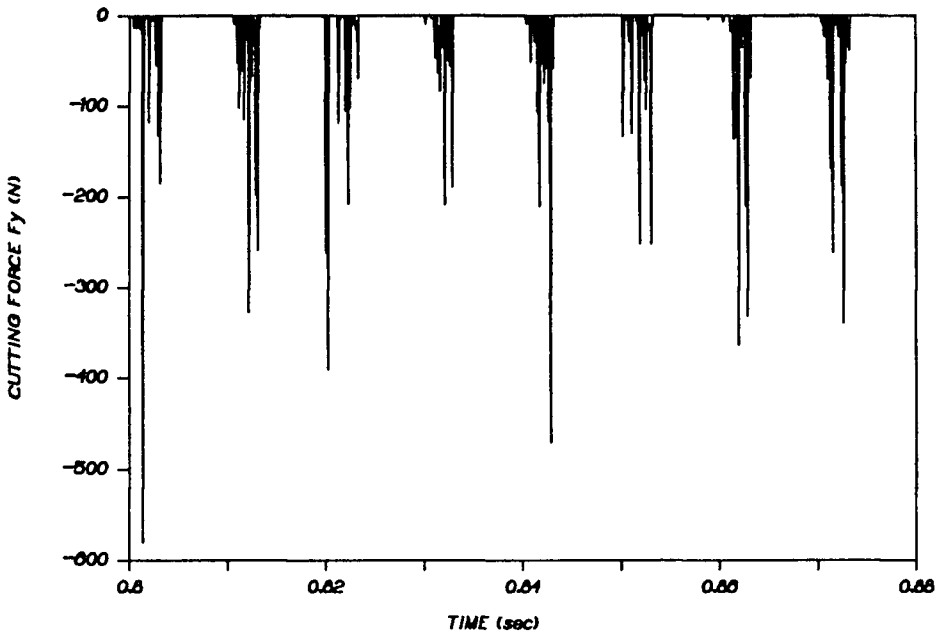

Figure 5.8: CASE 1: Simulated y-cutting force.

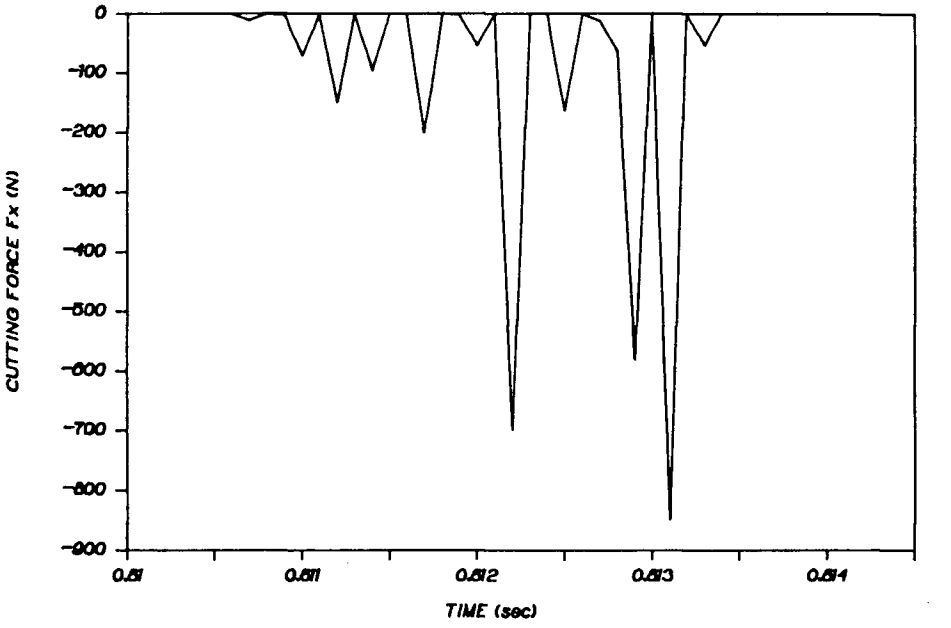

Figure 5.9: CASE 1: Simulated detailed x-cutting force.

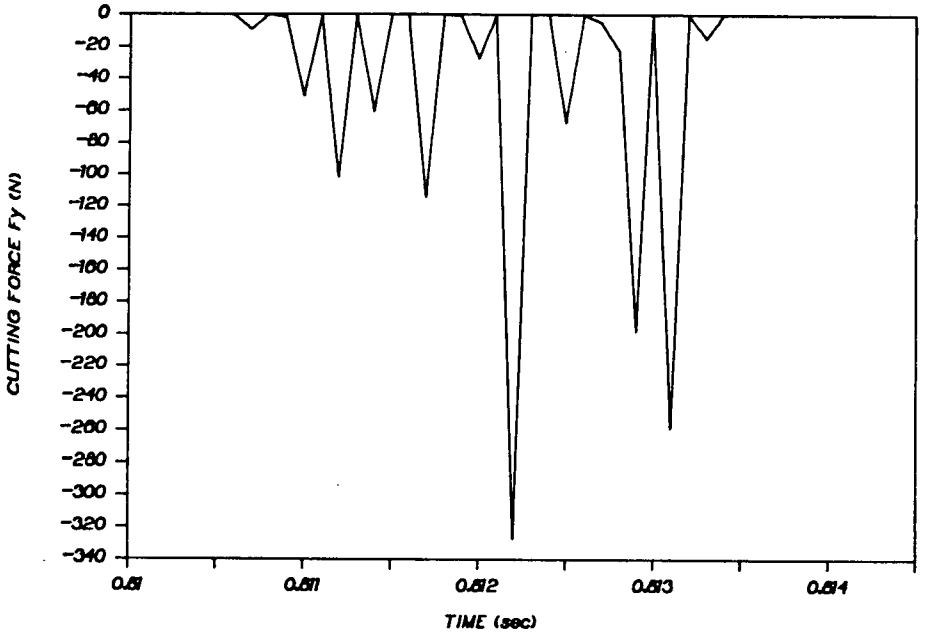

Figure 5.10: CASE 1: Simulated detailed y-cutting force.

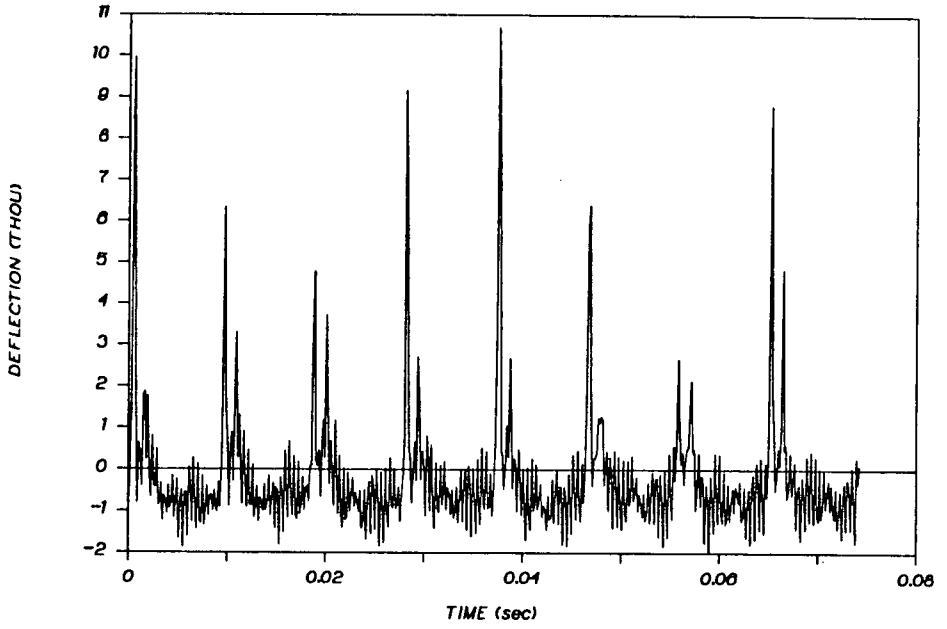

Figure 5.11: CASE 1: Experimental displacement at node 14.

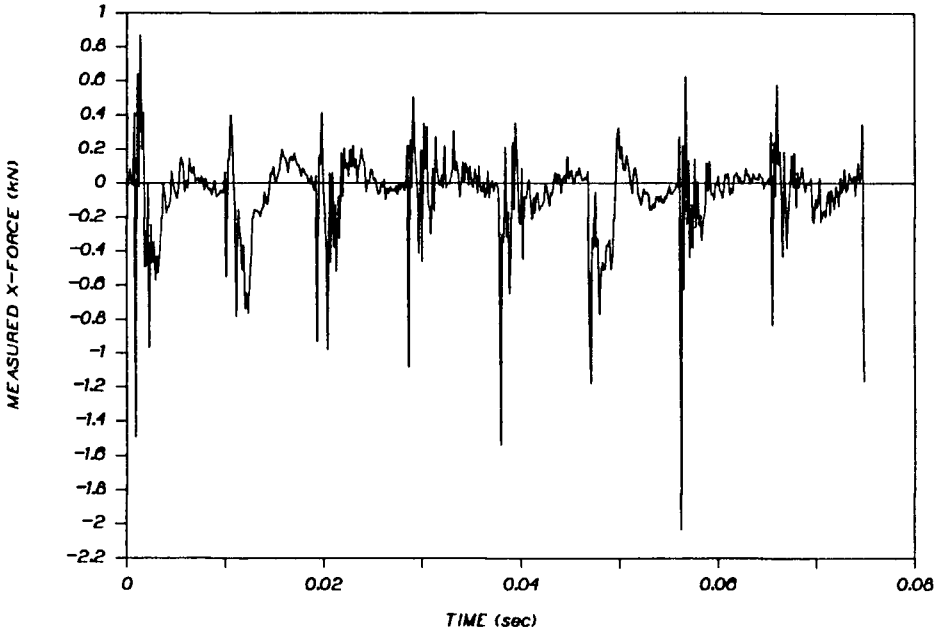

Figure 5.12: CASE 1: Experimental x-cutting force.

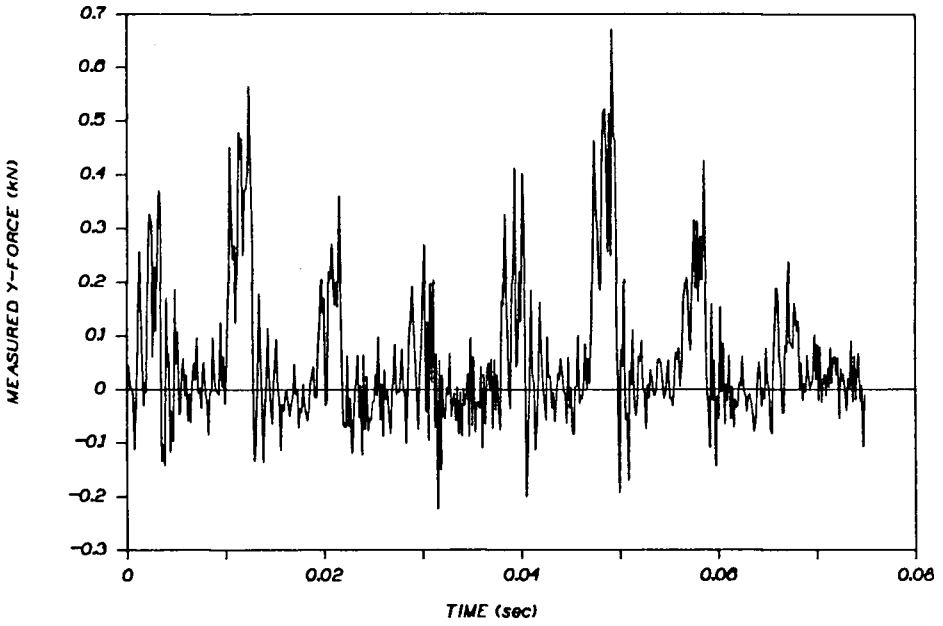

Figure 5.13: CASE 1: Experimental y-cutting force.

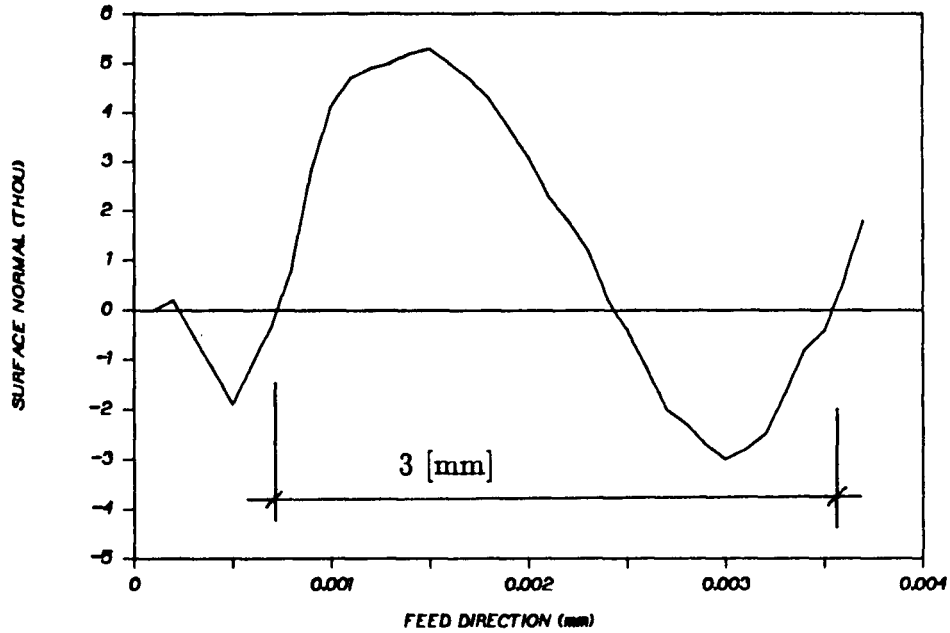

Figure 5.14: CASE 1: Experimentally measured surface finish at node 14.

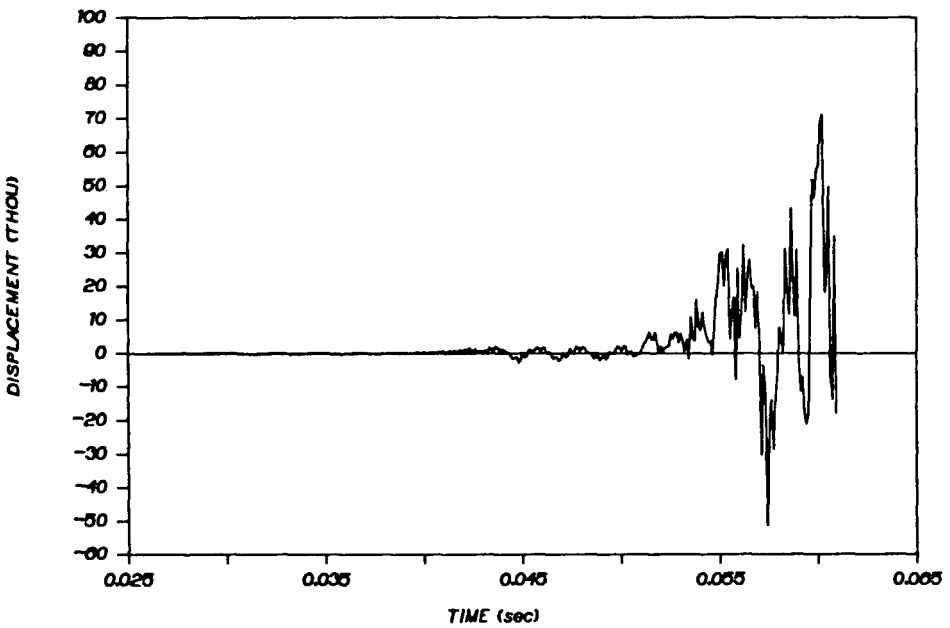

Figure 5.15: CASE 2: Simulated plate response at node 14 ($\zeta = 0.005$).

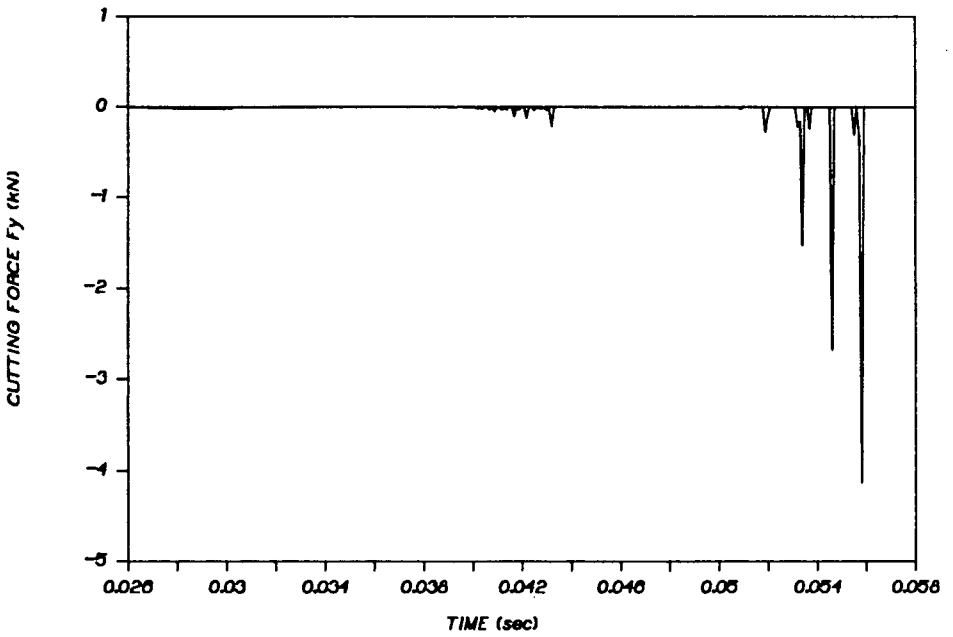

Figure 5.16: CASE 2: Simulated cutting force ($\zeta = 0.005$).

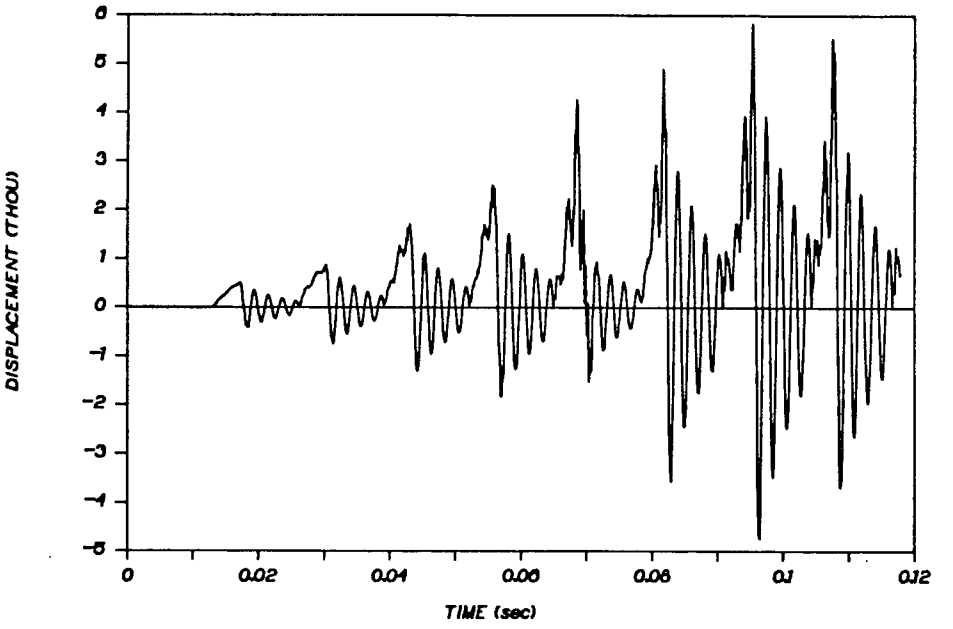

Figure 5.17: CASE 2: Simulated plate response at node 5 ($\zeta = 0.05$).

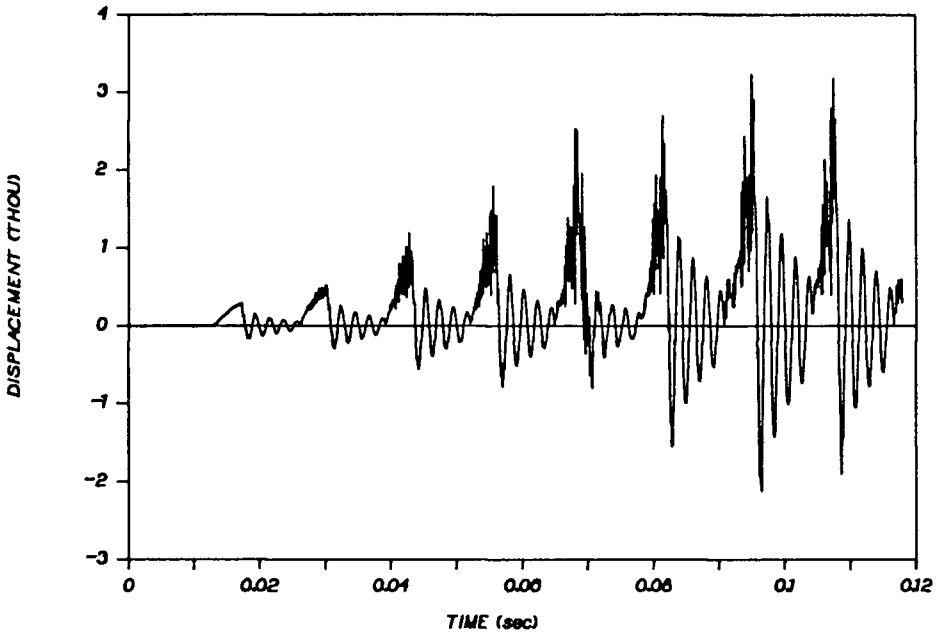

Figure 5.18: CASE 2: Simulated plate response at node 14 ($\zeta = 0.05$).

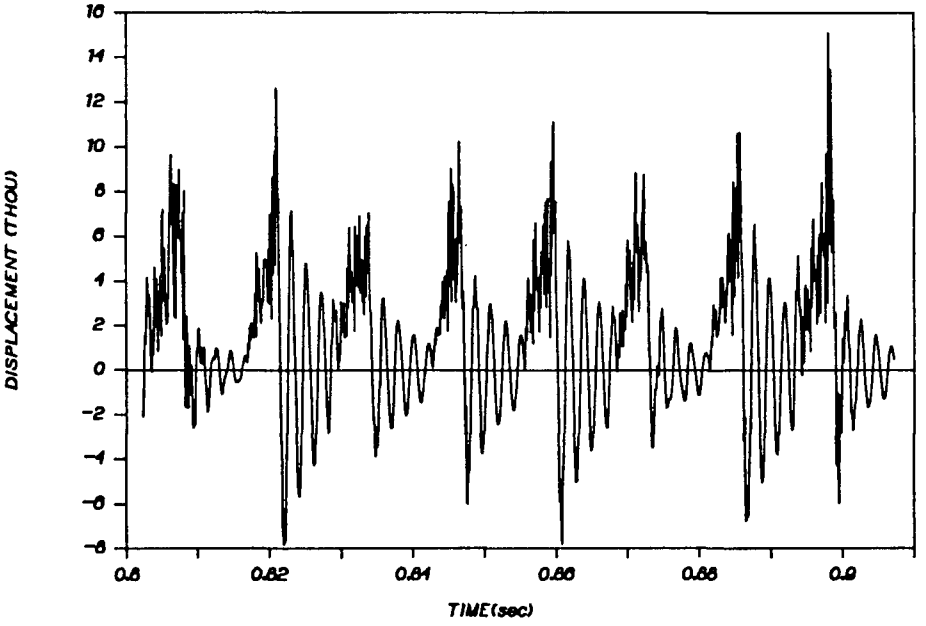

Figure 5.19: CASE 2: Simulated plate response at node 14 ($\zeta = 0.05$).

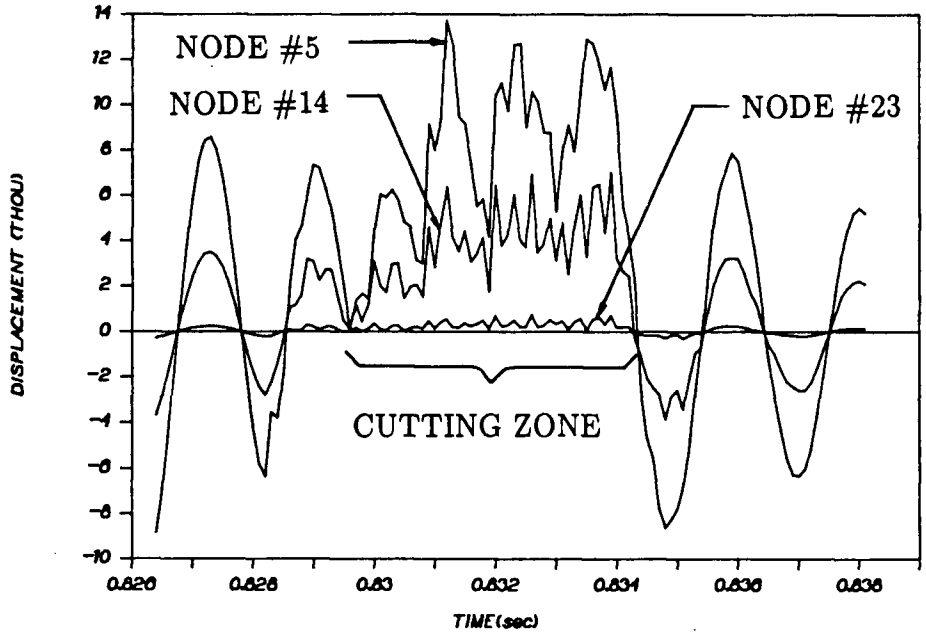

Figure 5.20: CASE 2: Simulated detailed plate response ($\zeta = 0.05$).

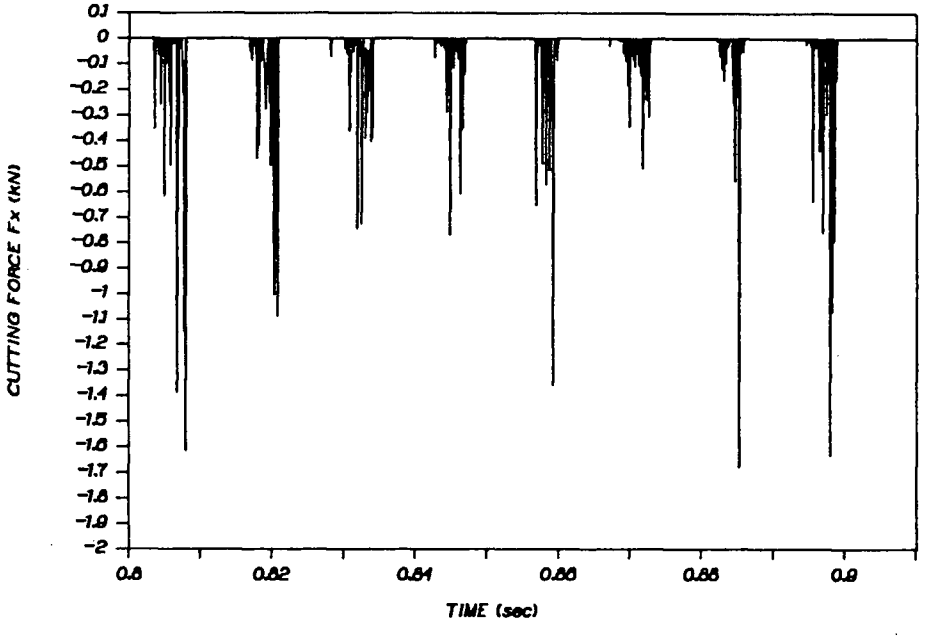

Figure 5.21: CASE 2: Simulated x-cutting force ($\zeta = 0.05$).

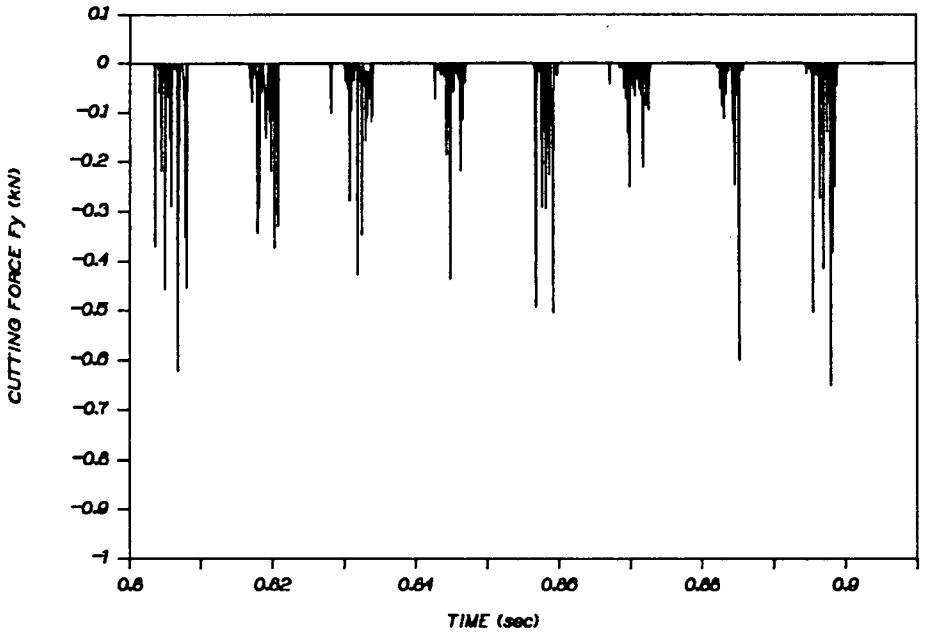

Figure 5.22: CASE 2: Simulated y-cutting force ($\zeta = 0.05$).

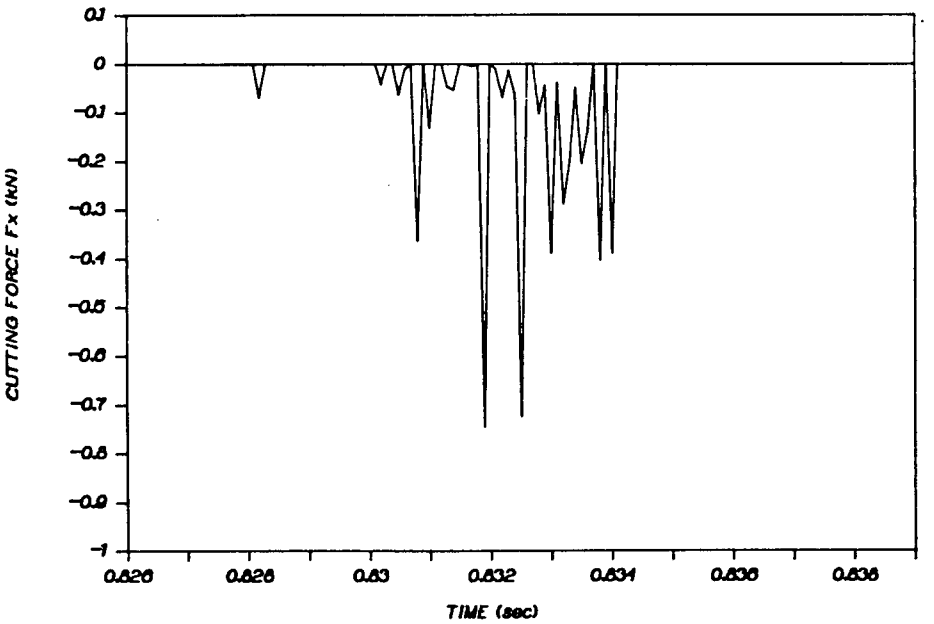

Figure 5.23: CASE 2: Simulated detailed x-cutting force ($\zeta = 0.05$).

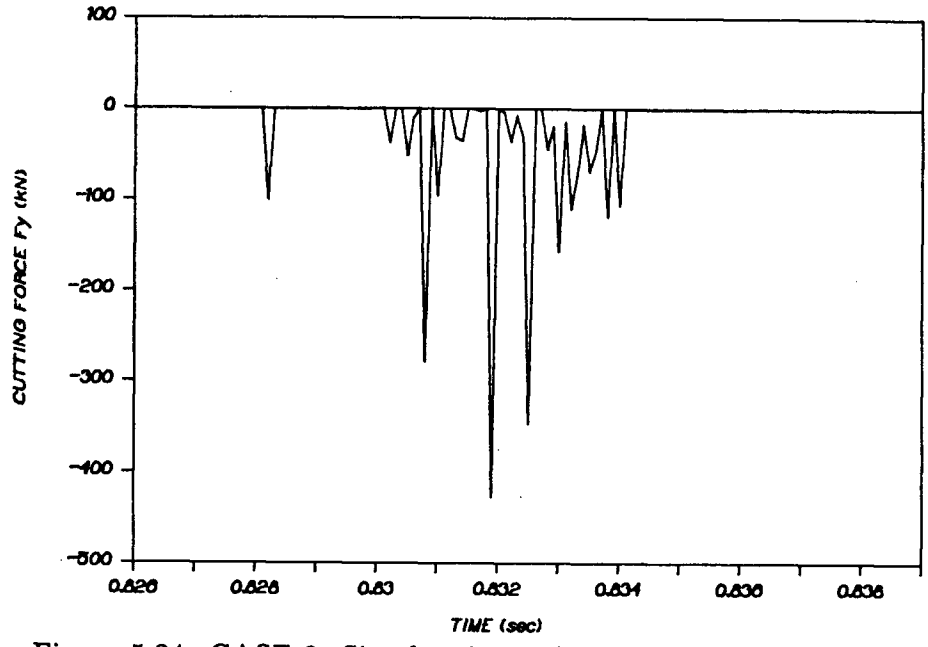

Figure 5.24: CASE 2: Simulated detailed y-cutting force ($\zeta = 0.05$).

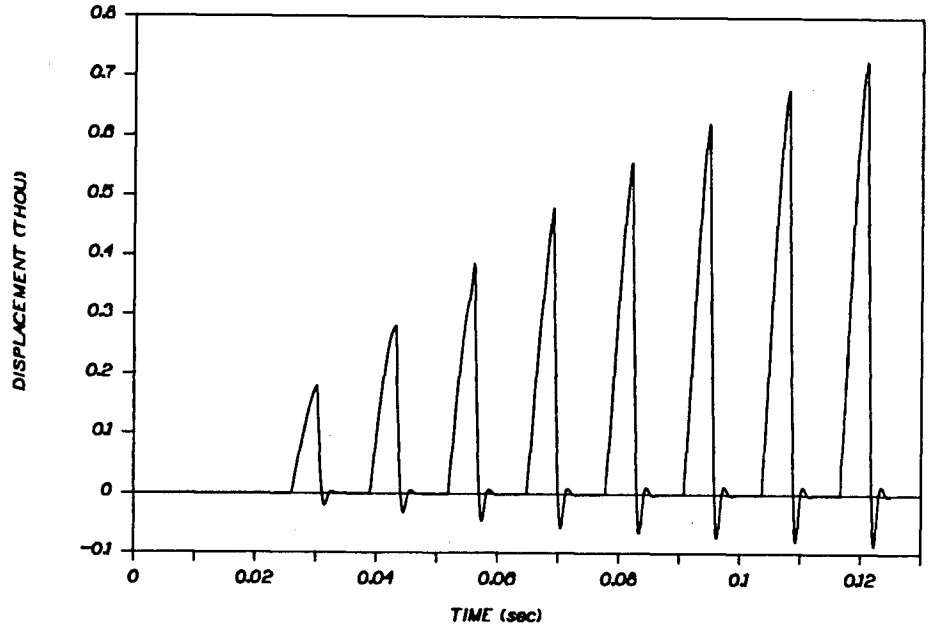

Figure 5.25: CASE 2: Simulated plate response at node 14 ($\zeta = 0.5$).

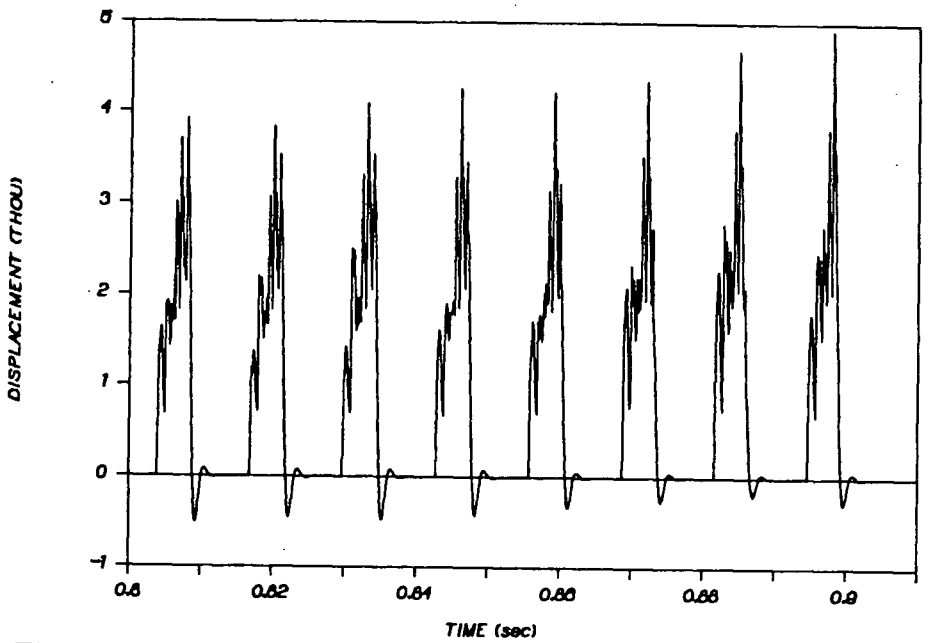

Figure 5.26: CASE 2: Simulated plate response at node 14 ($\zeta = 0.5$).

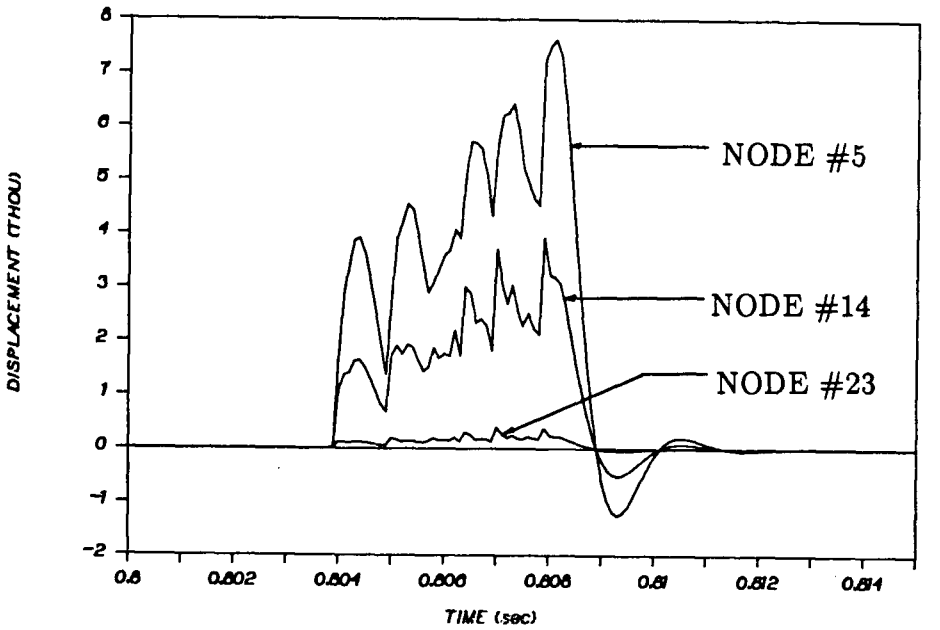

Figure 5.27: CASE 2: Simulated detailed plate response ($\zeta = 0.5$).

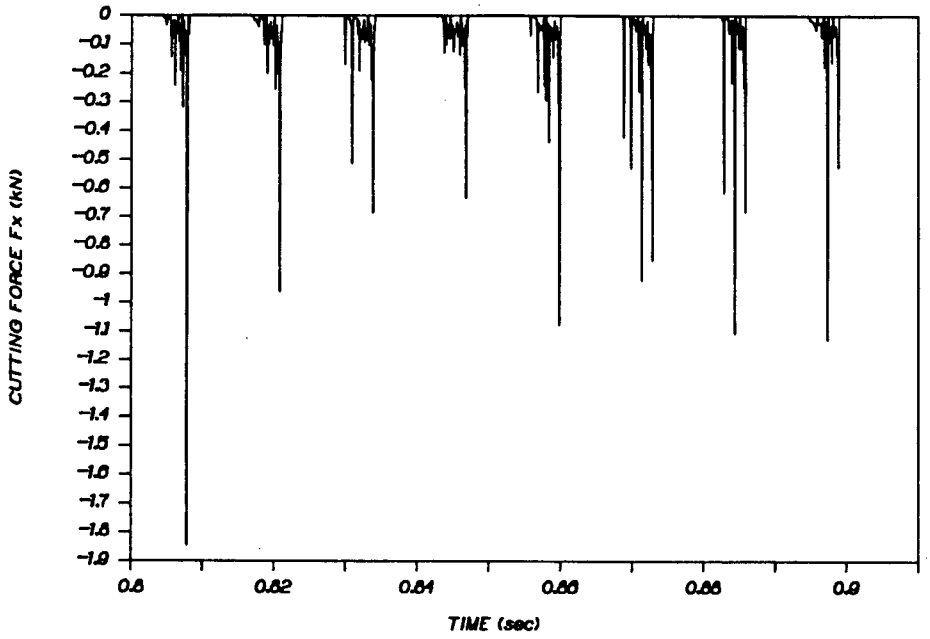

Figure 5.28: CASE 2: Simulated x-cutting force ($\zeta = 0.5$).

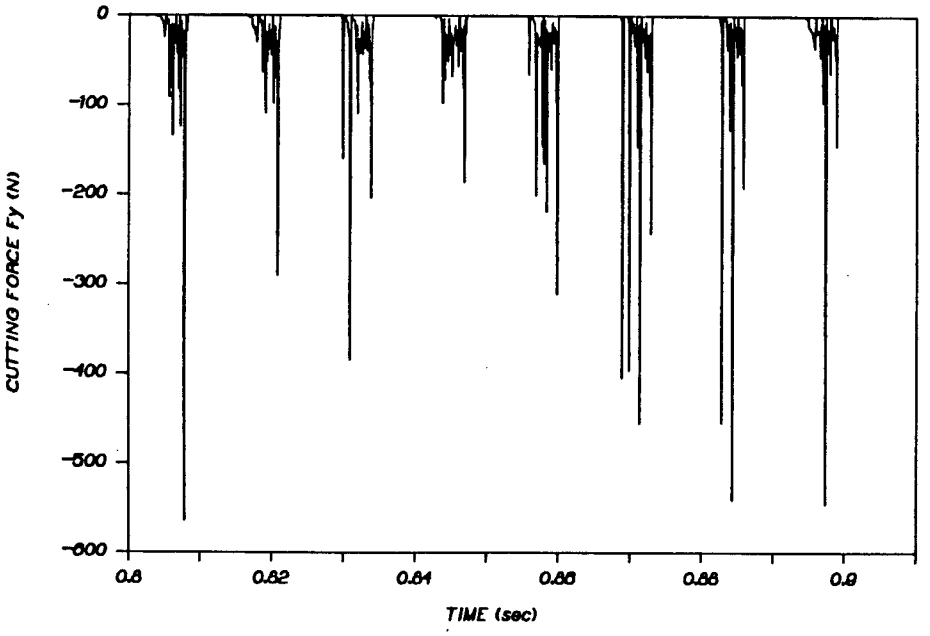

Figure 5.29: CASE 2: Simulated y-cutting force ($\zeta = 0.5$).

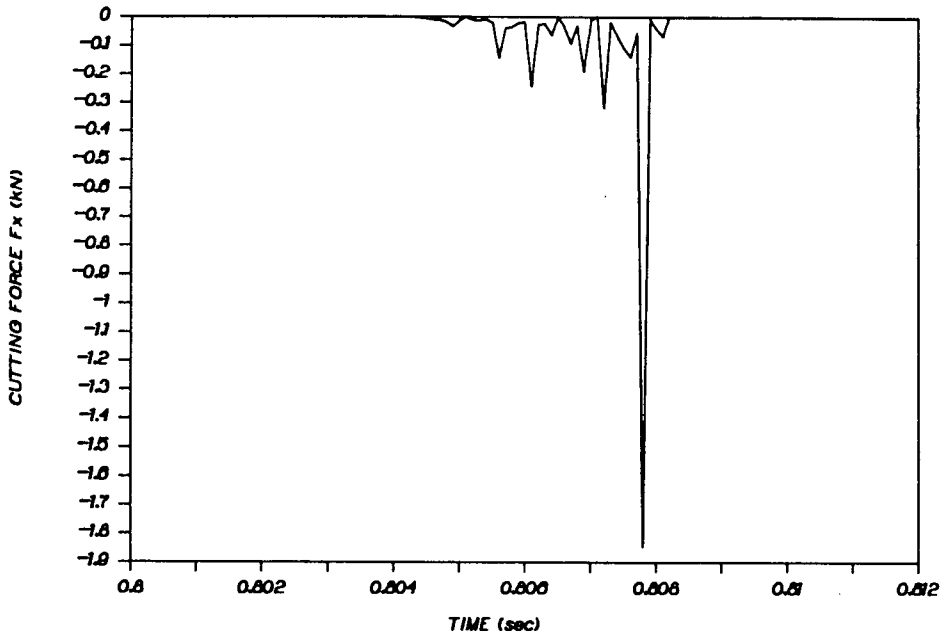

Figure 5.30: CASE 2: Simulated detailed x-cutting force ($\zeta = 0.5$).

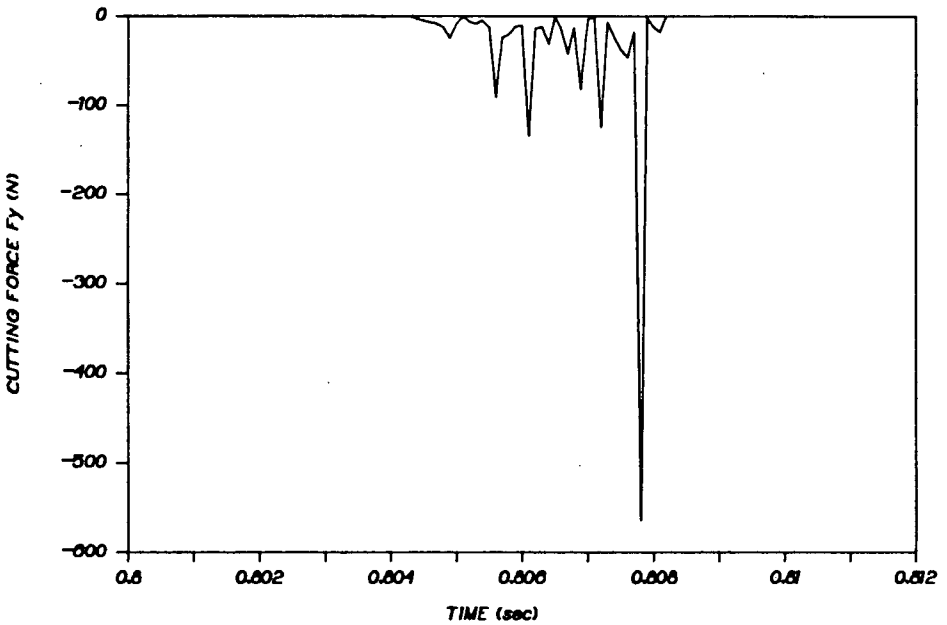

Figure 5.31: CASE 2: Simulated detailed y-cutting force ($\zeta = 0.5$).

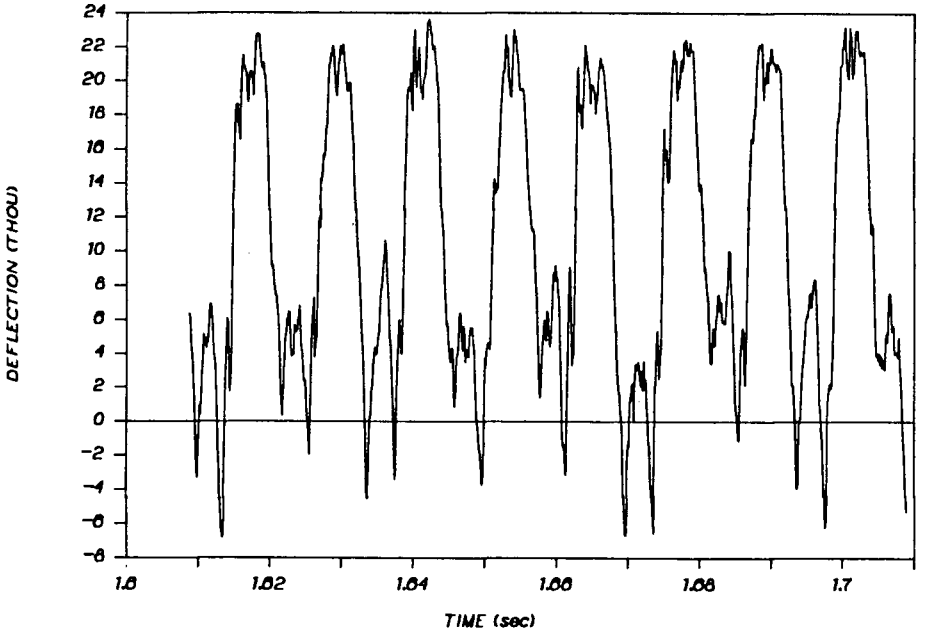

Figure 5.32: CASE 2: Experimental displacement at node 14.

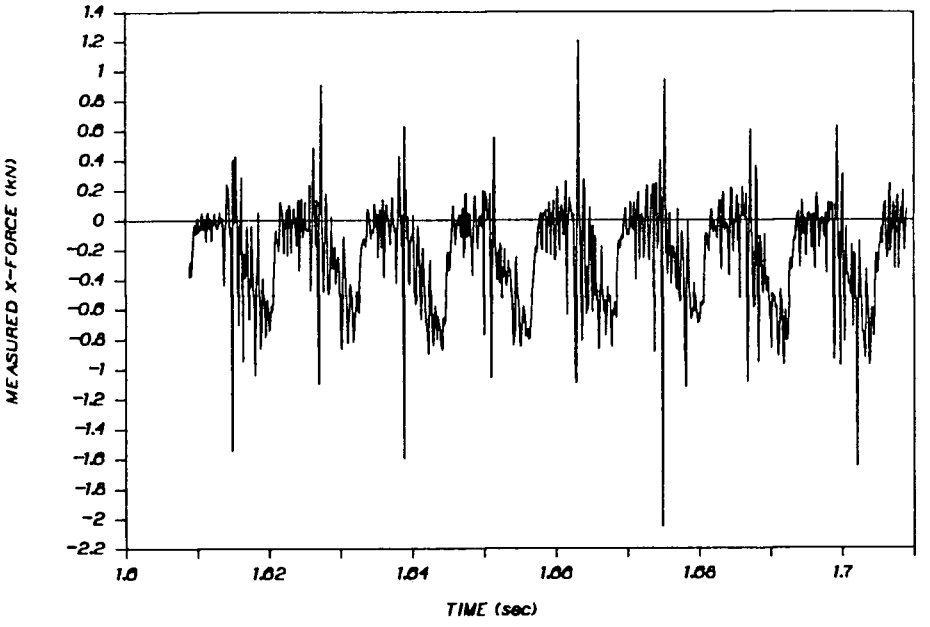

Figure 5.33: CASE 2: Experimental x-cutting force.

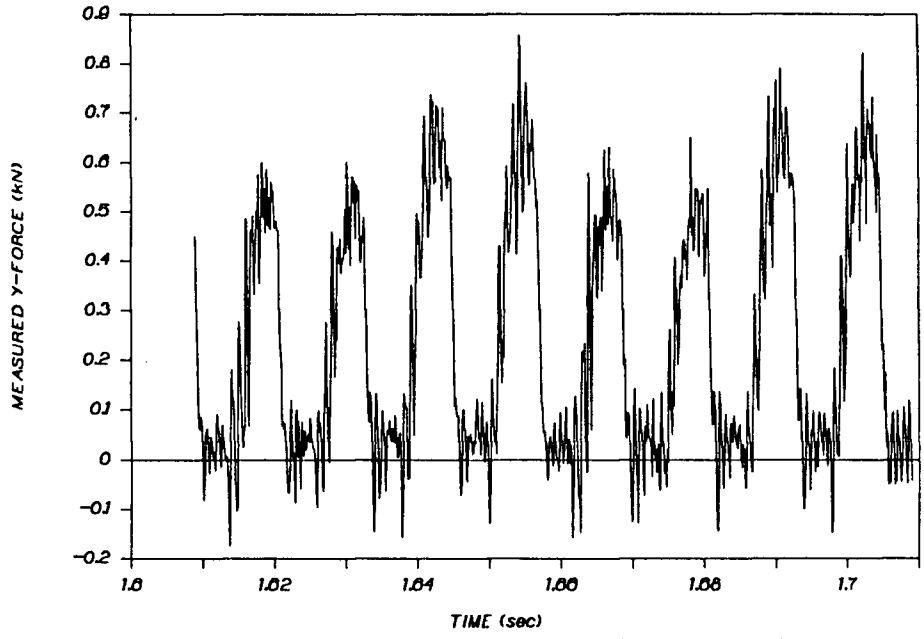

Figure 5.34: CASE 2: Experimental y-cutting force.

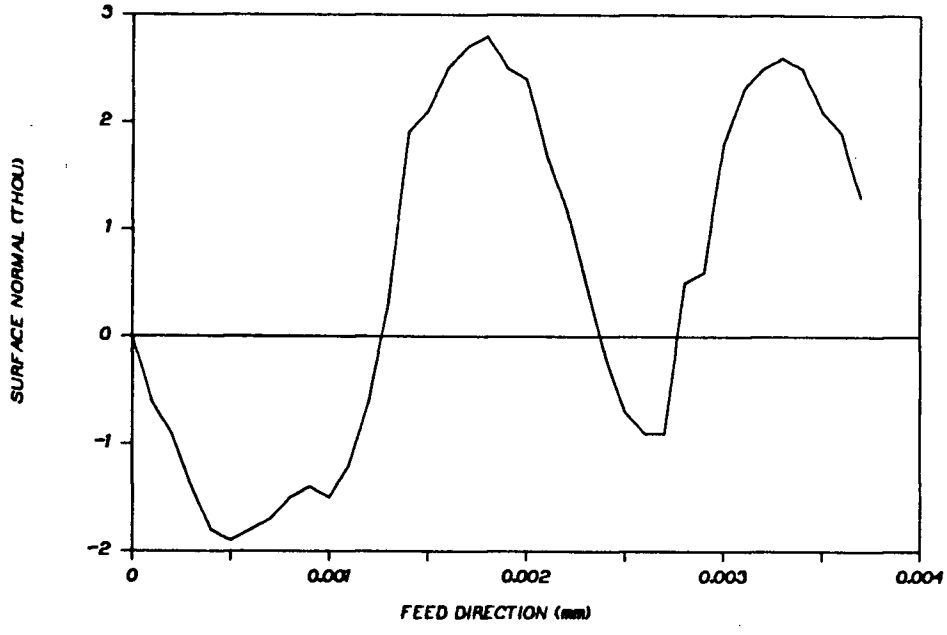

Figure 5.35: CASE 2: Experimentally measured surface finish at node 14.

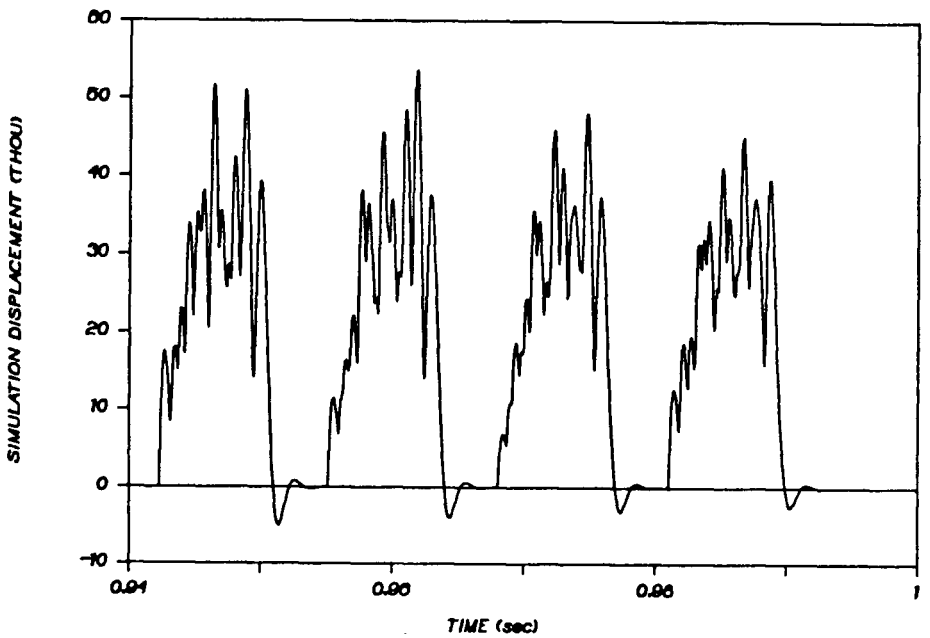

Figure 5.36: CASE 3: Simulated displacement at node 14 (no ploughing).

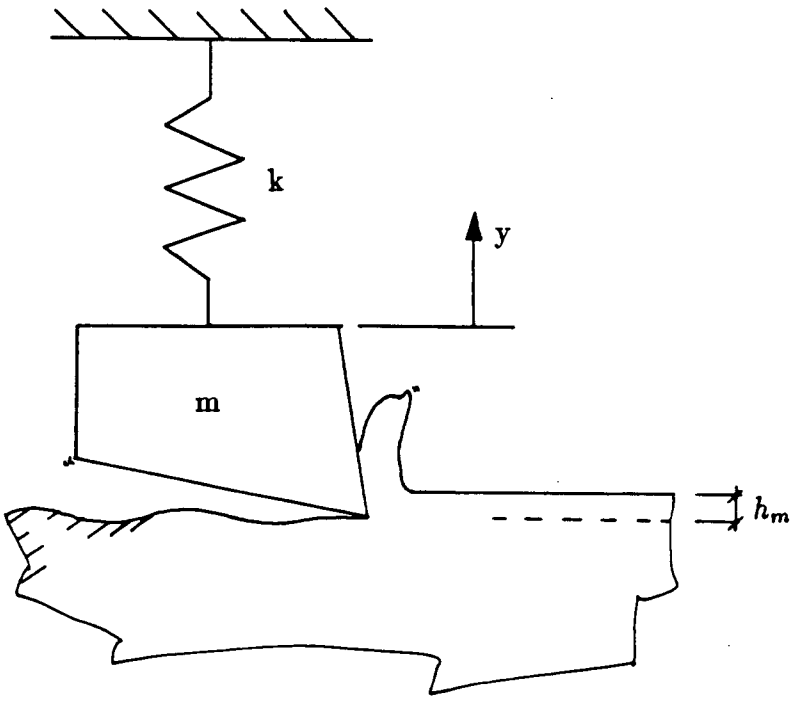

Figure 5.37: Simple case of dynamic cutting.

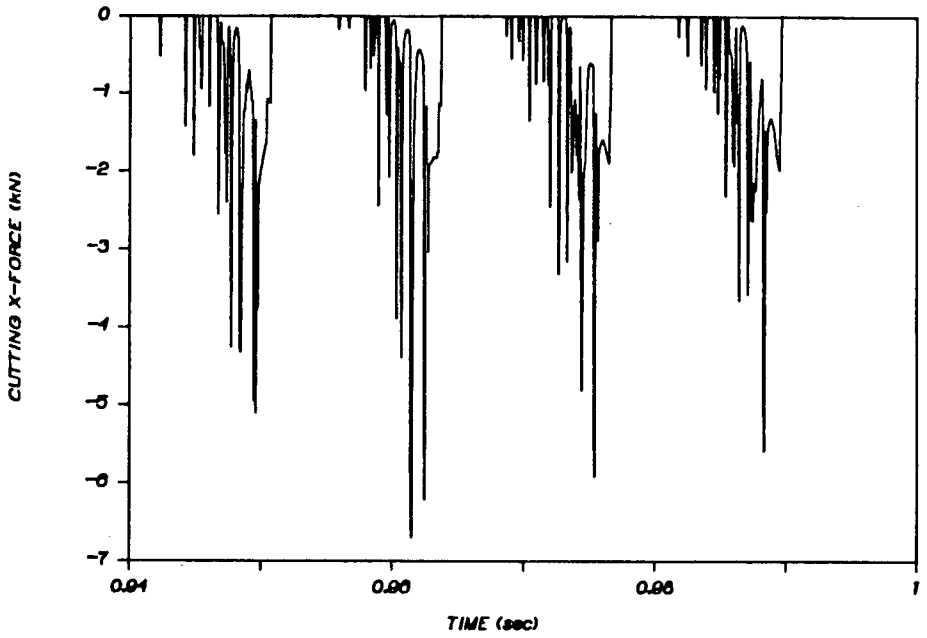

Figure 5.38: CASE 3: Simulated x-cutting force (no ploughing).

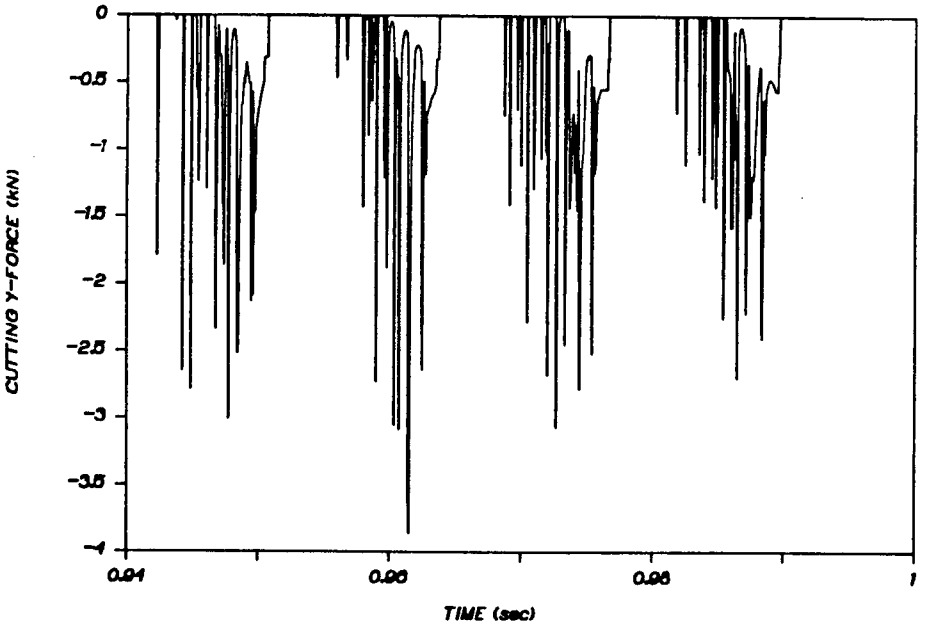

Figure 5.39: CASE 3: Simulated y-cutting force (no ploughing).

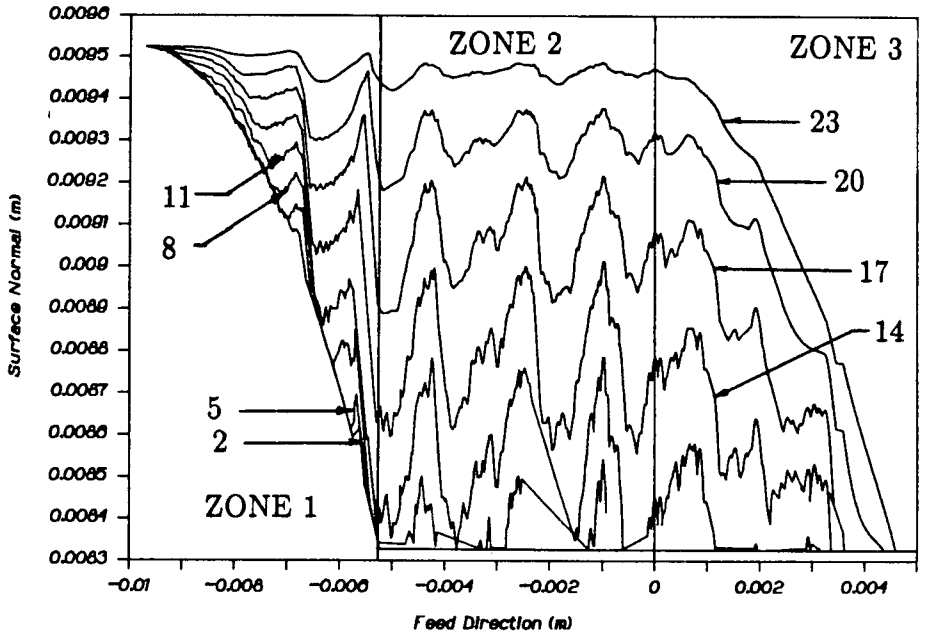

Figure 5.40: CASE 3: Simulated microscopic surface finish (no ploughing).

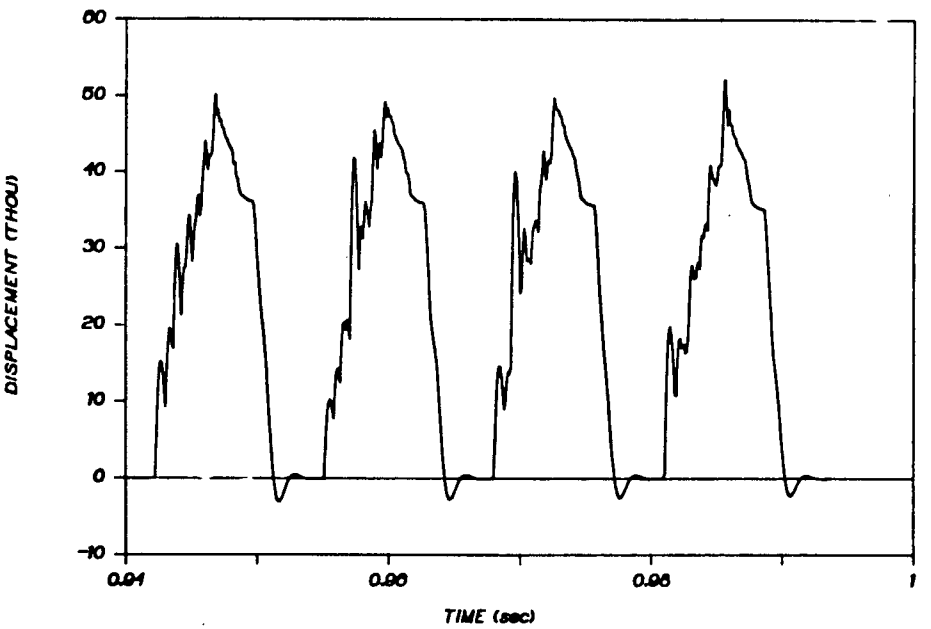

Figure 5.41: CASE 3: Simulated displacement at node 14 (ploughing incl.).

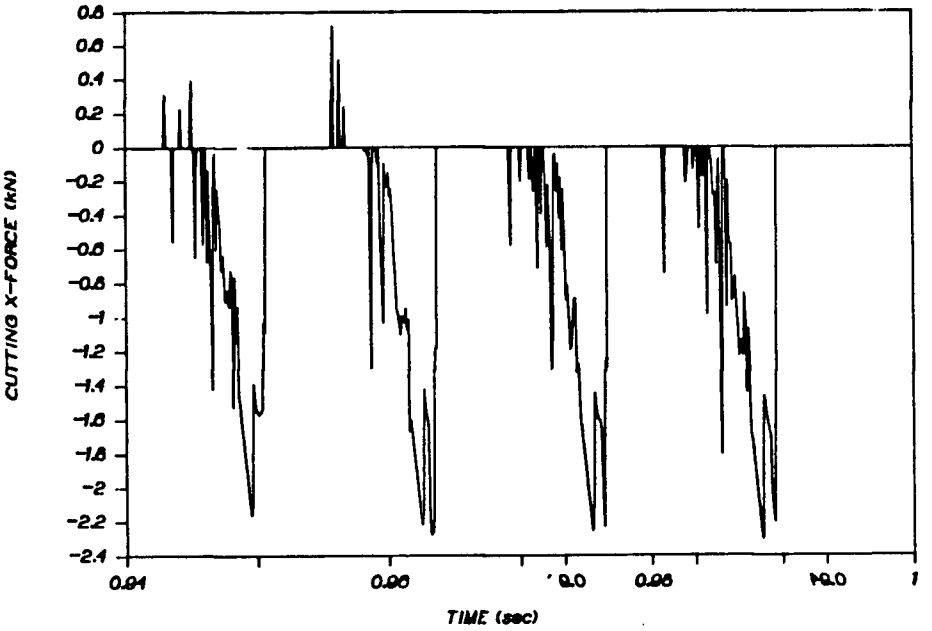

Figure 5.42: CASE 3: Simulated x-cutting force (ploughing incl.).

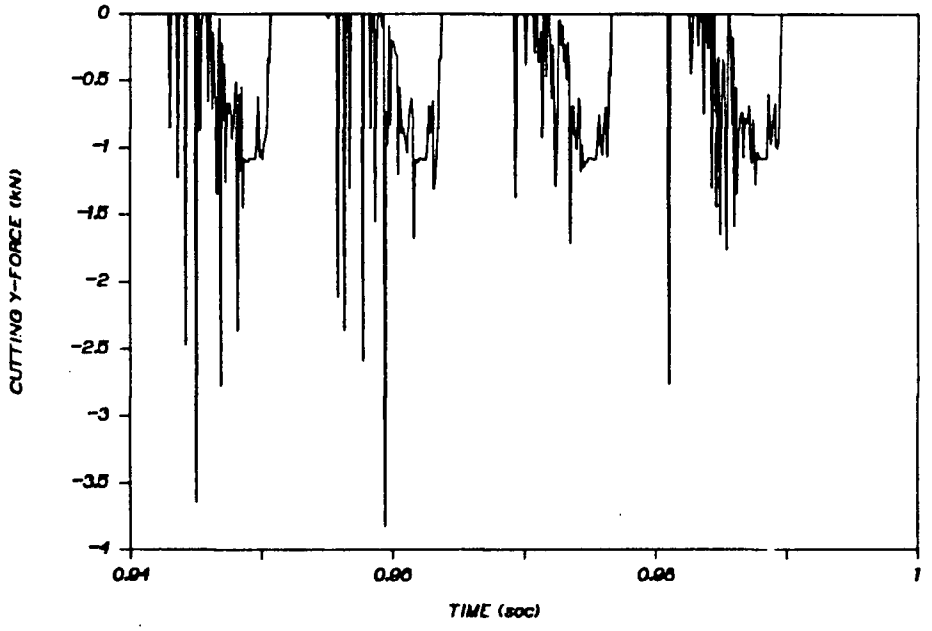

Figure 5.43: CASE 3: Simulated y-cutting force (ploughing incl.).

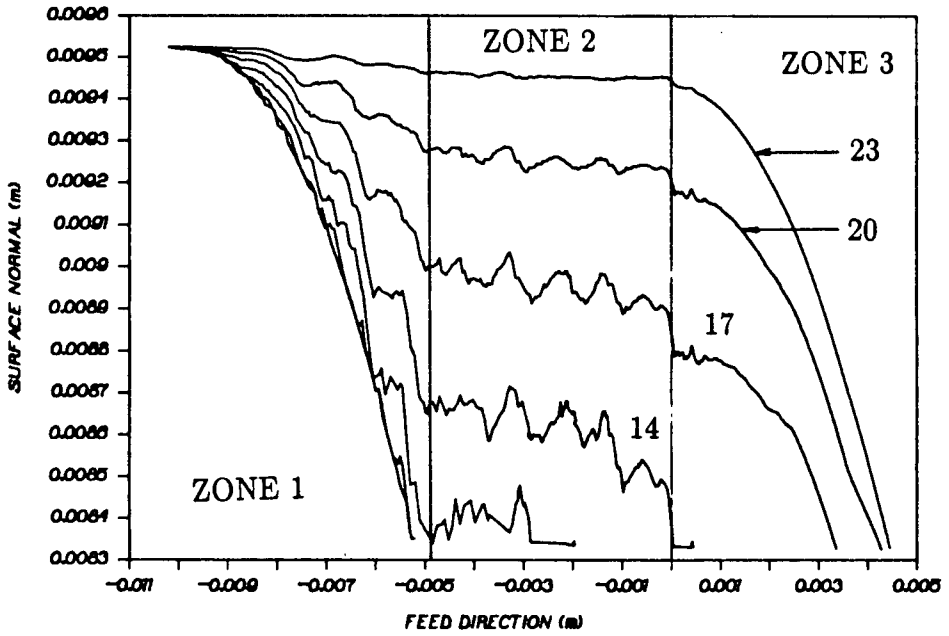

Figure 5.44: CASE 3: Simulated microscopic surface finish (ploughing incl.).

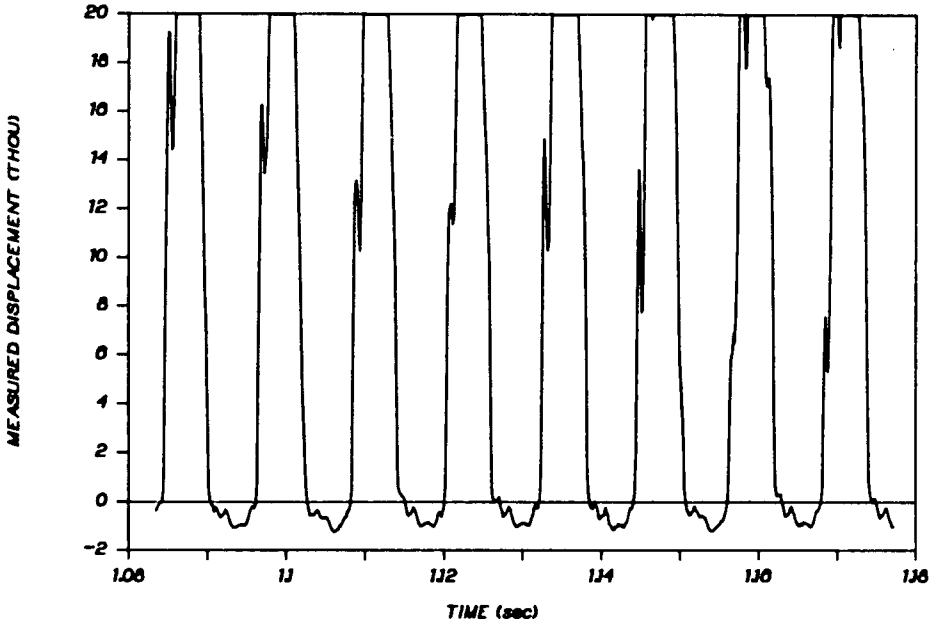

Figure 5.45: CASE 3: Experimental displacement at node 14.

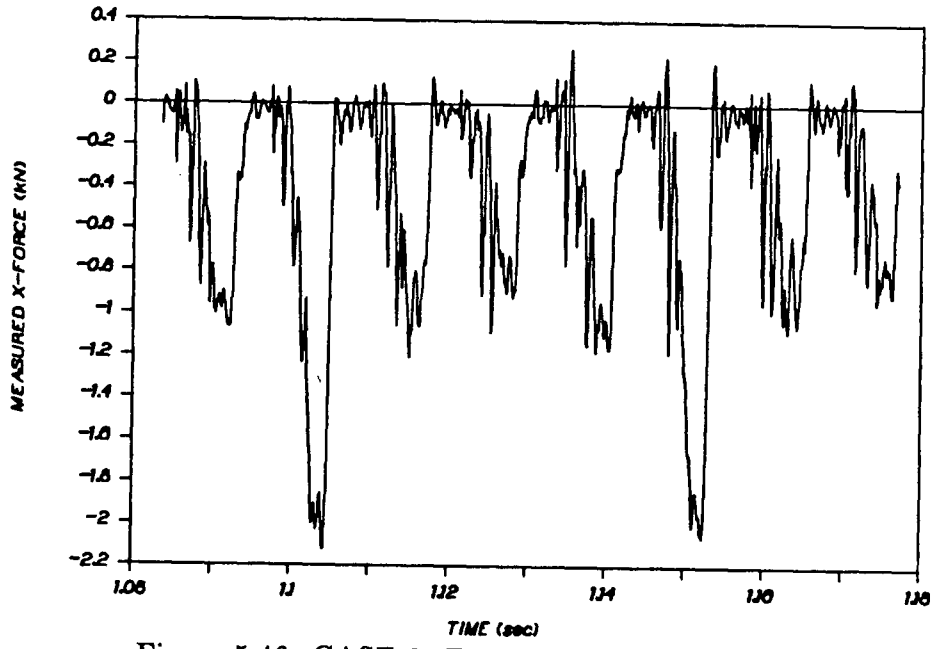

Figure 5.46: CASE 3: Experimental x-cutting force.

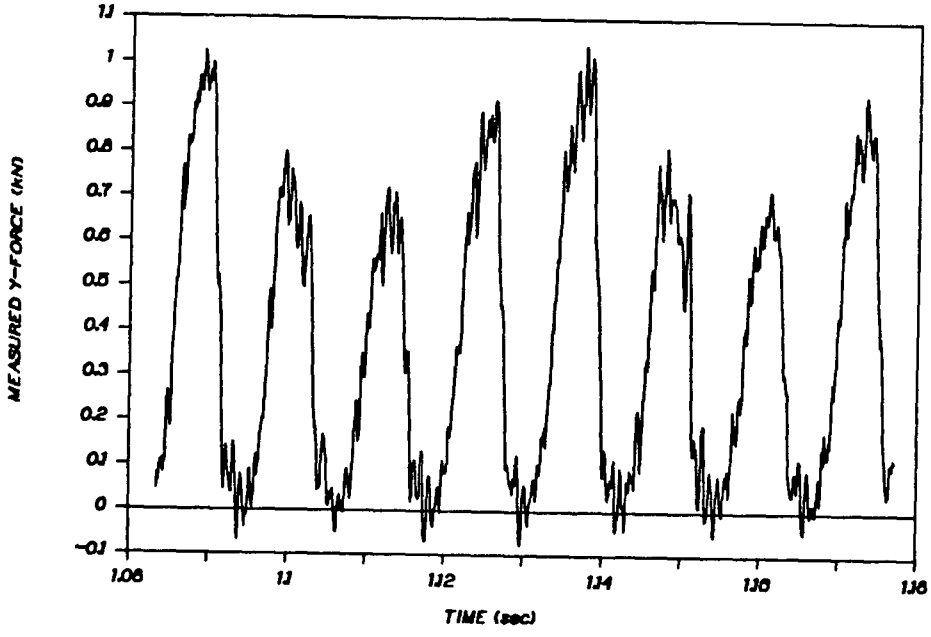

Figure 5.47: CASE 3: Experimental y-cutting force.

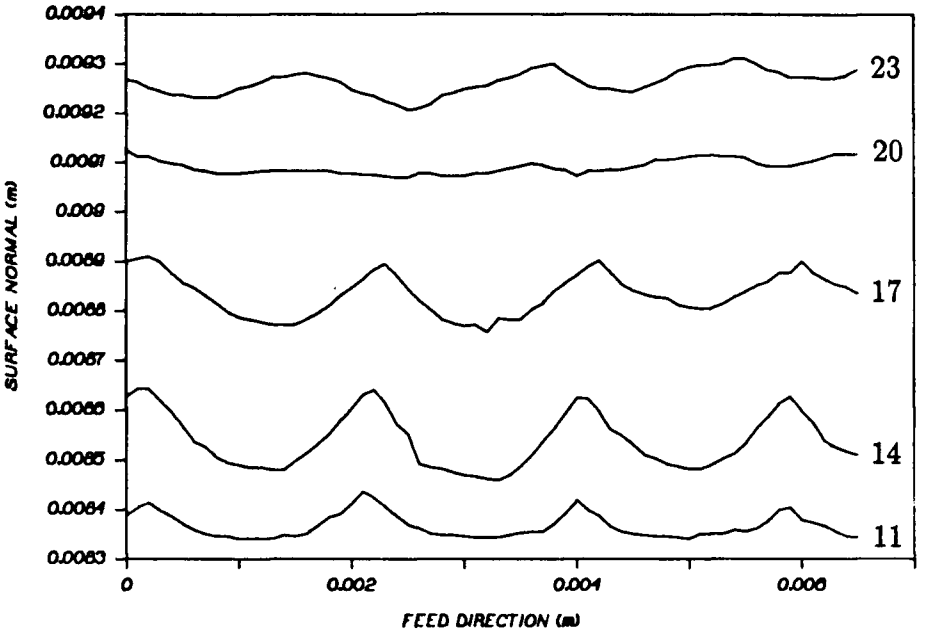

Figure 5.48: CASE 3: Experimentally measured surface finish at node 14.

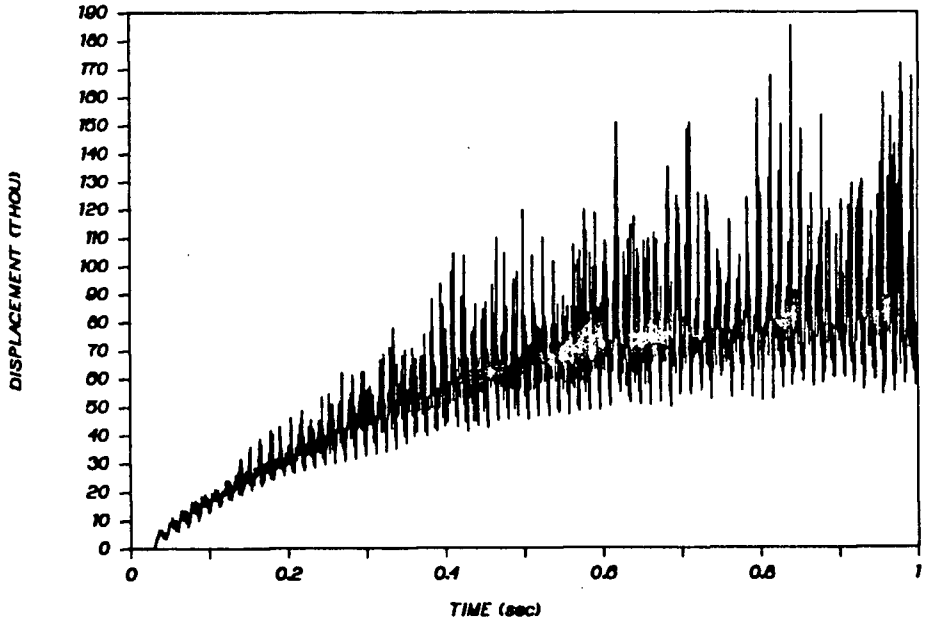

Figure 5.49: CASE 4: Simulated displacement at node 14 showing unstable cutting.

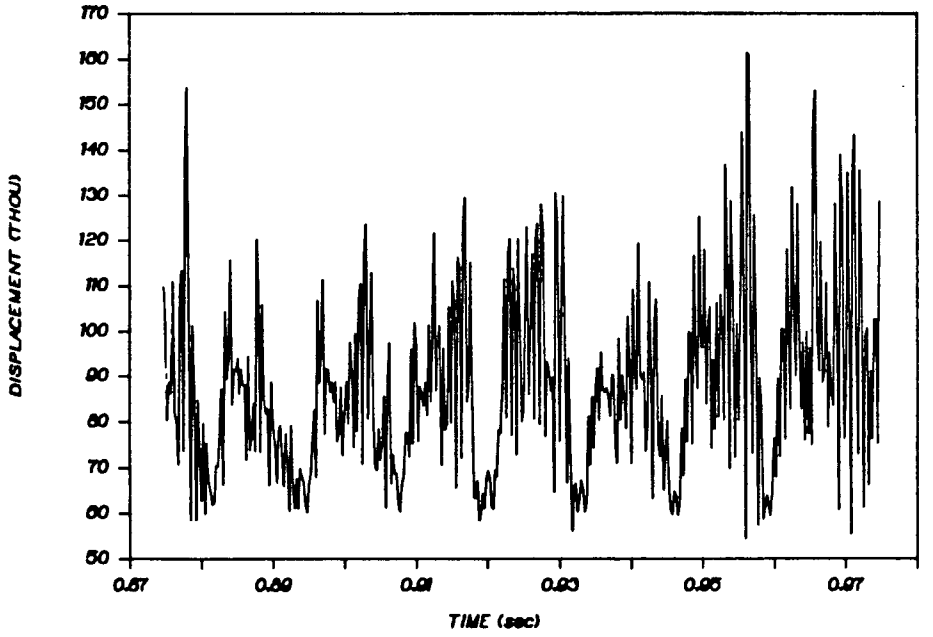

Figure 5.50: CASE 4: Simulated displacement at node 14.

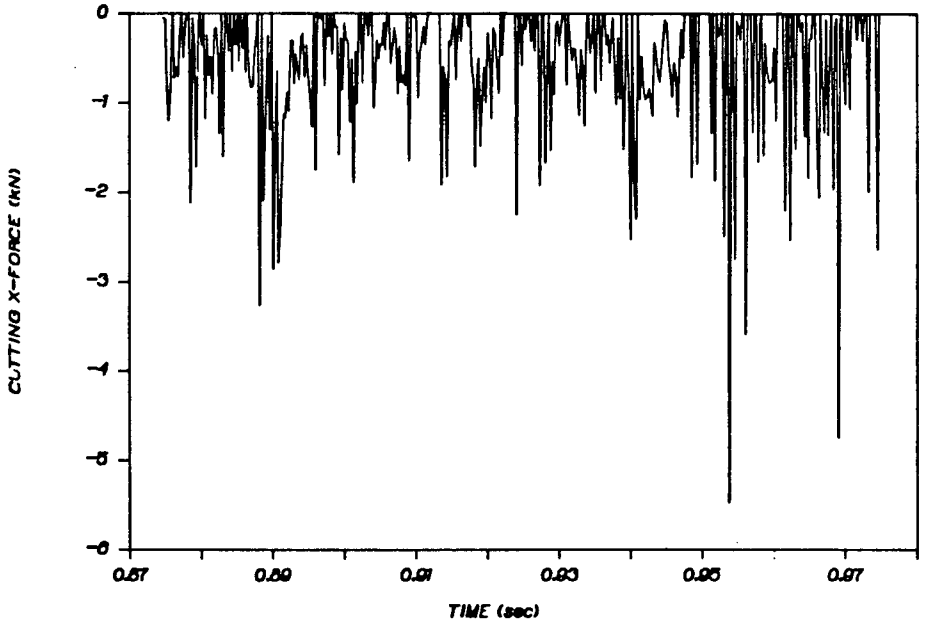

Figure 5.51: CASE 4: Simulated x-cutting force.

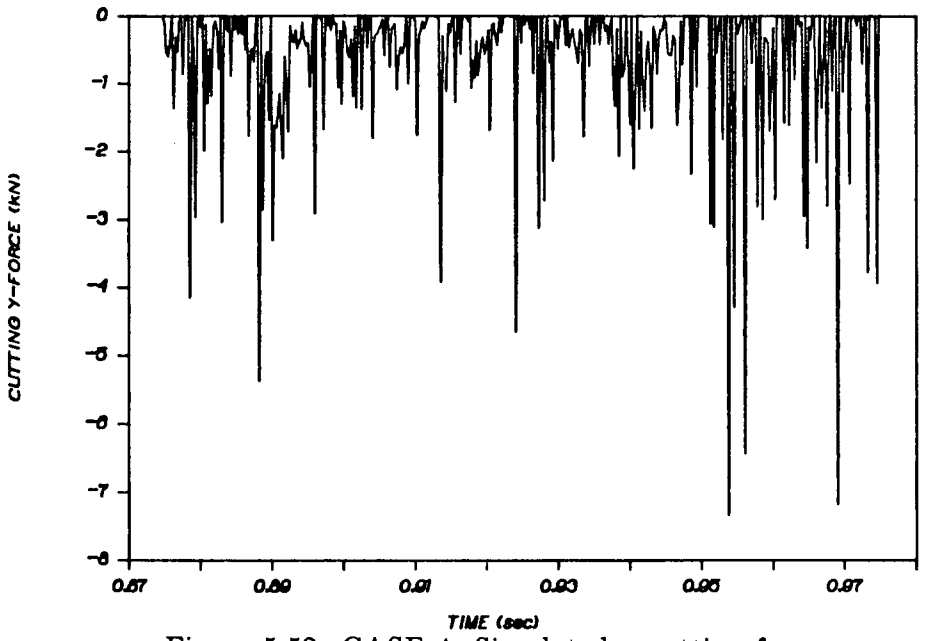

Figure 5.52: CASE 4: Simulated y-cutting force.

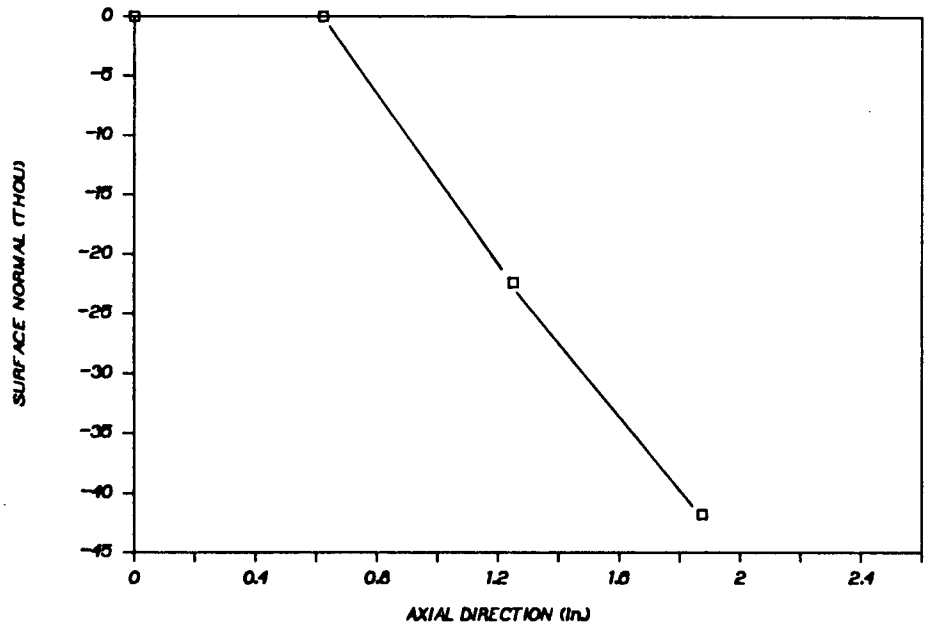

Figure 5.53: CASE 4: Simulated surface profile.

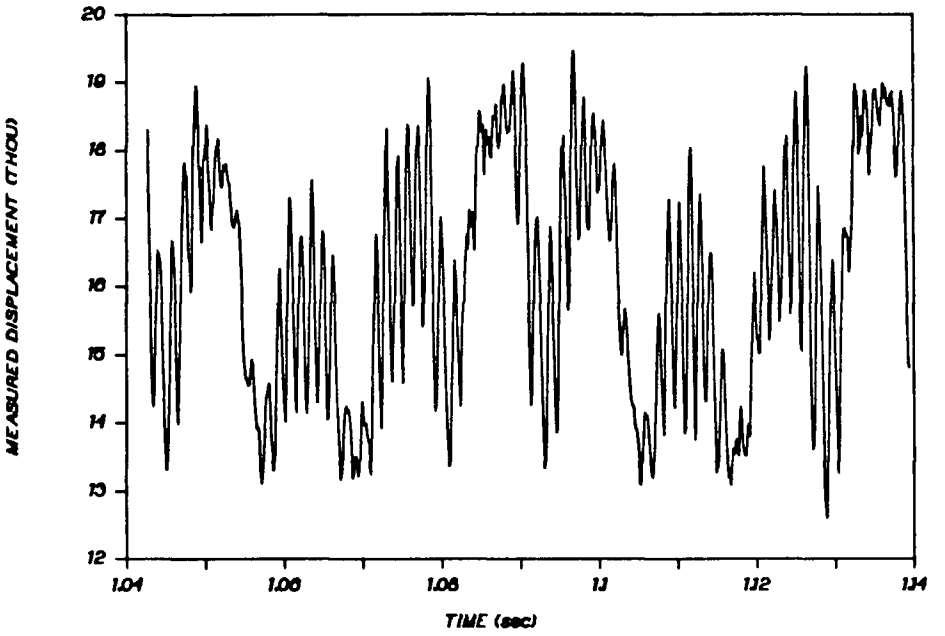

Figure 5.54: CASE 4: Experimental displacement at node 14.

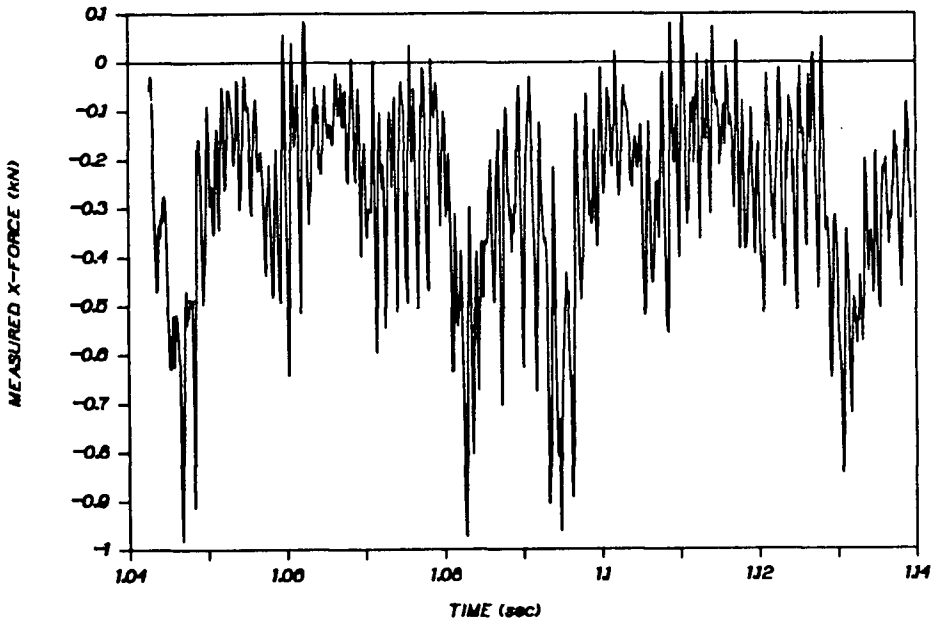

Figure 5.55: CASE 4: Experimental x-cutting force.

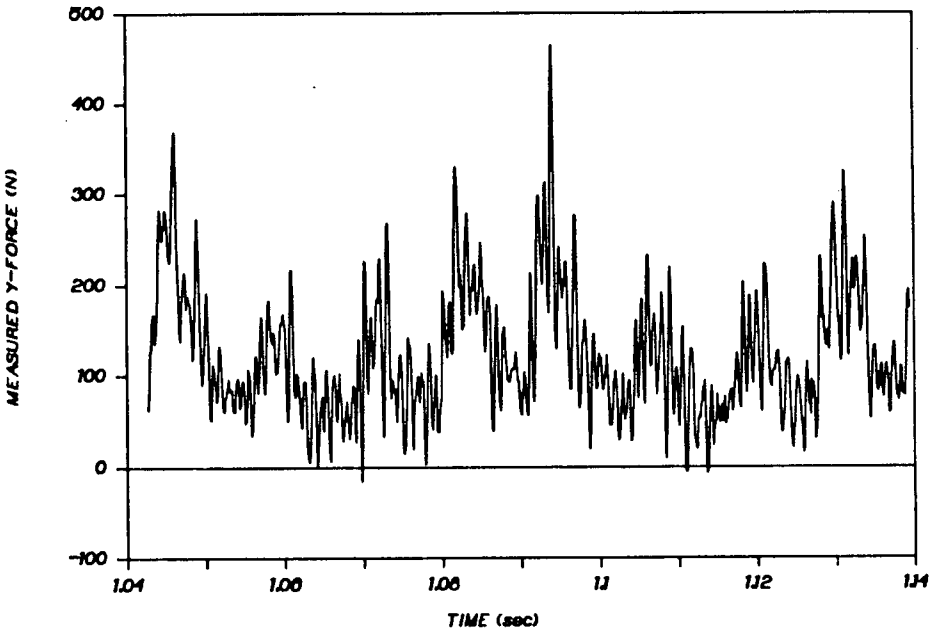

Figure 5.56: CASE 4: Experimental y-cutting force.

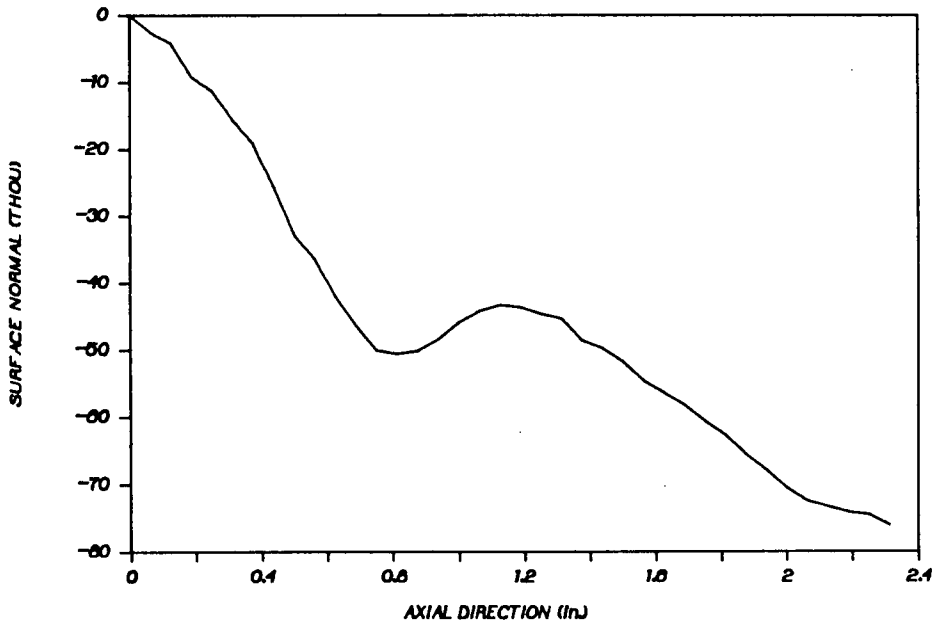

Figure 5.57: CASE 4: Experimentally measured surface profile.

Chapter 6

Concluding Remarks

The mechanisms of chip removal and surface generation have been studied in this thesis. An improved model of uncut chip thickness determination has been developed by employing the actual kinematics of milling. To the best knowledge of the author, this is an original approach to discrete modelling of the milling process. The use of an accurate model for the kinematics of tooth motion in milling is particularly important in machining workpieces with narrow chip thickness and large axial depths of cut. Errors introduced by earlier assumptions of circular tool motion may be significant for accurate determination of the uncut chip thickness.

It is shown in this thesis that the cutting edge of the milling tool may travel in several zones during its vibratory motion as a result of the dynamic interaction between the flexible structures of the tool and workpiece. The cutting force mechanism is governed by a different physical mechanism in each region. Previous dynamic milling models have used either generalized metal shearing laws or emperical cutting force coefficients, representing the process stiffness and damping, to estimate the cutting forces. In this study force contributions of shearing, tool flank-workpiece interaction and disengagement of the tool and workpiece are included separately and superimposed in a discrete time model of the process. Tool flank interference has been modelled as a simple ploughing mechanism.

The closed loop behaviour of the cutting process under structural vibrations has been modelled by employing the kinematics of milling, relative motion between the tool and

workpiece, the cutting force mechanism and surface finish generation. A discrete time simulation program has been developed to implement these mechanisms. The simulation has the versatility to incorporate dynamic models for both the tool and the workpiece. Two mechanisms, washboarding and vibration reproduction, have been identified in generating waves on the workpiece surface under different conditions of dynamic milling.

Peripheral milling of a very flexible workpiece (plate) has been investigated in this thesis. The time varying mass and stiffness of the workpiece have been reduced to a few degrees of freedom at the cutting zone where milling occurs. The workpiece was modelled using the finite element method and reduced by the system equivalent reduction expansion process. Four cases of machining flat plates have been examined by both simulation and experimental studies. Several important trends have been predicted by simulation which were realized in the experiments. These included: prediction of waves on the finished workpiece surface, lack of material removal at the top of the plate, an increased vibration frequency during cutting, high frequency components present in the cutting forces as a result of higher mode activity near the root of the plate and the reduction of dynamic cutting force amplitudes by the introduction of a ploughing force model. Although these trends qualitatively define milling of flexible workpieces the accuracy of many numerical results has been poor and future work is required to improve the model.

There are several problems remaining to be investigated in this research. These include inadequate cutting force prediction, limited tool geometries available and the inability to model the continuously changing dynamics of the plate. Therefore, future work should include the development of more appropriate static and dynamic cutting force models, implementation of more complex tool geometries (tool runout and ball end) and the investigation of changing workpiece dynamics during cutting. Also, the tool offset method should be verified as an acceptable first improvement to milling flexible workpieces by both experimental and simulation investigations.

Bibliography

[1] Altintas, Y. and Yellowley, I., "In Process Detection of Tool Failure in Milling Using Cutting Force Models," *Trans. of ASME, J. Eng. for Ind.* , Vol.111, pp.149-157, 1989.

[2] Armarego, E.J.A. and Brown, R.H., *The Machining of Metals* , Prentice-Hall Inc., 1969.

[3] Bailey, J.A., "Friction in Metal Machining - Mechanical Aspects," *J. of Wear*, Vol.31, 1975.

[4] Baumeister, Theodore (ed.), *Marks' Standard Handbook for Mechanical Engineers*, 8th Edition, McGraw-Hill Inc. 1978.

[5] Bishop, R. E. D. and Gladwell, G. M. L., "An Investigation Into The Theory Of Resonance Testing," *Proc Roy Soc Phil Trans*, Vol.255, A.1055, pp. 31-280, January 1963.

[6] Bishop, R.E.D., *Vibration*, Second Ed., Cambraidge University Press, pp.91-118, 1979.

[7] Boentgen, Rudolf R., "Some Things That Work and Some Things Don't In Experimental Modal Measurements," *Proceedings of the 7th International Modal Analysis Conference*, Vol.1, pp.1-4, 1989.

[8] Clough, Ray W., *Dynamics of Structures*, McGraw-Hill Inc., pp.69-77, 1975.

[9] Cook, Robert D., *Concepts and Applications of Finite Element Analysis*, Third Edition, John Wiley and Sons, pp.1-30, 1989.

[10] Ewins, D.J., *Modal Testing Theory and Practice*, Research Studies Press, England, 1984.

[11] Fu, H.J., DeVor, R.E. and Kapoor, S.G., "A Mechanistic Model for the Prediction of the Force Systems in Face Milling Operations," *ASME J. Eng. Ind.*, Vol.106, pp.81-88, 1984.

[12] Halling, J. (ed.), *Principles of Tribology*, The Macmillan Press Ltd., pp.72-91, 1983.

[13] Harris, Cyril M. (ed.), *Shock and Vibration Handbook*, Third Edition, McGraw-Hill, Inc., p.7-30, 1988.

[14] Hinkle, Roland T. *Design of Machines*, Prentice-Hall Inc. 1957.

[15] Kegg, R. L., "Cutting Dynamics in Machine Tool Chatter: Contribution to Machine-Tool Chatter," *Journal of Engineering for Industry*, pp.464-470, November 1985.

[16] King, Robert I.(ed.), *Handbood of High Speed Machining Technology*, Chapman and Hall, pp.48-153, 1985.

[17] Kline, W.A., and DeVor, R.E., "The Effect of Runout on Cutting Geometry and Forces in End Milling," *Int. J. Mach. Tool Des. Res.*, Vol.23, pp.123-140, 1975.

[18] Kline, William, *The Prediction of Cutting Forces and Surface Accuracy for the End Milling Process*, Ph.D. Thesis, Univ. of Illinois at Urbana-Champaign, 1981.

[19] Koren Yoram, *Computer Control of Manufacturing Systems*, McGraw-Hill Inc. 1983.

[20] Lin, S.C., DeVor, R.E. and Kapoor, S.G., "The Effects of Variable Speed Cutting on Vibration Control in Face Milling," *Proc. ASME 1988 Winter Annual Meeting*, Book PED-Vol.33, pp.41-51, 1988.

[21] Long, G. W. and Lemon, J. R., "Structural Dynamics in Machine-Tool Chatter: Contribution to Machine-Tool Chatter," *Journal of Engineering for Industry*, pp.455-463, November 1965.

[22] Martellotti, M., "Analysis of the Milling Process," *Trans. ASME*, Vol.63, pp.677-700, 1941 and Vol.67, pp.233-251, 1945.

[23] Marui, E., et al., "The Mechanism of Chatter Vibration in a Spindle-Workpiece System: Part 1 - Properties of Self-Excited Chatter Vibration in Spindle-Workpiece System," *Journal of Engineering for Idustry*, Vol.110, pp.236-241, August 1988.

[24] Meirovitch, L., *Computational Methods in Structural Dynamics*, Sijthoff and Noordhoff International Publishers, The Netherlands, pp.29-30,184-185, 1980.

[25] Merchant, M.E., "Mechanics of the Cutting Process," *J. Appl. Phys.*, 16, 1945.

[26] Merritt, H. E., "Theory of Self-Excited Machine-Tool Chatter: Contribution to Machine-Tool Chatter." *Journal of Engineering for Industry*, pp.447-454, November, 1965.

[27] Montgomery, D.T., "The Machining of Flexible Structures," *CAMROL Report No. 90-1*, The University of British Columbia, 1990.

[28] O' Callahan, Dr. John, et al., "System Equivalent Reduction Expansion Process (SEREP)," *Proceedings of the 7th International Modal Analysis Conference*, Vol.1, pp. 29-37, 1989.

[29] Ogata, Katsuhiko, *Discrete-Time Control Systems*, Prentice-Hall Inc., pp.315-318, 1987.

[30] Press, William H. et al., *Numerical Recipies, The Art of Scientific Computing*, Cambridge University Press, p.390, 1986.

[31] Ryffel, Henry H. (ed.), *Machinery's Handbook*, 22nd Edition, Industrial Press Inc. 1985.

[32] Schey, John A, *Introduction to Manufacturing Processes*, McGraw-Hill, Inc., pp.225-284, 1977.

[33] Smith, S. and Tlusty, J., "Update On High-Speed Milling Dynamics," *Proc. ASME 1987 Winter Annual Meeting*, PED Vol.25, pp.153-165, 1987.

[34] Sutherland, J.W., "A Dynamic Model of the Cutting Force System in End Milling," *ASME - Sensors and Controls for Manufacturing*, 1988.

[35] Sutherland, J. W. and DeVor, R. E., "An Improved Method for Cutting Force and Surface Error Prediction in Flexible End Milling Systems," *ASME, J. Eng. Ind.*, Vol.108, pp.269-279, 1986.

[36] Timoshenko, S., *Strength of Materials, Part I, Elementary Theory and Problems*, Third Edition, D Van Nostrand Company, Inc., pp.148-153,288,291, 1958.

[37] Tlusty, J., "Analysis of the State of Research in Cutting Dynamics," *Annals of CIRP*, Vol.27/2/1978, 1978.

[38] Tlusty, J., "Dynamics of High-Speed Milling," *Journal of Engineering for Industry*, Vol.108, pp.59-67, May 1986.

[39] Tlusty, J., *Stability Against Chatter," Machine Tool Structures*, Vol.1, by Koenigsberger, F. and Tlusty, J., Section 2, pp.115-339, Pergamon Press, 1967.

[40] Tlusty, J. and Ismail, F., "Basic Non-Linearity in Machining Chatter," *Annals of the CIRP*, Vol.30, pp.21-25, 1981.

[41] Tlusty, J. and Ismail, F., "Dynamic Structural Identification Task and Methods," *Annals of the CIRP*, Vol.29, January 1980.

[42] Tlusty, J. and Ismail, F., "Special Aspects of Chatter in Milling," *Journal of Vibration, Acoustics, Stress, and Reliability in Design*, Vol.105, pp.24-32, January 1983.

[43] Tlusty, J., Macneil, P., "Dynamics of Cutting Forces in End Milling," *Annals of CIRP*, Vol.21, pp.21-25, 1975.

[44] Tlusty, J. and Moriwaki, T., "Experimental and Computational Identification of Dynamic Structural Models," *Annals of the CIRP*, Vol.25, 1976.

[45] Tobias, S. A., *Machine-Tool Vibration*, Blackie and Son Ltd. London, pp.143-179, 1965.

[46] Trent, E.M., *Metal Cutting*, Butterworth and Co. Ltd., pp.1-48, 1977.

[47] Tse, Francis S., Morse, Ivan E. and Hinkle, Roland T., *Mechanical Vibrations, Theory and Applications*, Second Edition, Allyn and Bacon, Inc., 1978.

[48] *VAST Version 4.1 Users Manual*, Defence Research Establishment Atlantic, Canada, 1986.

[49] Vold, Harvard, "Insight, Not Numbers," *Proceedings of the 7th International Modal Analysis Conference*, Vol.1, pp.16-19, 1989.

[50] Wu, D.W., "A New Approach of Formulating the Transfer Function for Dynamic Cutting Process," *Trans. ASME, J. Eng. for Ind.*, Vol.111, pp.37-47, 1989.

[51] Zienkiewicz, O.C., *The Finite Element Method*, Third Edition, McGraw-Hill Inc. 1985.

Appendix A

Static Deflection Calculations

The following static deflections are calculated with reference to the loaded plate of Fig. 4.3.

Deflection due to F_x:

From beam bending theory the deflection of the plate at its tip due to the applied force (F_x) is given by [36]:

$$\delta = \frac{Pl^3}{3EI}$$

$$\delta = \frac{1(.0635)^3}{3E[1.27(10)^{-3}(.0635)^3/12]}$$

$$\delta = \frac{3(10)^3}{E}$$

Deflection due to M:

For a shaft of rectangular cross section, with the dimensions of the plate of Fig.4.2, the angular twist per unit length is given by [36]:

$$\theta = \frac{3M}{lt^3G}$$

where,

$$M = F_x t/2$$

and,

$$G = \frac{E}{2(1+\nu)}$$

If the displacement at the corner of the plate is estimated as:

$$\delta = \frac{\theta l}{2}$$

then the calculated maximum deflection of the plate due to applied (M) for a plate with $\nu = 0.3$ is:

$$\delta = \frac{3(.00127/2)(2)(1.3)(.0635)}{2(.0635)(.00127)^3 E}$$

$$\delta = \frac{77(10)^3}{E}$$

Deflection due to F_y:

The deflection of the plate due to force (F_y) is given by [36]:

$$\delta = \frac{(.168)Pl^2}{D}$$

where,

$$D = \frac{Et^3}{12(1-\nu^2)}$$

$$\delta = \frac{(.168)(1)(.0635)^2(12)(1-.3^2)}{E(.00127)^3}$$

$$\delta = \frac{3600(10)^3}{E}$$

Appendix B

Listing of Programs

- File transfers from VAST to formatted data.
- SEREP dynamic system reduction program.
- Point receptance FRF calculation for reduced dynamic systems.
- Forced response calculation for reduced dynamic systems.
- FFT analysis for a range of data.
- Simulation of dynamic milling with workpiece vibrations.

The programs listed above can be found in Report **, 1990 from UBC's Computer Aided Manufacturing and Robotics Library (CAMROL).**

Appendix C

Summary of Plate Machining Results

PLATE: **free - free - free - cantilevered (see Fig. 4.1)**
2.5 x 2.5 x 0.1 (in.) to 2.5 x 2.5 x 0.05 (in.)
63.5 x 63.5 x 2.54 (mm) to 63.5 x 63.5 x 1.27 (mm)

Yield Pressure = 496 MPa

TABLE OF PARAMETERS USED FOR FOUR CASES:

PARAMETER		CASE #1	CASE #2	CASE #3	CASE #4
Operation	(-)	up mill	up mill	up mill	up mill
Tool diameter	(in.)	3/4	3/4	3/4	1
Rake angle	(deg)	5	5	5	3
Clearance angle	(deg)	10	10	10	5
Primary land	(in.)	NA	NA	0.02	0.02
Flutes on cutter	(-)	4	4	4	4
Spec. cutting press.	(MPa)	1185	1185	1185	1185
Cutting force ratio	(-)	1	1	1	1
Axial depth of cut	(in.)	2.5	2.5	2.5	2.5
Spindle speed	(RPM)	1500	1157	1157	1157
Feedrate	(in./s)	0.015	0.02	0.4	0.4
Feed per tooth	(thou)	0.15	0.26	5.2	5.2
Immersion angle	(deg)	30	30	30	18
Max. uncut chip	(thou)	0.08	0.13	2.6	1.6
Sim. damping ratio	(-)	0.05	a) 0.005 b) 0.05 c) 0.5	0.5	0.5
Modes incl.	(-)	1-5	1-5	1	1
Sim. time step (micro sec)		10	10	10	10
Ploughing Incl.	(-)	no	no	a) no b) yes	no

SUMMARY OF RESULTS FOR FOUR CASES:

CASE NO. 1:

Figures:		5.4-5.14
Displacement:	Simulation	First mode dominant and strong out of cut. Higher modes stronger towards root of plate. Unstable machining operation. In cut frequency higher than out of cut frequency.
	Experiment	Poor correlation with simulation. In cut frequency (900 Hz) close to sim. value.
Forces:	Simulation	Very strong AC component. Very high frequency (5 kHz) variation during cut.
	Experiment	Significant AC and DC components are visible. Magnitude is close to simulation.
Surface:	Experiment	Wavelength = 2.8 mm, Amplitude = 0.2 mm. Theoretical wavelength is 1.7 mm.

CASE NO. 2:

Figures:		5.15-5.35
Displacement:	Simulation	a) Strongly unstable, simulation crashes.
		b) Unstable machining process. Strong first mode transients in cut. Higher frequency vibration in cut (890 Hz).
		c) Unstable machining process. Little transient vibration between cuts. In cut vibration frequency is about (890 Hz).
	Experiment	Overall poor correlation with simulation. In cut frequency (860 Hz) close to sim. value.
Forces:	Simulation	a) Strongly unstable, simulation crashes.
		b) Very strong AC component. Very high frequency (5 kHz) variation in cut.
		c) Slightly more DC component than case b). Very high frequency (5kHz) variation in cut.
	Experiment	Significant AC and DC components are visible. Peak magnitude is close to simulation.
Surface:	Experiment	Wavelength = 2 mm, Amplitude = 0.1 mm. Theoretical wavelength is 1.3 mm.

CASE NO. 3:

Figures:		5.36-5.48
Displacement:	Simulation	a) Strong AC (1.3 kHz) and DC components in cut. In cut frequency higher than fundamental freq.
		b) Strong DC component. Reduced AC (1.5 kHz) magnitude wrt. case a).
	Experiment	Poor results obtained, tops clipped off. Comparable with both simulation results.
Forces:	Simulation	a) Strong AC component on a small DC sig.
		b) Greatly reduced AC component wrt. case a). Similar DC wrt. case a).
	Experiment	Strong DC component due to increased feedrate. Significant runout visible. Magnitude is close to simulation case b).
Surface:	Simulation	a) Wavelength = 1.6 mm, Amplitude (#14) = 0.4 mm. No cutting at top of plate.
		b) Wavelength = 0.9 mm, Amplitude (#14) = 0.1 mm. No cutting at top of plate.
	Experiment	Wavelength = 2 mm, Amplitude (#14) = 0.15 mm. No cutting at top of plate.

CASE NO. 4:

Figures:		5.49-5.57
Displacement:	Simulation	Unstable machining operation. Strong DC and AC (1.35 kHz) components. Visible variation at tooth passing frequency.
	Experiment	Poor quantitative correlation with simulation. In cut frequency (700 Hz) not close to sim. value. Similar trend (ie. shape) with simulation.
Forces:	Simulation	Very strong AC component. Very high frequency variation during cut.
	Experiment	Significant AC and DC components are visible. Magnitude is not close to simulation. Runout is clearly visible.
Surface:	Simulation	No cutting at top of the plate. More material removed towards root of the plate. More detail required for further comments.
	Experiment	Similar trend with simulation result.